SYNTHESIS OF EARTHQUAKE GROUND MOTION AT THE 1915 ÇANAKKALE BRIDGE: STOCHASTIC SIMULATIONS WITH A REGIONAL PATH DURATION FUNCTION

by

Numan Büyükçapar

B.S., Civil Engineering, Balıkesir University, 2014

Submitted to the Kandilli Observatory and Earthquake Research Institute
in partial fulfillment of the requirements for the degree of
Master of Science

Graduate Program in Earthquake Engineering

Boğaziçi University

2021

ACKNOWLEDGEMENT

I would like to express deep appreciation to my thesis supervisor Assoc. Prof. Dr. Gülüm Tanırcan who has always encouraged and guided me throughout the most complicated and enduring sections of this study. It was a real privilege and great pleasure to study with her.

I would like to thank Assoc. Prof. Dr. A. Özgün Konca and Dr. Gail Atkinson for their contributions which are made either with documents or personal communications to my thesis.

I would also like to thank my managers Dinçer Mete and Ali Özener who have always enabled me to expedite the thesis process.

Finally, I would like to express my eternal gratitude to my parents Sevinç Büyükçapar, Mustafa Büyükçapar, and sisters Merve Büyükçapar, and Mine Ertuğrul who were extremely understanding and supportive in all phases of my life.

ABSTRACT

SYNTHESIS OF EARTHQUAKE GROUND MOTION AT THE 1915 ÇANAKKALE BRIDGE: STOCHASTIC SIMULATIONS WITH A REGIONAL PATH DURATION FUNCTION

Strong ground shaking duration has got to be taken into consideration realistically in ground motion simulations as it is a key parameter affecting structural damages. Total duration of an earthquake comprises source and path properties. Among them path duration which is one of the most important parameters for use in stochastic simulation studies has long been defined as multilinear functions of distance modelled with regional or global earthquake ground motion recordings. Up-to-date path duration models available in the literature are based on global (PEER-NGAWest2) or regional (such as NEAmerica, Japan) strong motion database. Therefore, they represent either a global estimation or can be used only for certain regions. Turkey-specific path duration-distance function is absent in the scientific literature. The main purpose of this thesis is to fulfill this absence and propose a path duration-distance function utilizing the abundant strong motion database of Turkey as well as performing stochastic simulation of strong ground motions at the 1915 Çanakkale Bridge by using path duration function that describes the behavior of Turkish earthquakes. For the latter part of the study, a stochastic simulation method of Motazedian and Atkinson (2005): EXSIM is utilized. Effect of generic and site-specific local site amplification on the simulation is another subject that is investigated in the thesis. Subsequent to this suggestion, the said original method, which is also present on the SCEC (Southern California Earthquake Center) Broadband Platform, was improved by Boore (2009) and Assatourians and Atkinson (2012). Following the analyses which are intrinsic to above-mentioned parts of the study, the obtained regional path duration function has been discussed in detail, and simulations that have been performed throughout the thesis have been thoroughly assessed and presented.

ÖZET

1915 ÇANAKKALE KÖPRÜSÜ'NDE DEPREM YER HAREKETİ SENTEZİ: BÖLGESEL YAYILIM YOL SÜRESİ FONKSİYONUYLA STOKASTİK SİMÜLASYONLAR

Güçlü yer hareketlerine yönelik süreler, yapısal hasarları etkileyen önemli bir parametre olduğu için yer hareketi simülasyonlarında gerçekçi bir şekilde dikkate alınmalıdır. Bir depremin toplam süresi, kaynak ve yayılım yolu özelliklerini kapsamaktadır. Bunlardan, stokastik simülasyon çalışmalarında kullanılan en önemli parametrelerden biri olan yayılım yol süresi, uzun zamandır bölgesel veya küresel deprem yer hareketi kayıtlarıyla modellenen mesafeye dayalı çoklu doğrusal fonksiyonlar olarak tanımlanmaktadır. Mevcut durumda, literatürde bulunan güncel yayılım yol süresi modelleri, küresel (PEER-NGAWest2) veya bölgesel (NEAmerica, Japonya gibi) kuvvetli yer hareketi veri tabanlarına dayanmaktadır. Dolayısıyla, söz konusu yayılım yol süresi modelleri ya küresel bir tahmini temsil etmekte ya da yalnızca belirli bölgeler için kullanılabilmektedir. Türkiye'ye özgü mesafeye dayalı yayılım yol süresi fonksiyonu ise bilimsel literatürde bulunmamaktadır. Bu tezin esas amacı, bu eksikliği gidermek ve bol miktardaki kuvvetli yer hareketi veri tabanını kullanarak mesafeye dayalı bir yayılım yol süresi fonksiyonu ortaya çıkarmak ve sonrasında Türkiye'de meydana gelen depremlerin davranışını tanımlayan bu yayılım yol süresi fonksiyonunu kullanarak 1915 Çanakkale Köprüsü'nde kuvvetli yer hareketlerinin stokastik simülasyonunu gerçekleştirmektir. Tezde incelenen diğer bir konu ise genel ve sahaya özel lokal saha amplifikasyonlarının simülasyona olan etkisidir. Çalışmanın ikinci kısmı için Motazedian ve Atkinson'a (2005) ait bir stokastik simülasyon yöntemi olan EXSIM kullanılmıştır. Sonrasında, SCEC (Southern California Earthquake Center) Geniş Bant Platformu'nda da bulunan söz konusu orijinal yöntem, Boore (2009) ve Assatourians ve Atkinson (2012) tarafından geliştirilmiştir. Çalışmanın yukarıda belirtilen kısımlarına özgü analizlerin ardından, elde edilen bölgesel yayılım yol süresi fonksiyonu ayrıntılı bir biçimde ele alınmış, tez boyunca gerçekleştirilen simülasyonlar kapsamlı bir biçimde değerlendirilmiş ve sunulmuştur.

TABLE OF CONTENTS

ACKNOWLEDGEMENT iii

ABSTRACT iv

ÖZET v

TABLE OF CONTENTS vi

LIST OF FIGURES viii

LIST OF TABLES xi

LIST OF SYMBOLS xii

LIST OF ACRONYMS / ABBREVIATIONS xiv

1. INTRODUCTION 1

2. LITERATURE SURVEY 3

2.1. Path Duration Modelling 3

2.2. Stochastic Ground Motion Simulation 4

3. AN INVESTIGATION OF REGIONAL PATH DURATION MODEL 9

3.1. Method 9

3.2. Ground Motion Set 12

3.3. Analysis & Results 16

4. STOCHASTIC SIMULATIONS OF STRONG GROUND MOTIONS 30

4.1. The Stochastic Simulation Method 31

4.1.1. Number of Trials 32

4.1.2. Residual Model 33

4.2. Propagation Path Parameters 33

4.3. Site Parameters 34

4.4. Point Source Stochastic Simulation of the Mw4.5 Gökçeada Event 35

4.5. Simulation of the 2014 (Mw6.9) Gökçeada Earthquake 42
4.5.1. Data Set 42
4.5.2. Source Parameters 43
4.6. Simulation 46
4.6.1. Basis of Comparisons for Results 46
4.6.2. Number of Trials 47
4.6.3. Model Validation 47
4.7. Analysis 47
4.8. Results and Discussions 58
5. SYNTHESIS OF STRONG GROUND MOTION AT THE 1915 ÇANAKKALE BRIDGE 60
5.1. Analysis and Results 61
6. CONCLUSION 63
REFERENCES 65
APPENDIX A: THE CHARACTERSITICS OF RECORDINGS 69

LIST OF FIGURES

Figure 2.1. The flow chart of ground motion simulation methods. 4
Figure 3.1. The median DP, in various magnitude and distance bins, revised DP belongs to Boore and Thompson (2014), AB95 (ENA) by Atkinson and Boore (1995), A14 by G. Atkinson, and A95 by Atkinson (1995). 11
Figure 3.2. The number of recordings based on various ranges of M_w, V_{s30}, and R_{RUP}. 14
Figure 3.3. Location of earthquakes and strong motion stations. 15
Figure 3.4. An example of recordings from May 19, 2011 Kütahya-Simav Earthquake, station 0302. It is removed from the calculation as it includes no proper data. 17
Figure 3.5. Corner frequency values corresponding to each seismic event. 19
Figure 3.6. Effective significant duration (D'_{95}) versus closest distance to rupture (R_{RUP}). 21
Figure 3.7. The difference between effective significant duration (D'_{95}), and source duration (D_S) versus closest distance to rupture (R_{RUP}). 21
Figure 3.8. Total duration (D_T) versus closest distance to rupture (R_{RUP}) for the different seismic events with magnitudes ranging from 5.5 to 7.5 22
Figure 3.9. The difference between effective significant duration (D'_{95}) and source duration (D_S) versus closest distance to rupture (R_{RUP}). 22
Figure 3.10. Segmented linear fittings involved in station recordings presented individually based on each magnitude bin up to 150 km, 200 km, and 300 km. 23
Figure 3.11. Segmented linear fitting together with the arithmetic mean of four magnitude groups up to 150 km, 200 km, and 300 km. 24
Figure 3.12. The plots are based on two groups (6.0>Mw≥5.5 and Mw≥7.0) having maximum dataset up to 150 km, 200 km, and 300 km. 24
Figure 3.13. Path duration function from events in Turkey following Boore and Thompson (2014), based on two groups (5.5>Mw≥7.0 and Mw≥7.0). 26
Figure 3.14. The medians of D'_{95}, $D_{5\text{-}95}$ vs R_{RUP} values in various magnitude and distance bins. 27
Figure 3.15. Mean of the rms duration minus the source duration, averaged by 15-km distance bins, Atkinson, G.M., and Boore, D.M. (1995). 28
Figure 4.1. Epicenter of two seismic events (red stars), focal mechanism (beachball), active faults (red lines), strong motion recording stations (downward-pointing blue triangles). ..30

Figure 4.2. Frequency dependent generic amplification factors, Karagöz et al. (2018).....35
Figure 4.3. The comparison of simulated Husid plots based on the path duration models from this study (top-left) and Herrmann (1985) (top-right) as well as recorded N-S (bottom-left) and E-W (bottom-right) at station 1701, Mw 4.5.....36
Figure 4.4. The comparison of simulated Husid plots based on the path duration models from this study (top-left) and Herrmann (1985) (top-right) as well as recorded N-S (bottom-left) and E-W (bottom-right) at station 1710, Mw 4.5.....37
Figure 4.5. The comparison of simulated Husid plots based on the path duration models from this study (top-left) and Herrmann (1985) (top-right) as well as recorded N-S (bottom-left) and E-W (bottom-right) at station 1711, Mw 4.5.....38
Figure 4.6. The comparison of simulated Husid plots based on the path duration models from this study (top-left) and Herrmann (1985) (top-right) as well as recorded N-S (bottom-left) and E-W (bottom-right) at station 1714, Mw 4.5.....39
Figure 4.7. The comparison of simulated Husid plots based on the path duration models from this study (top-left) and Herrmann (1985) (top-right) as well as recorded N-S (bottom-left) and E-W (bottom-right) at station 2201, Mw 4.5.....40
Figure 4.8. The comparison of simulated Husid plots based on the path duration models from this study (top-left) and Herrmann (1985) (top-right) as well as recorded N-S (bottom-left) and E-W (bottom-right) at station 2203, Mw 4.5.....41
Figure 4.9. The contour map of slip distribution (Konca et al, 2018), the region shown with dashed line is the slip area considered in the simulation. 44
Figure 4.10. Pseudo spectral accelerations and residuals of geometric mean of horizontal PSAs at station 1701, BJ97 – top, K18 – bottom. 49
Figure 4.11. Pseudo spectral accelerations and residuals of geometric mean of horizontal PSAs at station 1710, BJ97 – top, K18 – bottom. 50
Figure 4.12. Pseudo spectral accelerations and residuals of geometric mean of horizontal PSAs at station 1711, BJ97 – top, K18 – bottom. 51
Figure 4.13. Pseudo spectral accelerations and residuals of geometric mean of horizontal PSAs at station 1713, BJ97 – top, K18 – bottom. 52
Figure 4.14. Pseudo spectral accelerations and residuals of geometric mean of horizontal PSAs at station 1714, BJ97 – top, K18 – bottom. 53
Figure 4.15. Recorded and simulated acceleration time histories at stations 1701, 1710, 1711, 1713, and 1714 – based on BJ97. 54

Figure 4.16. Recorded and simulated acceleration time histories at stations 1701, 1710, 1711, 1713, and 1714 – based on K18. 55
Figure 4.17. Recorded and simulated velocity time histories at stations 1701, 1710, 1711, 1713, and 1714 – based on BJ97. 56
Figure 4.18. Recorded and simulated velocity time histories at stations 1701, 1710, 1711, 1713, and 1714 – based on K18. 57
Figure 5.1. Pseudo spectral accelerations at the 1915 Çanakkale Bridge, Side Span Pier, Asia (left), and Europe (right), respectively. 61
Figure 5.2. Simulated acceleration and velocity time histories at the 1915 Çanakkale Bridge, Side Span Pier, Asia (left), and Europe (right), respectively. 62

LIST OF TABLES

Table 3.1. List of Earthquakes Used in This Study. 15
Table 3.2. The comparison of significant duration results based on different databases for the same event, and station in order to check the accuracy of calculations. 17
Table 3.3. The comparison of corner frequency values for the same seismic event. 18
Table 3.4. Corner frequency values of all seismic events before the process of elimination, AFAD-TADAS. 19
Table 3.5. Data intensities based on each magnitude bins. 25
Table 3.6. Path duration (D_P) vs closest distance to the rupture (R_{RUP}) based on magnitudes. 25
Table 3.7. Coefficients of path duration (Dp) model used in this study. 26
Table 3.8. Significant duration ratios. 28
Table 4.1. Earthquake information of two different simulated seismic events. 31
Table 4.2. Geometrical spreading function used in this study, Akıncı et al. (2006). 33
Table 4.3. Comparison between simulated effective significant duration (D'_{95}) values for each station, Mw 4.5. 41
Table 4.4. The relevant parameters of strong ground motion stations. 43
Table 4.5. Boundary of Fault Segment (before trimming). 43
Table 4.6. Boundary of Fault Segment (after trimming). 45
Table 4.7. Input parameters of the finite fault simulation. 46
Table 4.8. Minimum average residual, stress drop, and pulsing percentage values. 48
Table 4.9. Comparison between recorded and simulated peak ground acceleration values for each station. 58
Table 4.10. Comparison between recorded and simulated peak ground velocity values for each station. 58
Table 5.1. Minimum average residual, stress drop, and pulsing percentage values. 61
Table 5.2. Simulated peak ground acceleration and velocity values for side span piers. 62
Table A.1. Selected recordings, and their key characteristics. 69

LIST OF SYMBOLS

$A(t)$	Total seismic signal
a(t)	Acceleration time history
a_{rms}	Root mean-square acceleration
d(f)	Displacement spectra at the source
D_P	Path duration
D_T	Total duration
$D_{5\text{-}95}$	Significant duration
D'_{95}	Effective significant duration
f_c	Source spectrum corner frequency
H_i	Normalization factor for the *i*th subsource
I_a	Arias Intensity
I_o	Epicentral Intensity
M_w	Moment magnitude
M_o	Seismic moment
M_{oi}	Seismic moment of the *i*th subsource
N	The total number of subsources
R	Hypocentral distance
R_{RUP}	Closest distance to the rupture
$R_{\theta\Phi}$	Radiation pattern/the rms value of shear excitation
T_d	Faulting duration
T_i	Fraction of rise time
v(f)	Velocity spectra at the source
V_{s30}	Average of the shear-wave velocity of uppermost 30 m soil
$Y_i(t)$	The signal of the $_i$th subsource
β	Shear-wave velocity in geophysical engineering
Δt_i	Delay time of the sub-source
Δσ	Constant earthquake stress drop
ρ	Density
Kappa	Near surface attenuation parameter

SD	Stress drop
PP	Pulsing percentage

LIST OF ACRONYMS / ABBREVIATIONS

AFAD	The Turkish Disaster and Emergency Management Presidency
BBP	Broadband Platform
DWNM	Discrete Way Number Method
EXSIM	Stochastic Extended Simulation
FD	Finite Difference
FE	Finite Element
KOERI	Kandilli Observatory and Earthquake Research Institute
NAFZ	North Anatolian Fault Zone
NEHRP	National Earthquake Hazards Reduction Program
PEER	Pacific Earthquake Engineering Research Center
SMSIM	Stochastic-Method Simulation
SCEC	Southern California Earthquake Center
SoF	Style of faulting
RVT	Random Vibration Theory
SmS	S-wave reflections

1. INTRODUCTION

Stochastic methods are extensively utilized to simulate ground motions in the world especially for the areas where the recordings related to destructive seismic events are not present. Strong ground motion simulations with stochastic methods require detailed information on regional propagation path and site properties. Amplitude variation of the high frequency ground motion can be assessed through combination of various factors such as earthquake source functions, local site amplification, intrinsic attenuation and geometrical spreading factors. Duration of the high frequency strong ground motion, on the other hand, has a random behavior hidden in the phase spectrum and hence is difficult to quantify. For simplicity, duration has long been defined with a distance-dependent simple function in stochastic simulations. Total duration of the ground motion comprises source and path properties. Total duration comprises source and path properties. Path duration has been considered as multilinear functions of distance modelled with global earthquake ground motion recordings. Recent path duration models available in the literature are based on global (PEER-NGAWest2) or regional (such as NEAmerica, Japan) strong motion database, hence they represent either a global estimation or can be utilized only for certain regions. Turkey-specific path duration-distance function is absent in the scientific literature. Hence our motivation in this thesis is to fulfil this absence and propose a path duration-distance function utilizing the abundant strong motion database of Turkey.

In this study stochastic simulations are performed for two seismic events that occurred at Gökçeada Region in the North Aegean Region. The method of Motazedian and Atkinson (2005), "[22]" is adopted for the stochastic simulation. The first earthquake is Mw4.5 dated May 24, 2014 14:49:15. This event is one of the aftershocks of May 24, 2014 Mw6.9 Gökçeada Earthquake. The purpose of this small event simulation is to visualize the effect of path duration on simulated time series when using conventional (0.05R) and region-dependent (this study) path duration functions. For large magnitude events, source duration dominates the total duration of ground excitation and consequently path duration effect shall not be seen adequately. Hence such a validation may not be clearly seen with the simulation of the Mw.6.9 Gökçeada Earthquake. Therefore, a point source stochastic simulation is performed for validation purposes.

Second objective of this study is to investigate the effect of different site amplification functions on the simulation. May 24, 2014 Mw6.9 Gökçeada Earthquake simulation is done considering two sets of amplification functions with one from microtremor array measurements and the other from a generic soil sites.

Finally, the stochastic simulation of 2014 Mw 6.9 Gökçeada Earthquake at the side span piers of the 1915 Çanakkale Bridge shall be performed by using the regional path duration model obtained in this study.

2. LITERATURE SURVEY

This section is presented under two subsections "Path Duration Modelling", and "Stochastic Ground Motion Simulation.

2.1. Path Duration Modelling

When it comes to earthquake key parameters, strong ground shaking duration becomes more of an issue as it has an influence on damaging results. The duration of motion, which has various definitions, comes into existence the sum of source duration and path duration which is suggested by Herrmann (1985). The equation in question is a function of source, path and site parameters just as the rest of duration definitions obtained by several recent studies (Kempton and Stewart, 2006; Ghofrani and Atkinson, 2014) do. Since the total duration is contributed by source and path individually, Boore and Thompson (2014) which is followed in this study have adopted the formulation of Kempton and Stewart (2006) where duration is described as the so-called additive function of parameters mentioned above. The logic behind the preference of Kempton and Stewart (2006) is that the source and path effects are divided into different categories in stochastic methods. The path duration (D_P in sec.), which boosts as the distance increases, has been stated as a function of distance (R in km) from the source by Herrmann (1985) as $D_P=0.05R$. On a closer inspection, the terms of durations such as source, path, total durations, and significant duration alike are used in an attempt to carry out simulations. This simple formula which is intrinsic to calculation of stochastic simulation is extensively used in total duration estimation. Recent studies performed with abundant strong motion data as Atkinson and Boore (1995), Boore and Thompson (2014), on the other hand, reveal that the equation of Hermann underestimates the path duration. In addition, they proposed several linear segments for duration-distance relationships. These comparisons are presented in Chapter 3. Among them, Boore and Thompson (2014) study was performed with PEER-NGAWest2 strong motion database. This database includes very limited strong motion recordings from Turkey. Hence, the path duration function they have suggested represents a global estimation and is not region specific, i.e., Turkey-specific path duration-distance function is absent in the scientific literature.

2.2. Stochastic Ground Motion Simulation

Ground motion simulations are divided into two categories; those are deterministic and stochastic methods. Each method is subdivided into smaller sections. Point source modelling and finite-fault source modelling alike are the subsections of stochastic simulation methods as shown in Figure 2.1 below. Hybrid methods are composed of *deterministic methods* such as Finite Element (FE), Finite Difference (FD), and Discrete Way Number Method (DWNM), and *stochastic methods* such as Boore (1981).

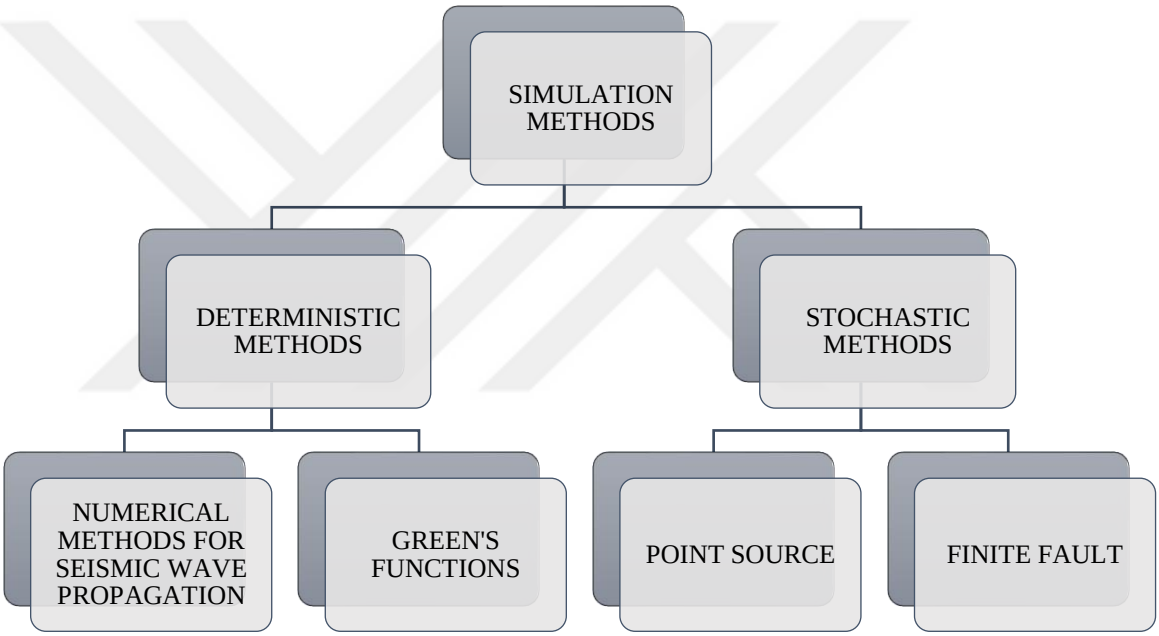

Figure 2.1. The flow chart of ground motion simulation methods.

Stochastic methods are extensively utilized in an attempt to simulate ground motions in the world especially for the areas where the recordings related to destructive seismic events are not present. Seismological models of the ground motion spectral amplitude and the engineering aspect are integrated by the Hanks and McGuire (HANKS, 1979; McGUIRE and HANKS, 1980; HANKS and McGUIRE, 1981), and the stochastic method used in this study is based on this concept.

Boore (1983) presented an elaborated study which is associated with the random vibration theory (RVT) in consideration of strong ground motion prediction. However, on closer inspection, Boore (1983) is not suitable for the distances farther than some focal depths from the fault (Herrmann, 1985), because in that case the duration of earthquake signals is governed by propagation through the earth instead of source duration.

Boore and Joyner (1984) put emphasis on the significance of source duration when it comes to the modelling response spectra. Boore and Joyner (1984) developed RVT in order to calculate the response spectra. Since the peak amplitude of ground velocity, acceleration, and seismograms are readily modeled, the RVT is regarded as by far general. In the words of Herrmann, R. B., the essence of this theory is that earthquake ground motion can be represented by a windowed, filtered stationary noise sequence, please refer to "[16]". As a fundamental information, the spectra, duration, and frequency content details can be enough for the characterization of peak ground motions.

Basic steps to be followed in stochastic simulation are as follows.

- Generate a normally distributed random signal having zero mean and unit variance.
- Window the signal by multiplying it by a window function.
- Calculate the Fourier transform of the windowed signal.
- Normalize the result so that the RMS amplitude spectrum equals unity
- Calculate the theoretical (deterministic) point-source spectrum.
- Multiply the above equation by the normalized random-signal complex spectrum to obtain the FAS.
- Calculate the inverse Fourier transform of the site spectrum to obtain the time history.

High-frequency strong ground motion duration is highly critical from the point of view of structural damage, where high frequency strong ground motion stands for the frequency range which is greater than or equal to 1 Hz. Meanwhile, it should be kept in mind that it is relatively complex to define strong ground motion features when the frequency range is greater than or equal to 2 Hz. The simulation of higher-frequency ground motions which are taken center stage in the studies of engineers closely correlated with the stochastic methods – besides, the ground motion data intrinsic to high-frequency

become more of an issue for seismologists since the mentioned data are being used to ascertain dynamic stress differences.

According to Boore, "stochastic method" represents the means of simulating ground motions whereas "stochastic model" of the ground motion means a specific application of the method. Thus, "the stochastic method" and "the stochastic model" terms differ from each other, and this difference becomes more of an issue due to the fact that the ground motions for different applications of the method might be extremely different.

One of the basic characteristics of the stochastic method is to divide the various parameters that have an influence on the ground motions (source, path, and site) into basic useful forms.

For the finite fault simulation methods, fault planes, whose dimensions are determined in accordance with seismic moment (M_o) of an earthquake are subdivided into sub-sources, and these sub-sources are considered as stochastic point sources separately. The calculation of sub-faults synthetics is performed utilizing a stochastic point source w-square spectrum proposed by Boore (1983). Shear wave amplitude spectrum of each sub-fault follows the Equation 2.1 and 2.2. Then contributions from each sub-fault with proper time delays are superposed at the location of the station. The duration of motion is derived from the summation of source duration and path duration. Time series which are associated with the sub-sources are gathered in the time domain. In the words of Atkinson et al. "[15]", the shear wave amplitude spectrum in the frequency domain is the product of filter functions representing the source, propagation and site effects.

$$Acc(M_0, R, f) = Source(M_0, f)Path(R, f)Site(f) \tag{2.1}$$

$$A_{jj}(f) = CM_{oij}H_{ij}\left(\frac{(2\Pi f)^2}{1+\left(\frac{f}{f_0 ij^{(t)}}\right)^2}\right)e^{\frac{-\Pi f R_{ij}}{Q(f)\beta}}G\left(R_{ij}\right)D(f)e^{-\Pi f \kappa_0} \tag{2.2}$$

where:

M_0 Seismic moment

f_0 Corner frequency

β Shear wave velocity in km/s in the vicinity of earthquake source

R_{ij} Epicentral distance

κ_0 A factor which is effective in amplification and propagation path effective

C Constant to account for average source radiation pattern for S waves, near surface amplification, the average crustal density and partitioning of the total shear wave energy into the horizontal components and calculated through Eq. 2.3.

$G(R_{ij})$ Geometrical spreading function

$Q(f)$ Quality factor that represents the intrinsic attenuation characteristics of the medium.

H_{ij} Scaling factor, Motazedian and Atkinson (2005), Eq. (9)

$D(f)$ Site amplification

$e^{-\Pi f \kappa_0}$ High cut filter to include the spectral decay at high frequencies described with the κ factor of soils, Anderson and Hough (1984)

$$C = R_{\theta\Phi}.\mathrm{FS}.\mathrm{PRTITN}/(4\pi\rho_S\beta_S^3 R_0) \tag{2.3}$$

where:

ρ Density

FS Amplification factor due to the free surface

PRTITN Reduction factor that accounts the for the partitioning of energy into two horizontal components (taken as $1/\sqrt{2}$)

$R_{\theta\Phi}$ Radiation pattern

The w-square model is the most widely adopted earthquake source spectrum model and in implementation of simulation methods. Where, the term used as "w-square model" in the literature which is obviously recognized as a constant-stress-drop model derived by KEITI AKI (1967) whose finding has been adopted consciously or not by means of many

seismologists so as to estimate ground motions for seismic events especially at high frequencies (f > 0.1 Hz), please refer to "[17]". In general, engineers are interested in the high frequency component of the ground motion in order to obtain the ground motions which are going to be applied to the structures with low to intermediate predominant periods so as to check whether they are resistant against seismic activities or not.

One of the most substantial characteristics of these estimations was that these were intrinsic to a described seismic moment which is a long-term effect of K., AKI in this field. To put it simply, his research regarding the determination of seismic moment of an earthquake for the first time was the basis of simulating ground motions method, "[17]". The model adopted in order to characterize the ground motion spectrum belongs to the Brune (1970) model. The characteristics of the Brune model adopted in random vibration theory are described below.

- The geometrical spreading of the spectra is R^{-1},
- The time domain duration is considered as $T = f_c^{-1}$,

where:

R: The hypocentral distance.

Only the source parameters do not represent the certain corner frequency-seismic moment scaling, but to Brune (1970, 1971) scaling, the source spectra are characterized by means of a single corner-frequency model that is based on the magnitude of an earthquake. They have developed an extraordinarily plain relation in consideration of peak acceleration which was well correlated with the earthquake recordings, and this work is broadened to the simulation of time series by considering the measures of ground motions such as response spectra by Boore, 1983.

Based on Boore's approach stochastic simulation techniques have been improved and newer parameters have been introduced such as dynamic corner frequency (Motazedian and Atkinson (2005)). This method will be explained in the following chapters.

3. AN INVESTIGATION OF REGIONAL PATH DURATION MODEL

This section of the study shall be addressed under three subsections that titled "Method", "Ground Motion Set", and "Analysis and Results".

3.1. Method

The strong-motion duration intensity measure is defined as significant-duration. The significant duration is closely associated with the structural damage and used in the geotechnical earthquake engineering applications. Significant-duration which shows a more stable behavior considers the characteristics of the entire accelerogram and defines a continuous time window motion may be considered as strong. The related duration parameter makes use of Husid plots in order to estimate time elapsed between the two definite levels of energy. Duration of motion for horizontal components which is based on the accumulation of energy in the accelerogram is the time interval between the points at which 5% and 95% of total energy (D_{95}). It is simply calculated from the Arias Intensity (Arias 1970). Arias Intensity is an indicator of a potential destructiveness in ground motions as the integral of the square of the acceleration-time history (Eq. 3.1). So, it is extensively used among engineers and researchers for the seismic slope stability, soil liquefaction, building damage, seismic performance of pile foundations and bridges which means this intensity measure becomes more of an issue especially in engineering applications. The equation of Arias intensity is given below.

$$I_a = \frac{\pi}{2g} \int_0^{\infty} a(t)^2 dt \tag{3.1}$$

where:

Ia represents the Arias intensity whereas *a(t)* stands for the acceleration time history.

In contrast to the conventional definition of Trifunac and Brady (1975), Boore and Thompson (2014) defined an effective measure of significant duration (D'_{95}) for use in the stochastic simulations. It is given in the Eq. 3.2. The philosophy behind this change is having the results inconsistent with the assumption of stochastic method due to the fact that the time at which the chunk of 0.05 is arrived at may be too early by reason of strong P-wave energy, and the time for the portion of 0.95 to be arrived at may be too late. The reason for the latter is either the late reaching longer period of energy or the existence of strong aftershocks.

$$D'_{95}=2.0(D_{80}-D_{20}) \tag{3.2}$$

where:

D'_{95} is effective measure of significant duration,
$D_{80}-D_{20}$ is the duration (based on the accumulation of energy in the accelerogram) differences between the points at which % 80 and 20% of total energy (a subjective choice of Boore and Thompson (2014)).

Total duration of the ground motion is composed of source duration (D_s) and path duration (D_p). In order to define the path duration, source duration should be removed from the total duration, i.e., $D_P= D'_{95}- D_s$. It is simply assumed that source duration is inversely proportional to corner frequency, i.e., $D_S=0.5/f_c$, please refer to "[1]". Hence corner frequency of each individual event is necessary for the calculation. The New Path Duration Model obtained by Boore, D. M. and Thompson, E. M. (2014) as a red line is presented in Figure 3.1 below.

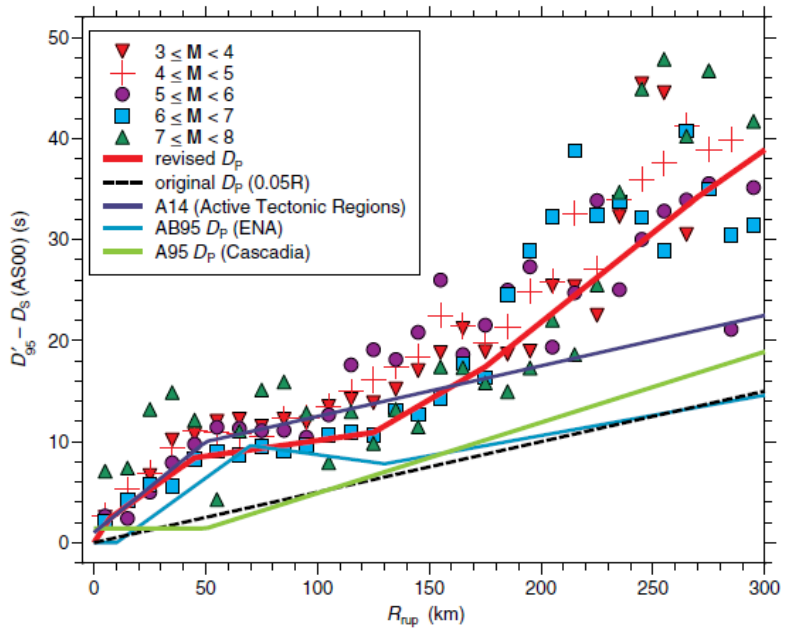

Figure 3.1. The median DP, in various magnitude and distance bins, revised DP belongs to Boore and Thompson (2014), AB95 (ENA) by Atkinson and Boore (1995), A14 by G. Atkinson, and A95 by Atkinson (1995).

A method proposed by Andrews "[2]" has been used so as to compute the corner frequency value, f_c. The equation is given below.

$$fc = \frac{1}{2\pi}\sqrt{\frac{S_{v2}}{S_{d2}}} \tag{3.3}$$

where:

S_{v2}, and S_{d2} are calculated by the following expressions:

$$S_{d2}=\int_0^{\infty} d^2\,(f)df \tag{3.4}$$

$$S_{v2}=\int_0^{\infty} v^2\,(f)df \tag{3.5}$$

where:

v(f) and d(f) are the velocity and the displacement spectra at the source, respectively.

3.2. Ground Motion Set

In the selection of ground motions, the earthquake data set which is intrinsic to Turkey is considered for the seismic events that occurred in between 1976 and 2017. The minimum and maximum epicenter coordinates of all earthquakes used in this study are 35.7°- 41.8° N latitude and 24.26° - 43.46° E longitude. Please refer to Table 3.1 for more detail.

The ground motion databases utilized in this study are Reference database for Seismic grOund-motion pRediction in Europe (RESORCE) by Akkar S. et al. "[24]", Pacific Earthquake Engineering Research Center (PEER NGA-West2) "[26]", and Turkish Accelerometric Database and Analysis System (AFAD-TADAS) "[25]", respectively. RESORCE database includes the recording of earthquakes up to Nov. 09, 2011 excluding 1999 Kocaeli Earthquake. Recordings of this event obtained from PEER-West2. All details intrinsic to the earthquakes, and stations such as moment magnitude (Mw), closest distance to the rupture (R_{RUP}), time-based average of the shear-wave velocity of uppermost 30 m soil (V_{s30}) are presented in Table A.1 within this document.

The recordings of earthquakes that occurred between 2010 and 2017 are provided from Prof. Tanırcan. Those raw recordings belong to AFAD-TADAS and contain only the earthquakes greater than 5.5-magnitude inclusive and are recorded by at least 3 stations. A total of 16 seismic events have been downloaded in the first place. The number of events has been decreased by 2 as there are no V_S30 values intrinsic to the stations within the scope of these two events. The next step was to eliminate 3 more earthquake recordings from the remaining 14 events as they contain just one station having V_S30 value. Furthermore, one more earthquake having 4 stations is removed from the calculation as the number of stations drop to 1 as a consequence of considering proper data. Consequently,

10 seismic events obtained have been utilized. A total of 6 events have been included in this study as it can be observed in Table A.1, and the remaining four seismic events have been used for the verification since they overlap the events which were already dealt with. Please refer to Table 3.4 for the events which are addressed at the beginning of the analyses.

In order not to neglect any events ranged from 2010 to 2017 inclusive, the relevant list is also checked through the Regional Earthquake-Tsunami Monitoring Center of Kandilli Observatory and Earthquake Research Institute (RETMC-KOERI) earthquake catalog by filtering the earthquakes Mw≥5.5. The earthquakes have been neglected under the latitude of 36° such as Crete in an attempt to eliminate the seismic events occurred in a location out of Anatolian Plate.

These two packages of databases coincide with each other from 2010 to 2011 inclusive in that RESORCE contains the events occurred between 1983 and 2011 whereas AFAD-TADAS incorporates the dataset from 2010 to 2017 inclusive. Therefore, these overlapping years are useful from the point of view of verification.

All magnitudes are in moment magnitude, Mw, for all seismic events, as is documented in this study. The overall criterion is to use motions having Mw values greater than 5.5 (inclusive), and (V_{s30}) values greater than 150 m/s. As for the number of stations, there are 38 seismic events recorded by at least 3 stations as well as 12 events having two stations. The earthquakes occurred between Aug. 1976, and Jul. 1983 have been omitted from the list as they have only one station recordings, so the catalogue automatically starts from Jul. 1983 and goes up to Jul. 2017. The final dataset comprises 477 two horizontal components recordings from 50 earthquakes having moment magnitudes of 5.5 to 7.4. The said earthquakes occurred on various faults such as strike-slip, normal, and reverse and at a depth of 0.0 to 46.6 km. Please refer to Table A.1 for more detail.

On closer inspection, this selection process has been made as three-pronged since all Turkish earthquake recordings are not available in above-mentioned website. For instance, 1999 Kocaeli Earthquake which is occurred in this time interval is not present in RESORCE Database. This being the case, the related missing recordings have been

obtained by means of AFAD-TADAS as well as PEER-West2. Once the determination of catalogue is made, all station recordings associated with missing recordings have been acquired as subsequent steps. There are 50 earthquakes (Table 3.1) and 477 stations related to these seismic events indicated dates within the catalogue in this range. All this information together with the station numbers which are already present in site are downloaded and documented. Please refer to Figure 3.2 for the number of recordings based on various ranges of Mw, V_{s30}, and R_{RUP} used in this study. Location of earthquakes and recorded stations are presented in Table 3.1 (based on AFAD-TADAS, "[25]") and Figure 3.3 below. In addition to Table 3.1, Table A.1 summarizes the selected recordings and their key characteristics such as magnitude, distance, style of faulting (SoF), approximate duration of motion so forth.

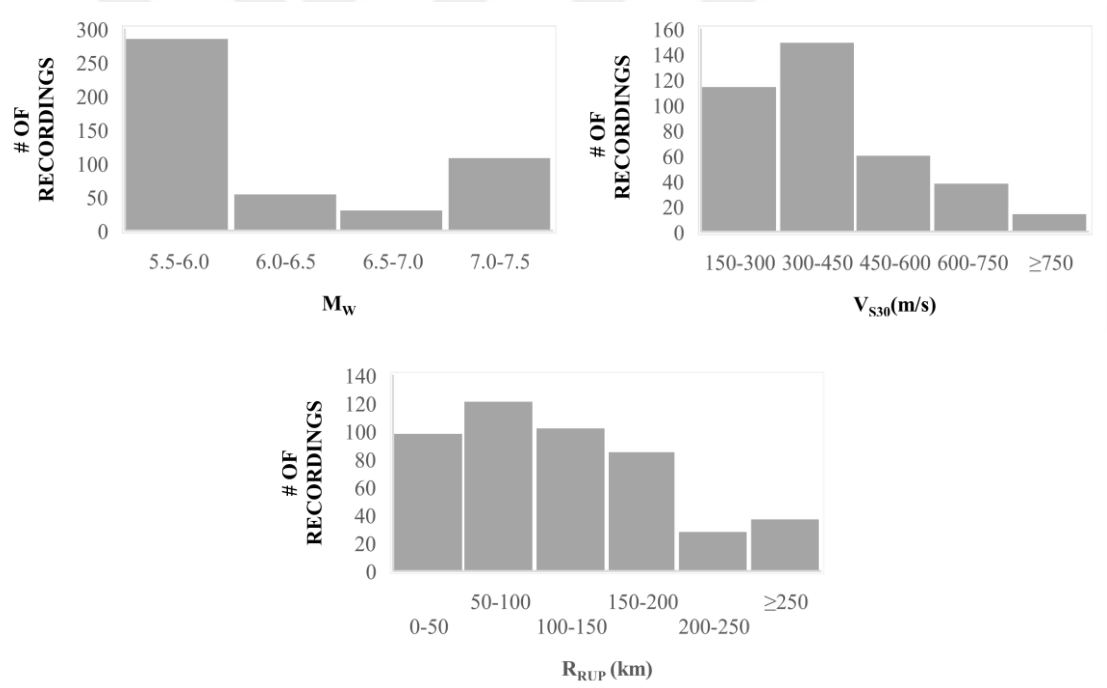

Figure 3.2. The number of recordings based on various ranges of M_w, V_{s30}, and R_{RUP}.

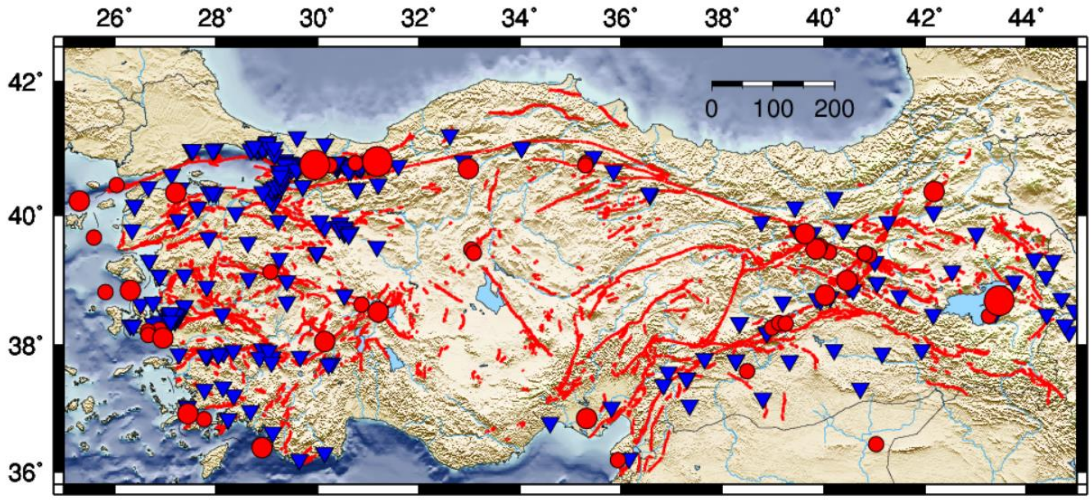

Figure 3.3. Location of earthquakes and strong motion stations.

Table 3.1. List of Earthquakes Used in This Study.

Set	Date	Time	Latitude (N)	Longitude (E)	Depth (km)	Mw
1	Jul. 05, 1983	12:01:27	40.3323	27.2101	6.9	6.1
2	Oct. 30, 1983	04:12:28	40.3522	42.1798	16.1	6.6
3	Mar. 13, 1992	17:18:39	39.7159	39.6292	22.6	6.7
4	Mar. 15, 1992	16:16:16	39.5278	39.929	28.5	5.9
5	Nov. 06, 1992	19:08:09	38.1091	26.956	17.2	6.0
6	Oct. 01, 1995	15:57:13	38.0561	30.1515	5.0	6.5
7	Dec. 05, 1995	18:49:32	39.4336	40.1083	25.5	5.8
8	Aug. 14, 1996	01:55:02	40.7461	35.2965	11.9	5.7
9	Aug. 14, 1996	02:59:41	40.7829	35.3061	2.7	5.6
10	Jan. 22, 1997	17:57:19	36.1852	35.9419	45.4	5.7
11	Nov. 14, 1997	21:38:49	38.8243	25.8212	2.3	5.9
12	Jun. 27, 1998	13:55:52	36.8451	35.325	46.6	6.3
13	Aug. 17, 1999	00:01:39	40.756	29.955	17.0	7.4
14	Sep. 13, 1999	11:55:30	40.75	30.079	10.4	5.8
15	Nov. 11, 1999	14:41:23	40.747	30.248	7.5	5.6
16	Nov. 12, 1999	16:57:21	40.806	31.187	10.4	7.1
17	Jun. 06, 2000	02:41:53	40.7	32.982	10.0	6.0
18	Aug. 23, 2000	13:41:28	40.782	30.76	10.5	5.5
19	Jul. 26, 2001	00:21:36	39.097	24.268	19.0	6.4

Set	Date	Time	Latitude (N)	Longitude (E)	Depth (km)	Mw
20	Feb. 03, 2002	07:11:28	38.52	31.202	22.1	6.5
21	Feb. 03, 2002	09:26:43	38.628	30.876	24.9	5.8
22	Jan. 27, 2003	05:26:23	39.4794	39.8481	10.0	6.0
23	Apr. 10, 2003	00:40:14	38.2466	26.8895	11.3	5.7
24	May 01, 2003	00:27:04	38.9987	40.4637	10.0	6.3
25	Jul. 06, 2003	19:10:43	40.4502	26.0413	17.1	5.7
26	Jul. 13, 2003	01:48:19	38.2716	38.9762	12.9	5.5
27	Aug. 04, 2004	03:01:07	36.8365	27.7679	10.0	5.5
28	Aug. 11, 2004	15:48:26	38.3403	39.2527	7.4	5.6
29	Jan. 23, 2005	22:36:06	35.7519	29.5737	12.1	5.8
30	Mar. 14, 2005	01:55:57	39.4186	40.8183	9.9	5.8
31	Mar. 23, 2005	21:44:52	39.4164	40.8094	12.0	5.6
32	Jun. 06, 2005	07:41:30	39.3888	40.9038	10.5	5.7
33	Oct. 17, 2005	05:45:18	38.1921	26.677	20.5	5.5
34	Oct. 17, 2005	09:46:56	38.2202	26.6586	18.6	5.8
35	Oct. 20, 2005	21:40:02	38.1535	26.6708	15.4	5.8
36	Feb. 09, 2007	02:22:57	38.343	39.119	8.4	5.5
37	Feb. 21, 2007	11:05:27	36.44	41.04	10.0	5.7
38	Dec. 20, 2007	09:48:27	39.4208	33.0926	0.0	5.7
39	Dec. 26, 2007	23:47:09	39.4735	33.0453	0.0	5.6
40	Mar. 08, 2010	02:32:39	38.7752	40.0295	5.0	6.1
41	Mar. 08, 2010	07:47:44	38.7355	40.009	5.0	5.6
42	May 19, 2011	20:15:23	39.1328	29.082	24.46	5.9
43	Oct. 23, 2011	10:41:13	38.689	43.4657	19.02	7.1
44	Nov. 09, 2011	19:23:33	38.4472	43.2638	6.09	5.6
45	Jun. 10, 2012	12:44:15	36.3858	28.9153	6.82	6.1
46	Jan. 08, 2013	14:16:04	39.6553	25.5912	26.83	5.8
47	May 24, 2014	09:25:00	40.2108	25.3073	25.02	6.5
48	Mar. 02, 2017	11:07:25	37.5955	38.4866	9.76	5.5
49	Jun. 12, 2017	12:28:37	38.8488	26.3126	15.86	6.2
50	Jul. 20, 2017	22:31:10	36.9198	27.4435	19.44	6.6

3.3. Analysis & Results

In the first part of the analysis, D'_{95} of recordings are calculated through Eq. 3.1 and Eq. 3.2. To do that the acceleration database obtained from raw AFAD-TADAS are

visually inspected. Thus, the strong ground motion recordings which are inappropriate have been eliminated. An example as to such plots is presented in Figure 3.4.

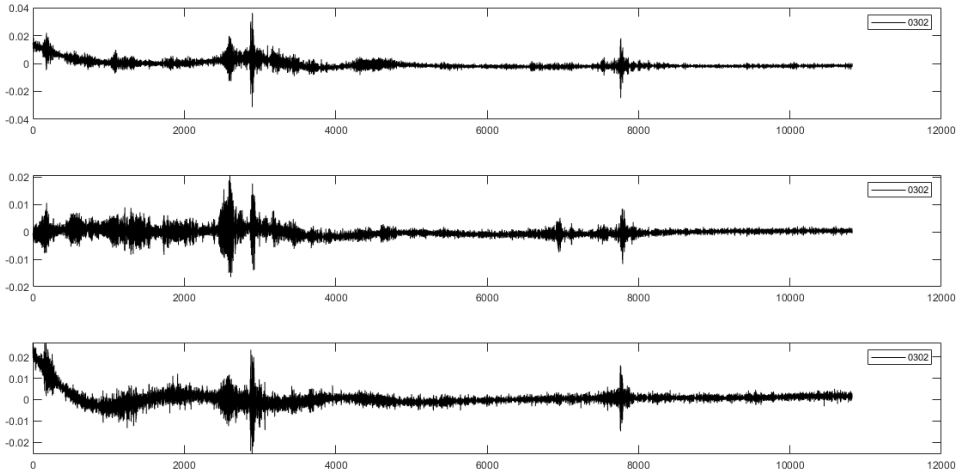

Figure 3.4. An example of recordings from May 19, 2011 Kütahya-Simav Earthquake, station 0302. It is removed from the calculation as it includes no proper data.

Baseline correction has been applied to data. This process enables us to focus our analysis on the fluctuations in data about the trend.

In an attempt to verify accuracy of the calculation of significant duration values, the related values which are already available in PEERWest2 that contain modest recordings associated with the earthquakes occurred in Turkey have been compared with the results. For instance, a spot check is done on significant durations of two different databases to check the accuracy of our calculation considering Oct. 1, 1995 Dinar Earthquake at station 0105. The results are shown in Table 3.2 below.

Table 3.2. The comparison of significant duration results based on different databases for the same event, and station in order to check the accuracy of calculations.

Databases	Station	Effective significant duration, $D_{5\text{-}95}$
PEERNGAWEST2	0105/Denizli	62.4 sec
Resorce	0105/Denizli	64.0 sec

*Note that our calculation is based on Resorce Database.

In the second step, corner frequencies of earthquakes are calculated utilizing recorded stations and the arithmetic mean of all values for a single earthquake has been estimated. The stations with higher Vs30 values are used in calculations as much as possible. Where, stations having fc, equal to zero have been also removed completely from the list in order not to deviate the related value as the mean value is considered while estimating the corner frequency of an earthquake. Furthermore, it is compared with median values for each seismic event for the sake of correctness. The corner frequency values corresponding to each seismic event are presented for comparison in Figure 3.5. As expected, corner frequencies are inversely proportional to the moment magnitude of seismic events. Please refer to Figure 3.5 for the distribution of f_c vs. M_w.

Moreover, Simav, Bodrum, and Lesbos earthquakes are spot checked by "[3]" to examine the accuracy of estimation. For instance, the result of corner frequency regarding Simav Earthquake, and the value obtained by means of spectral inversion which is presented in paper "[3]" are shown in Table 3.3 below.

Table 3.3. The comparison of corner frequency values for the same seismic event.

	Corner frequency, fc
Simav Mainshock [3]	0.69 Hz
Simav Mainshock [our analysis]	0.41 Hz

The corner frequency, fc, for the Simav Earthquake dated on 2011-05-19 presented in "[3]" is 0.69 Hz. whereas the related value is found as 0.41 Hz in our calculation. After all these verifications, and spot checks, all key characteristics obtained via analysis have been tabulated. Please refer to Table A.1 that contains essential values related to events.

The figures associated with the f_c values, and minimum V_s30 value considered in the calculations are presented below.

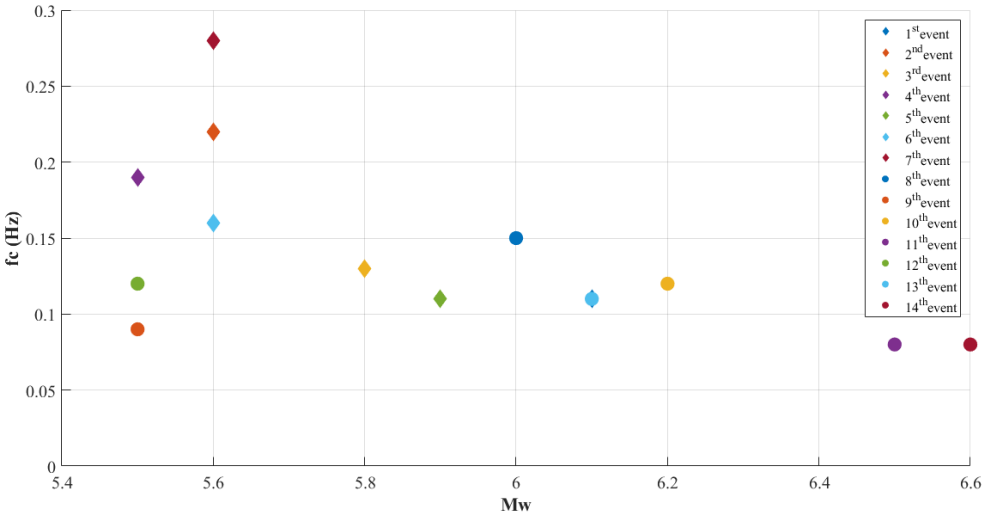

Figure 3.5. Corner frequency values corresponding to each seismic event.

Table 3.4. Corner frequency values of all seismic events before the process of elimination, AFAD-TADAS.

Name	Date	Time	M_w	f_c, mean
1st event	2010-03-08	02:32:29	6.1	0.11
2nd event	2010-03-08	07:47:37	5.6	0.22
3rd event	2011-05-19	20:15:22	5.8	0.13
4th event	2011-09-22	03:22:42	5.5	0.19
5th event	2011-10-23	20:45:42	5.9	0.11
6th event	2011-10-25	14:55:08	5.6	0.16
7th event	2011-11-09	19:23:33	5.6	0.28
8th event	2012-06-10	12:44:15	6.1	0.15
9th event	2012-06-14	05:52:51	5.2	0.09
10th event	2013-01-08	14:16:04	6.2	0.12
11th event	2014-05-24	09:25:00	6.5	0.08
12th event	2017-03-02	11:07:25	5.5	0.12
13th event	2017-06-12	12:28:37	6.1	0.11
14th event	2017-07-20	22:31:10	6.6	0.08

Figure 3.6 shows the D'_{95} corresponding to R_{RUP} for each seismic event range in terms of M_w. Figure 3.7, Figure 3.8, and Figure 3.9 are obtained as the results of calculations which are going to be utilized as the stochastic simulation input data.

The method adopted by Boore and Thompson, please refer to “[1]”, is employed for the significant duration calculation. The explanation as to which equation to use is given in

detail below. The adoption of Boore and Thompson method is assessed by way of comparison with the new path duration model which is presented in "[1]". The plots associated with the effective significant duration (D'_{95}) versus closest distance to the rupture (R_{RUP}), and the difference between effective significant duration and source duration versus closest distance to rupture are presented below. So as to compare the results, the following plots have been obtained by using the medians, in various magnitude and distance bins in accordance with the equation suggested in "[1]". Please refer to Figure 3.6 and 3.7. Where, considering the amount of data, the distance bins, and magnitude bins are determined as 10 km, and 0.5, respectively. Furthermore, the closest distance to the rupture, R_{RUP}, is restricted to 300 km.

The missing rupture distance R_{RUP} information of the stations has been calculated based on Kaklamanos et al. (2011), Boore and Atkinson (2007), and Wells and Coppersmith (1994). Strike, dip, and rake values of those 14 earthquakes have been obtained via www.globalcmt.org, and these values have been compared with results incorporated in "[6, 8, 9]" for the sake of accuracy.

When it comes to the comparison between RESORCE and AFAD as regards corner frequencies, a simple data analysis which was applied in Matlab to RESORCE data shall be also performed in AFAD so as to compare the differences between RESORCE and AFAD results.

f_C calculation phase of analysis has produced some different results. Therefore, acceleration data is plotted for each recording, and the arrivals of P wave and S wave (T_P and T_S) are read. Finally, the only data included in time package from 2-3 sec in advance of P-onset to the end of S-wave energy package window has been selected to run. Once this data is plotted, it is tapered at the final part. In other words, it is tapered as cosine to the data from beginning of T_P-F_S to (T_P-F_S) + 3 x (T_S-T_P).

A 4th order *Lowpass Butterworth Filter design* is used with the frequencies between 0.05 Hz, and 20 Hz for the data above-mentioned. The scripts including necessary functions in this analysis are provided by Prof. Tanırcan.

Figure 3.6 to 3.8 have been presented after the completion of analysis subsequent to obtaining input. As it can be seen clearly in Figure 3.9, the relation suggested by Boore and Thompson generates the lower bound of our data results.

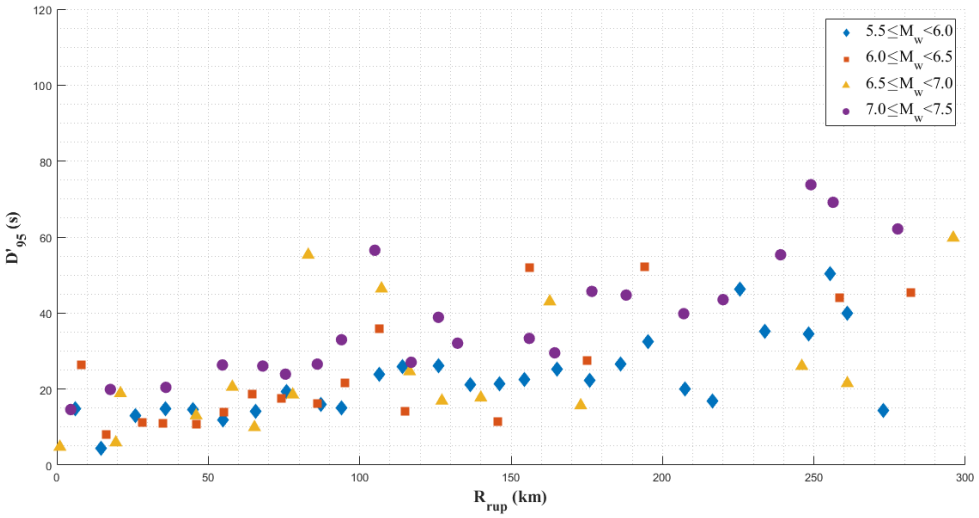

Figure 3.6. Effective significant duration (D'_{95}) versus closest distance to rupture (R_{RUP}).

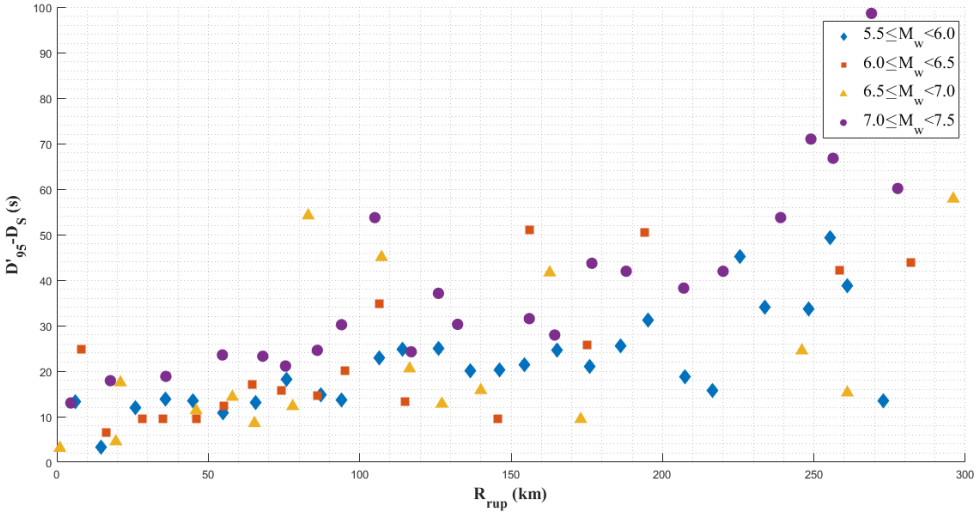

Figure 3.7. The difference between effective significant duration (D'_{95}), and source duration (D_S) versus closest distance to rupture (R_{RUP}).

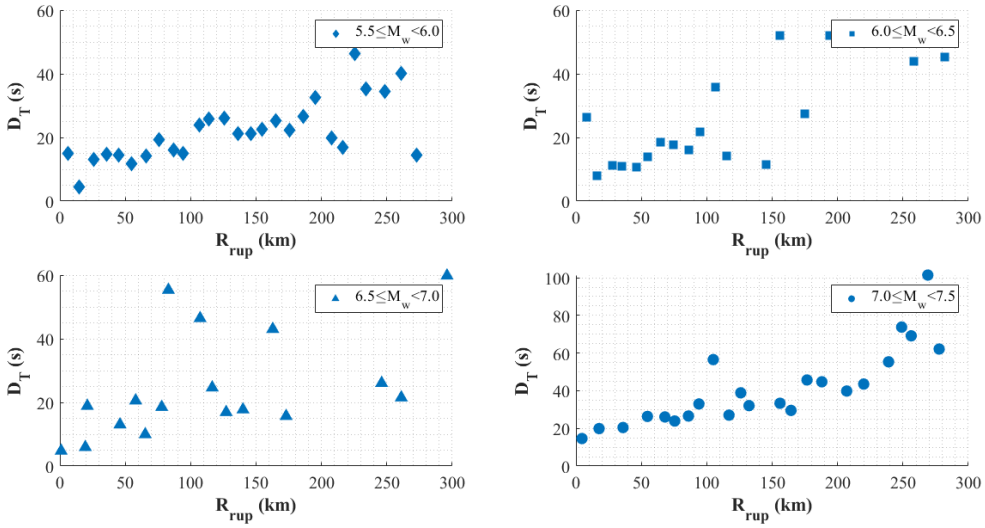

Figure 3.8. Total duration (D_T) versus closest distance to rupture (R_{RUP}) for the different seismic events with magnitudes ranging from 5.5 to 7.5.

Furthermore, the graphs incorporating basic linear fits associated with the figures are shown above. The difference between D_P=0.05R (Herrmann 1985) and fittings obtained in this study has been presented in the following figures. Please refer to Figure 3.9 to 3.12.

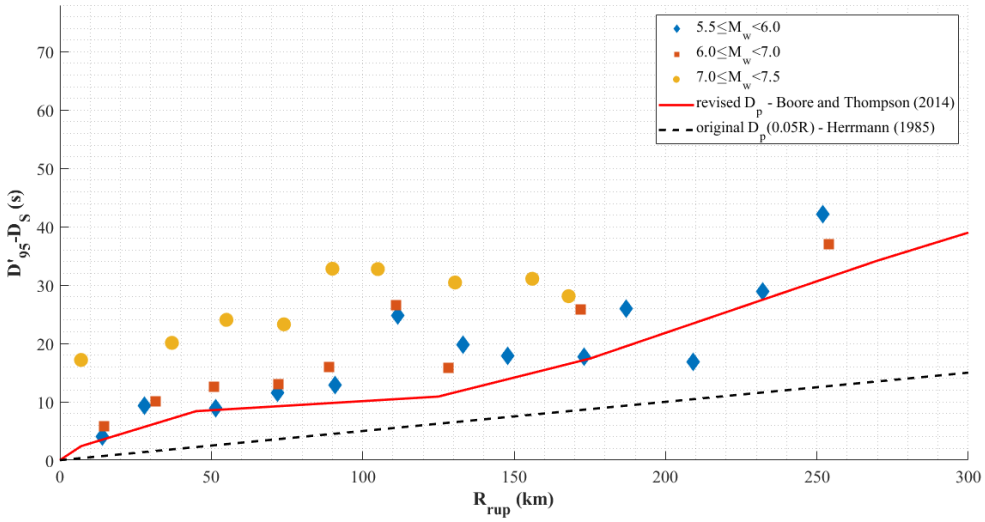

Figure 3.9. The difference between effective significant duration (D'_{95}) and source duration (D_S) versus closest distance to rupture (R_{RUP}).

The segmented lines are fitted by following the Boore and Thompson model. When it comes to followings, segmented linear fittings involved in station recordings are presented individually based on each magnitude bin. In addition to this, a segmented linear fitting together with the arithmetic mean of four magnitude groups, and the plots based on two groups (6.0>Mw≥5.5 and Mw≥7.0) having maximum dataset are shown below, respectively.

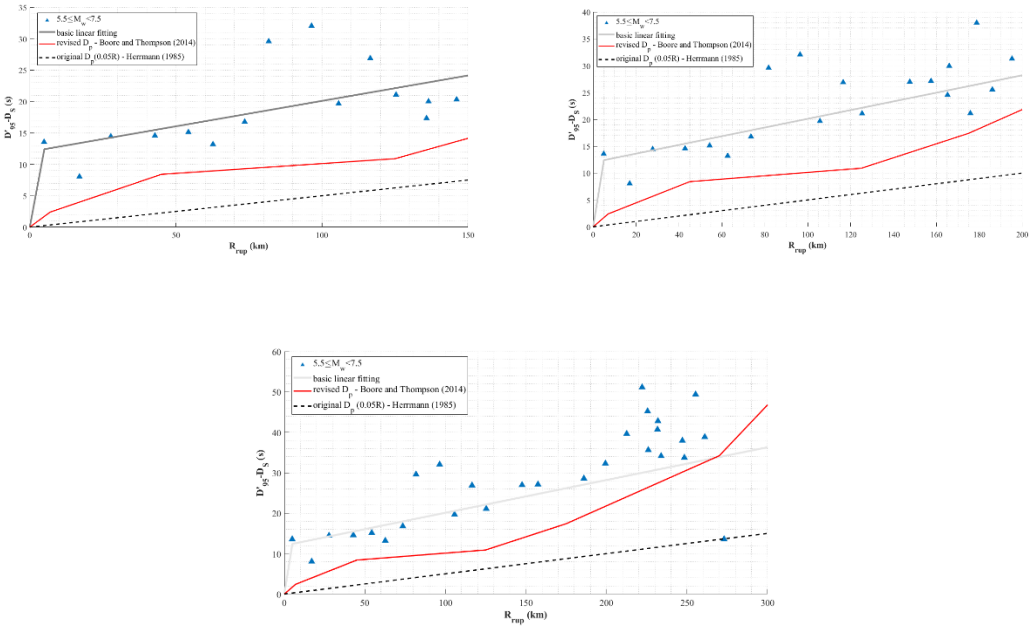

Figure 3.10. Segmented linear fittings involved in station recordings presented individually based on each magnitude bin up to 150 km, 200 km, and 300 km.

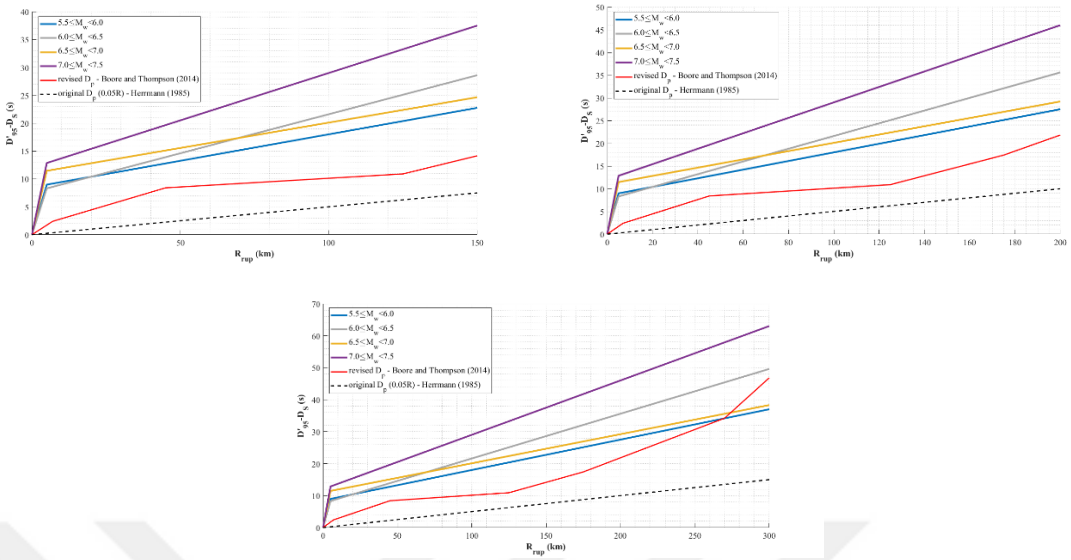

Figure 3.11. Segmented linear fitting together with the arithmetic mean of four magnitude groups up to 150 km, 200 km, and 300 km.

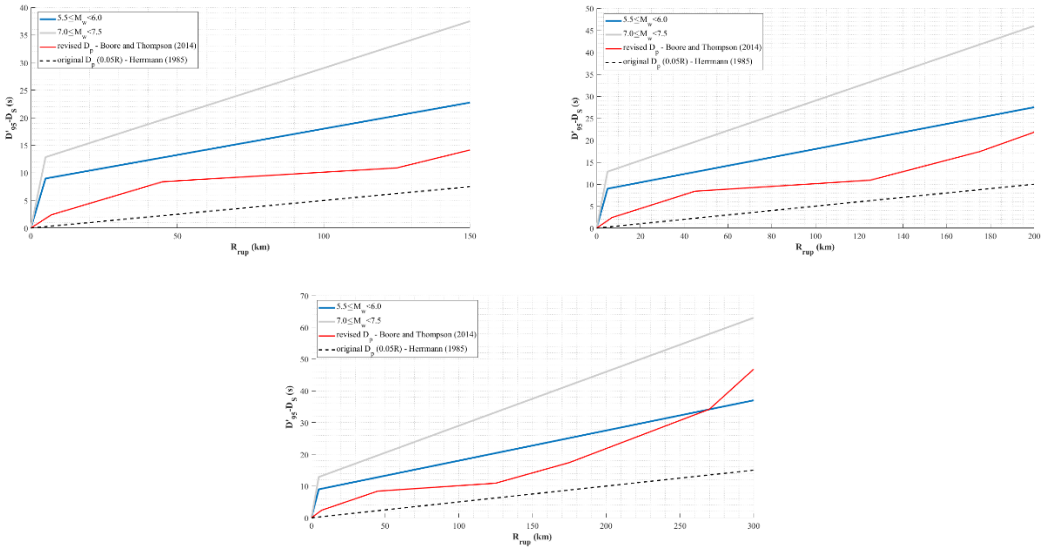

Figure 3.12. The plots are based on two groups (6.0>Mw≥5.5 and Mw≥7.0) having maximum dataset up to 150 km, 200 km, and 300 km.

Where, 20 km-distance bins are used. Moreover, the recordings of less than four are ignored. In other words, one in between M_w 6.0 and 7.0, 3 recordings over 7.0 (including) have been neglected as a consequence of this elimination.

The main object of these plots is to find best fitting in accordance with our data. These figures starting from zero plotted for both R_{RUP} and path duration results prove that a linear fit for our dataset should not be used for all along R_{RUP} (cut off 300 km). The percentage of data intensities are summarized below.

Table 3.5. Data intensities based on each magnitude bins.

Magnitude, M_w	Percentage, %
$5.5 \leq M_w < 6.0$	35
$6.0 \leq M_w < 6.5$	15
$6.5 \leq M_w < 7.0$	20
$7.0 \leq M_w < 7.5$	30

Table 3.6. Path duration (D_P) vs closest distance to the rupture (R_{RUP}) based on magnitudes.

7≤Mw>7.5		5.5≤Mw>7.0		Boore and Thompson	
D_P	R_{RUP}	R_{RUP}	D_P	R_{RUP}	D_P
14.21	7.61	14.25	4.946	7	2.4
14.96	33.00	29.75	9.672	45	8.4
24.05	55.00	51.25	10.7	125	10.9
20.69	67.35	72.03	12.34	175	17.4
32.81	90.00	90	14.42	270	34.2
29.13	130.00	111.3	25.66	-	-
31.09	155.50	130.7	17.82	-	-
26.21	167.00	160	21.79	-	-
71.00	256.94	213.5	27.42	-	-
73.48	275.00	252	42.11	-	-

Path duration function found by using the seismic events in Turkey is used as is obtained in this study, and the corresponding coefficients are presented in Table 3.7 below.

Table 3.7. Coefficients of path duration (Dp) model used in this study.

Rrup (km)	0.0	29.75	90.0	111.0	130.0	213.0	252.0	Slope of last segment
Dp (s)	0.0	9.6	14.0	25.0	17.8	27.4	42.1	0.379

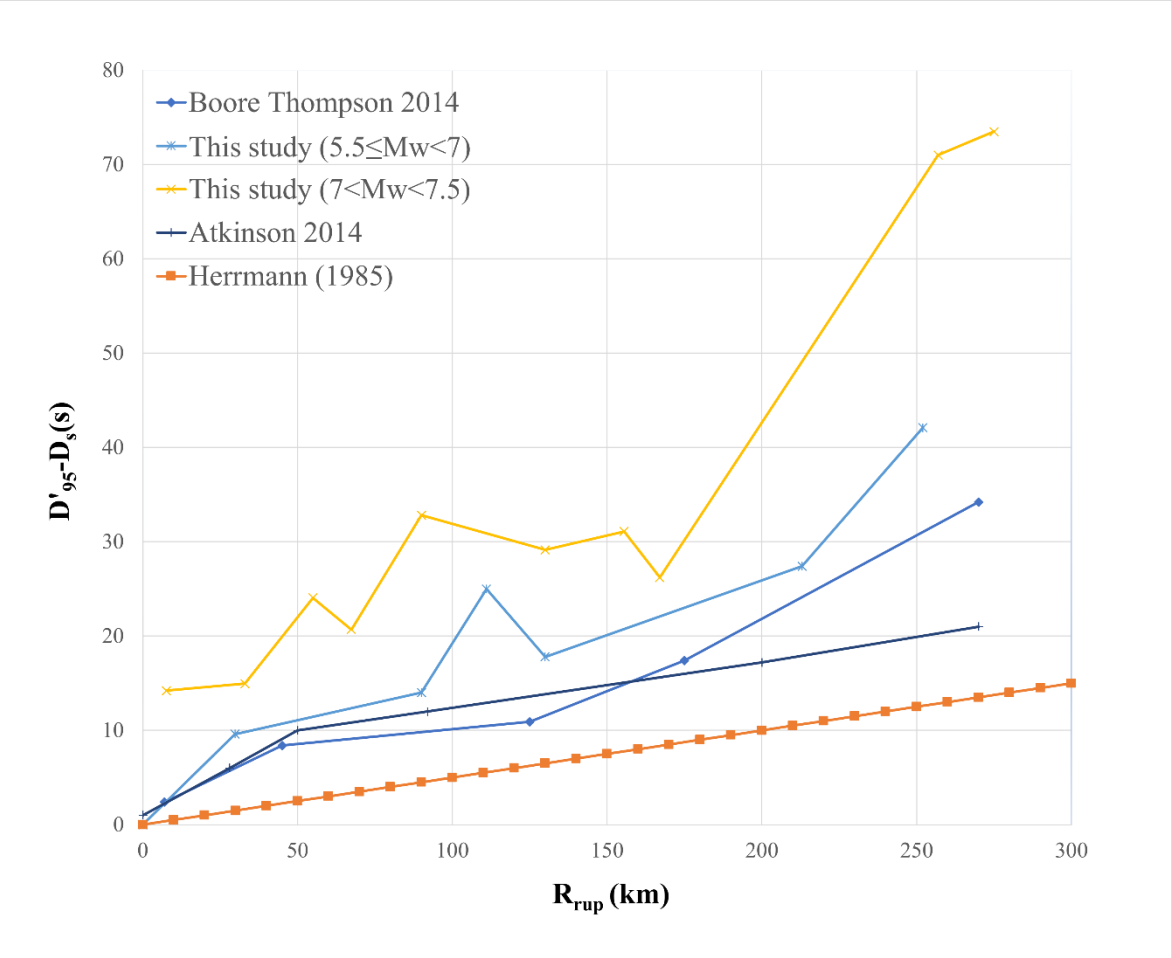

Figure 3.13. Path duration function from events in Turkey following Boore and Thompson (2014), based on two groups (5.5>Mw≥7.0 and Mw≥7.0).

Where, the distance bins are determined according to data intensities. Please note that the distance value of 111 km corresponding to 25 sec-duration shown in Figure 3.13 accounts for that S waves coincides with the intervals having greater S-wave reflections (SmS) from the Mohorovicic discontinuity (Moho). A similar behavior is observed in Figure 3, "[10]" which is also included in this document in Figure 3.15. Therefore, it is possible to see SmS that may generate larger amplitudes following the direct S. When this

being the case, $D_{5\text{-}95}$ / 2 x (D80-D20) may come out less than 2. For this reason, $D_{5\text{-}95}$ vs 2x(D80-D20) distributions of 5.5≤Mw≤7 and Mw>7 in different distances have been addressed separately together with dataset in an attempt to make sure that the estimation of 2x(D80-D20) used by Boore and Thompson is correct.

The ratio of $D_{5\text{-}95}$ to 2 x (D_{80}-D_{20}) with corresponding distances are tabulated. It can be observed whether the results are around or different from 2. Please refer to Table 3.8. The plot associated with the medians of D'_{95}, $D_{5\text{-}95}$ vs R_{RUP} values in various magnitude and distance bins is presented in Figure 3.14 below.

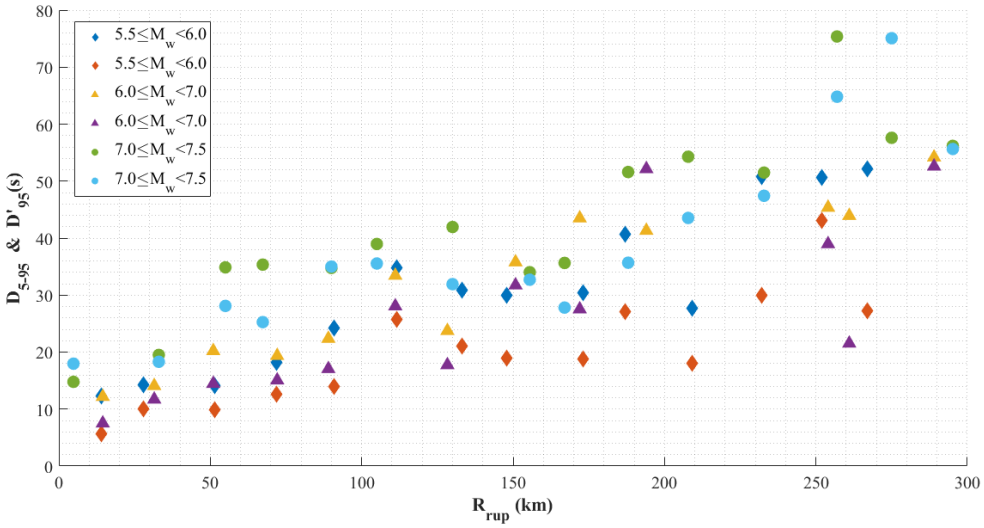

Figure 3.14. The medians of D'_{95}, $D_{5\text{-}95}$ vs R_{RUP} values in various magnitude and distance bins.

Please note that the greater significant duration values represent the effective significant duration.

Table 3.8. Significant duration ratios.

5.5≤Mw<6.0		6.0≤Mw<7.0		7.0≤Mw<7.5	
$D_{5\text{-}95}/D'_{95}$	R_{RUP}	$D_{5\text{-}95}/D'_{95}$	R_{RUP}	$D_{5\text{-}95}/D'_{95}$	R_{RUP}
2.20	14	1.62	14.5	0.82	4.83
1.41	28	1.20	31.5	1.07	33
1.42	51.5	1.40	51.0	1.24	55
1.44	72	1.29	72.1	1.40	67.4
1.74	91	1.31	89.0	0.99	90
1.35	111.5	1.19	111.1	1.10	105
1.47	133	1.34	128.3	1.31	130
1.58	148	1.13	150.8	1.04	155.5
1.62	173	1.58	172.0	1.28	167
1.50	187	0.79	194.0	1.45	188
1.54	209	1.16	254.0	1.25	207.8
1.70	232	2.04	261.0	1.09	232.9
1.17	252	1.03	289.0	1.16	256.9
1.91	267	-	-	0.77	275
-	-	-	-	1.01	295.2

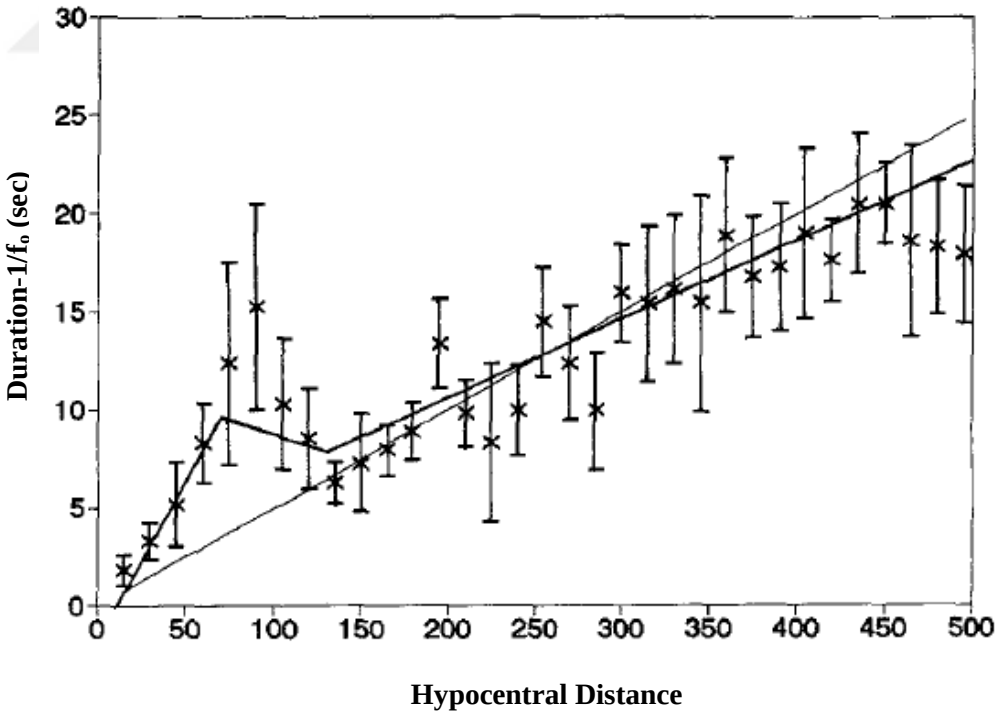

Figure 3.15. Mean of the rms duration minus the source duration, averaged by 15-km distance bins, Atkinson, G.M., and Boore, D.M. (1995).

Please note that Figure 3.1 is also presented in order to document that there is no negative slope in transition zone (A14) in contrast to Figure 3.13 in favor of simplification.

At this point, two results which are already obtained in the papers published by Atkinson, G.M., and Boore D.M. “[10]” and Boore D.M. and Eric M. Thompson “[1]”, respectively, have been acquired.

In the first model the distance dependence of duration is modeled as trilinear, using the transition distances 70 and 1.5 I 130 km for consistency with the attenuation model, and negative slope in the transition zone has been founded by Atkinson, G.M., and Boore D.M. “[10]”. In a similar vein, we have also found a negative slope between the distances of 110-130 km for 5.5<M<8. Please see Figure 3.13.

In the second reference, Boore D.M. and Eric M. Thompson “[10]”, the proposal of Atkinson2014 is referred. The proposal consists of 2 segments as a positive slope linear function. It is expected that Atkinson2014 and our equation are quite similar as we have dealt with active crustal events of Turkey. Nonetheless, it is obvious that there is no negative trend in Atkinson 2014, i.e., Moho bounce effects do not appear at any distance ranges in the related paper. However, there is a catch; a piece with negative slope in transition has been excluded which means the actual function is trilinear just as our function is. In other words, it has been eliminated for the sake of simplification, and only two segments have been used in Atkinson (2014), so it can be concluded that the actual function is trilinear and there is a piece of negative slope in transition in many cases. Please note that this is verified by means of personal communication with Gail M. Atkinson.

4. STOCHASTIC SIMULATIONS OF STRONG GROUND MOTIONS

In this study stochastic simulations are performed for two seismic events that occurred at Gökçeada Region in the North Aegean Region. The first one is Mw4.5 dated May 24, 2014 14:49:15. This event is one of the aftershocks of May 24, 2014 Mw6.9 Gökçeada Earthquake. The purpose of this small event simulation is to visualize the effect of path duration on simulated time series when using conventional (0.05R) and region-dependent (this study) path duration functions. For large magnitude events, source duration dominates the total duration of ground excitation and consequently path duration effect shall not be seen adequately. Hence such a validation may not be clearly seen with the simulation of the Mw.6.9 Gökçeada Earthquake. Therefore, a point source stochastic simulation is performed for validation purposes. Then May 24, 2014 Mw6.9 Gökçeada Earthquake simulation is done considering a finite fault model. Earthquake locations are shown in Figure 4.1 and Table 4.1, respectively.

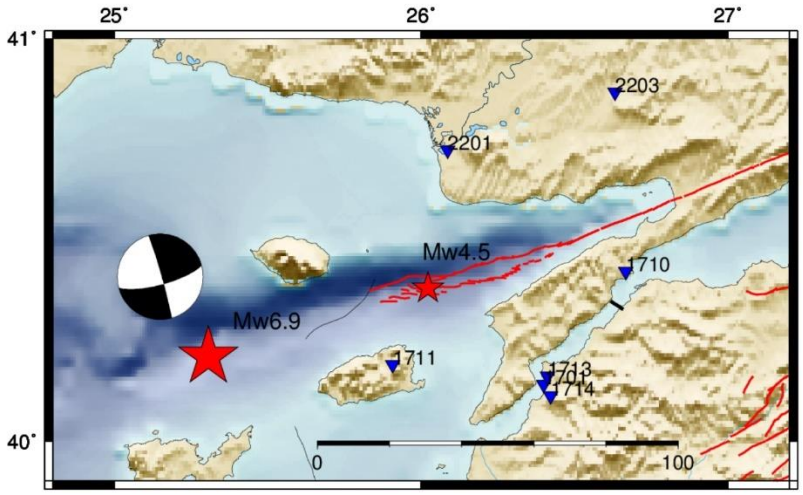

Figure 4.1. Epicenter of two seismic events (red stars), focal mechanism (beachball), active faults (red lines), strong motion recording stations (downward-pointing blue triangles).

Table 4.1. Earthquake information of two different simulated seismic events.

Date	Time	Latitude (N)	Longitude (E)	Mw	Depth (km)	Strike/Dip/Rake (°)	Source
May 24, 2014	12:01:27	40.2108	25.3073	6.9	25.02	73/85/-177	Konca et al. (2018)
May 24, 2014	14:49:15	40.3816	26.0231	4.5	11.87	283/55/-62	AFAD-TADAS

4.1. The Stochastic Simulation Method

In this study, a stochastic simulation method; EXSIM (Extended Simulation) is utilized for the simulation. The method was proposed by Motazedian and Atkinson (2005) "[22]". Boore (2009) and Assatourians and Atkinson (2012) improved the original method. The method is also present on the SCEC (Southern California Earthquake Center) Broadband Platform for the sake of implementation and verification. Improved methods introduce 2 parameters, dynamic corner frequency, fcij(t), and pulsing area percentage parameters in that the dynamic frequency regulates the radiated energy of subfaults whereas pulsing area percentage parameters represent amount of fault area that slips in an active way at any moment in the rupture, and so the contribution to dynamic corner frequency, which is expressed as a function of time in Eq. 4.1 below, is made.

$$f_{cij}(t) = 4.9\,E + 6\,N_R(t)^{-1/3} N^{1/3}\,\beta\,(\Delta\sigma/M_o\,)^{1/3} \tag{4.1}$$

where:

$f_{cij}(t)$ Dynamic corner frequency of an ijth subfault

N The total number of subfaults in the model

N_R The cumulative number of ruptured subfaults at time t

*Please note that i=1:nw, j=1:nl, and nl & nw represents the number of subfaults along the length and width of the main fault, respectively.

In accordance with dynamic frequency approach, a scaling factor of H_{ij}, which is given in Eq. 4.2 below, shall be applied in an attempt to preserve the whole energy of the simulation at high frequencies.

$$H_{ij} = N\Sigma\{f^2/[1 + (f/fc)^2]\}/\Sigma\{f^2/[1 + (f/fcij)^2]\}^{1/2} \quad (4.2)$$

It should be noted that EXSIM objects to assess finite-fault effects in consideration of geometric point of view. In other words, it does not attempt to elaborate on the physics of rupture propagation.

Once a filter on white noise that is time series generated by the software is applied, the Fourier amplitude spectrum of white noise (random signal) in question sets the spectrum in accordance with the seismic moment that is inserted. This method is called as point source stochastic method. This method, which is widely being used in simulations, was suggested by David Boore in 1993. The superposition of time histories is generated stochastically on the surface for each small fault plane in order to obtain the actual earthquake recording.

4.1.1. Number of Trials

Actually, a random noise sample is generated in Boore 1981 technique. Once we take and filter that white noise in the frequency domain, that matches up to the moment magnitude of an earthquake that we target. This approach is called as the stochastic simulation method which is adopted in EXSIM as well. One seed number is given in an attempt to generate a random white noise, but it can produce a different time series every time as it is randomly generated. This is why it does not make sense to develop one time history. Number of trials shall be entered as 10 which is considered here as an optimum choice. Please note that entering the number of trials as much more value like 100 shall generate smooth waveforms which is not ideal. On the other hand, doing only one run for each simulation will not make good sense as it would not represent the optimum range.

4.1.2. Residual Model

The comparison between simulated and recorded results is based on pseudo spectral accelerations. Residuals of spectral accelerations are calculated at 22 discrete periods (from 0.02 to 2.0 sec.) as per the following equation which is applied for all stations so as to find the smallest residual value.

Please note that EXSIM does not make calculations of both N-S and E-W components, it only estimates the geomean component.

$$|residual| = \frac{1}{N_{sta}N_T} \sum_{1}^{N_{sta}N_T} |log10(PSA_{rec})/(log10(PSA_{syn})| \quad (4.3)$$

where:

$|residual|$: the average absolute residual

PSA_{rec} : residuals of recorded

PSA_{syn} : residuals of simulated

N_T : the number of spectral periods

N_{sta} : the number of stations

4.2. Propagation Path Parameters

High-Frequency ground motion model parameters that represent the source characteristics such as geometrical spreading and anelastic attenuation are taken in accordance with Akıncı et al. (2006), "[19]". Geometrical spreading function used in this study is presented in Table 4.2 below.

Table 4.2. Geometrical spreading function used in this study, Akıncı et al. (2006).

Range	R≤30	30 < R≤ 60 km	60 < R ≤ 100 km	R > 100 km
Geometrical spreading	R^{-1}	$R^{-0.6}$	$R^{-0.9}$	$R^{-0.1}$

Quality factor, Q(f) is adopted in accordance with Akıncı et al. (2006) as it is specified in Table 4.7, and in Eq. 4.4 as well.

$$Q(f)=180\ (f\ /1.0)^{0.45} \tag{4.4}$$

Path duration function found by using the seismic events in Turkey is used in simulation as it is obtained in this study. Please refer to Chapter 3, Table 3.7 for the corresponding coefficients.

4.3. Site Parameters

Karagöz et al. (2018) "[13]", performed a detailed analysis on the site amplification factors at the AFAD-TADAS stations at Çanakkale and Gökçeada Regions. Amplification spectra of stations coded as 1701, 1710, 1711, 1713 and 1714 are given in Figure 4.2. Please note that amplification factors have been divided into two as free surface effect is already defined within the constant 'C' in EXSIM. In addition to that generic site amplification functions for site NEHRP-C and NEHRP-D site are also utilized following Boore and Joyner (1997) for comparison purpose.

Kappa (κ) regulates the rapid decay of spectral waveforms and is a critical factor that affects the waveforms in the simulations of earthquake strong ground motions. In this work, distance independent kappa value is based on the empirical studies that suggest it as 45 milliseconds for Northwestern Turkey, Aşkan et al. (2014), "[27]", and Akıncı et al. (2006), "[19]".

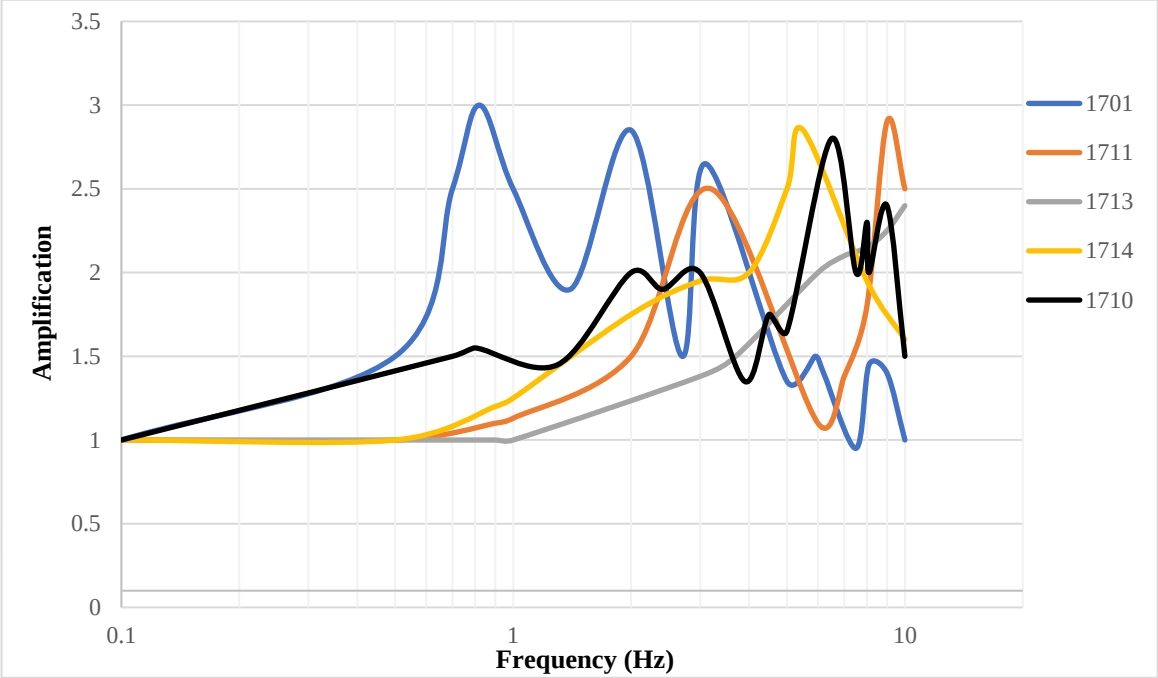

Figure 4.2. Frequency dependent generic amplification factors, Karagöz et al. (2018).

4.4. Point Source Stochastic Simulation of the Mw4.5 Gökçeada Event

For large magnitude events, source duration dominates the total duration of ground excitation and consequently path duration effect shall not be seen adequately. The path duration effect shall be seen as significant as the distance increases and the magnitude decreases. In order to see the effect of path duration on simulated time series a point source simulation is performed based on a small magnitude class earthquake.

The simulation has been performed from 0.1 MPa through 6 MPa range for stress drop where the stress drop is increased by 0.2 MPa. Moreover, the pulsing percentage values are applied between 10 and 60 by increasing 10 percent in an attempt to find the most suitable source parameters. The stress drop, and the pulsing percentage value applied for both simulations are 1 MPa and 30 %, respectively. The generic site amplification functions of Boore and Joyner (1997) are considered for both NEHRP-C and NEHRP-D sites in stochastic point source method. Comparison between simulated effective significant duration (D'_{95}) values for each station are presented in Table 4.3. According to the results, simulated effective significant duration (D'_{95}) values which are obtained as per

the path duration function of this study are closer to the recorded values (around 20-50 sec.). Meanwhile, the reason for the longer duration of the real recordings is the other reflections which are observed following the S-waves. Note that the only S-waves can be simulated through the EXSIM, and the real duration values are greater than the simulated ones due to the local site effect which is not considered in the simulation.

The comparison of simulated Husid plots based on the path duration model from this study (top-left) and Herrmann (1985) (top-right) as well as recorded N-S (bottom-left) and E-W (bottom-right) at five stations (1701, 1710, 1711, 1714, and 2201) are presented in Figure 4.3 through Figure 4.8 below.

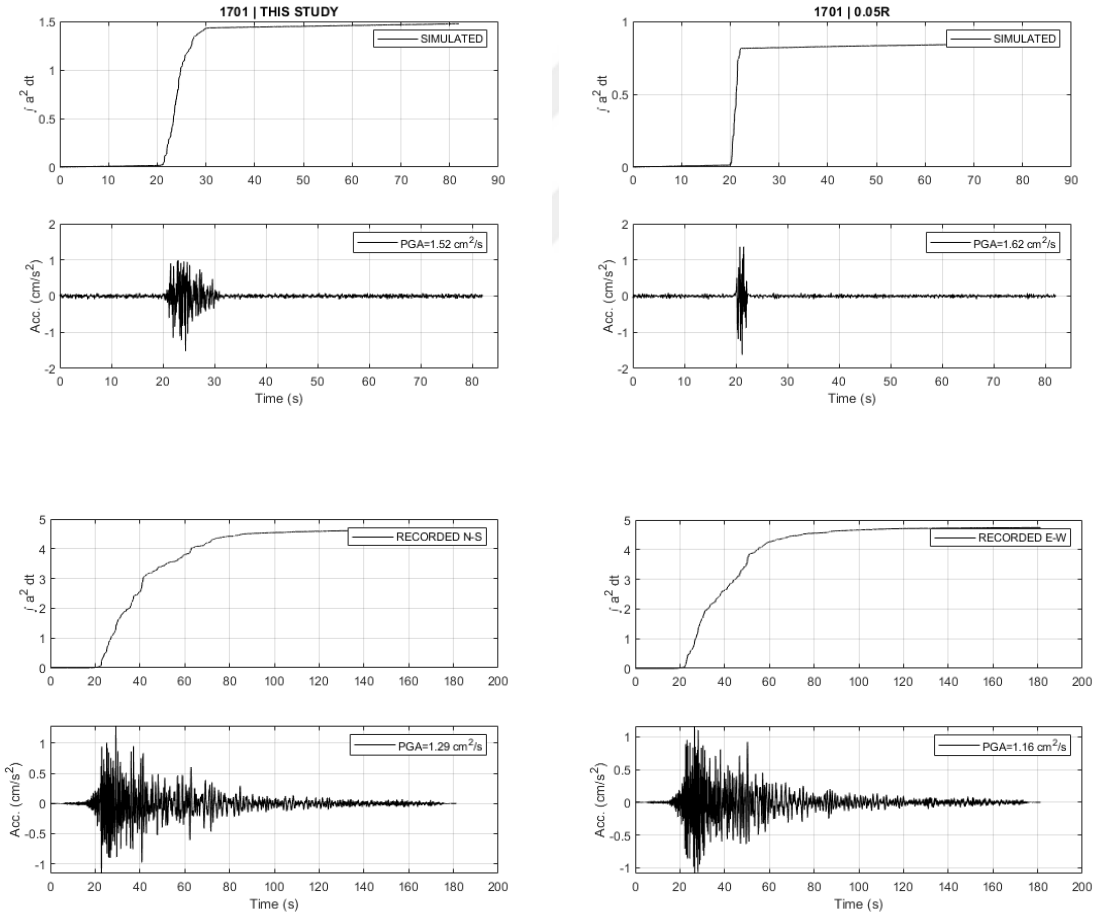

Figure 4.3. The comparison of simulated Husid plots based on the path duration models from this study (top-left) and Herrmann (1985) (top-right) as well as recorded N-S (bottom-left) and E-W (bottom-right) at station 1701, Mw 4.5.

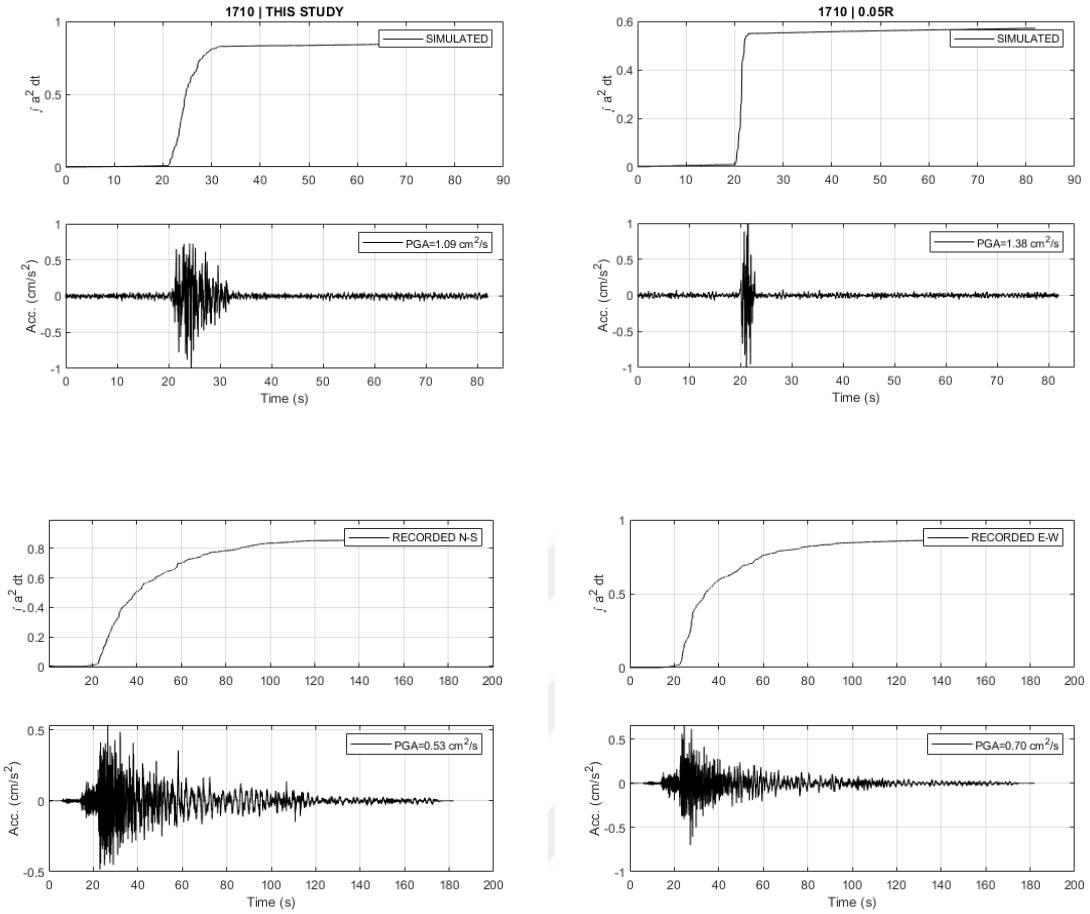

Figure 4.4. The comparison of simulated Husid plots based on the path duration models from this study (top-left) and Herrmann (1985) (top-right) as well as recorded N-S (bottom-left) and E-W (bottom-right) at station 1710, Mw 4.5.

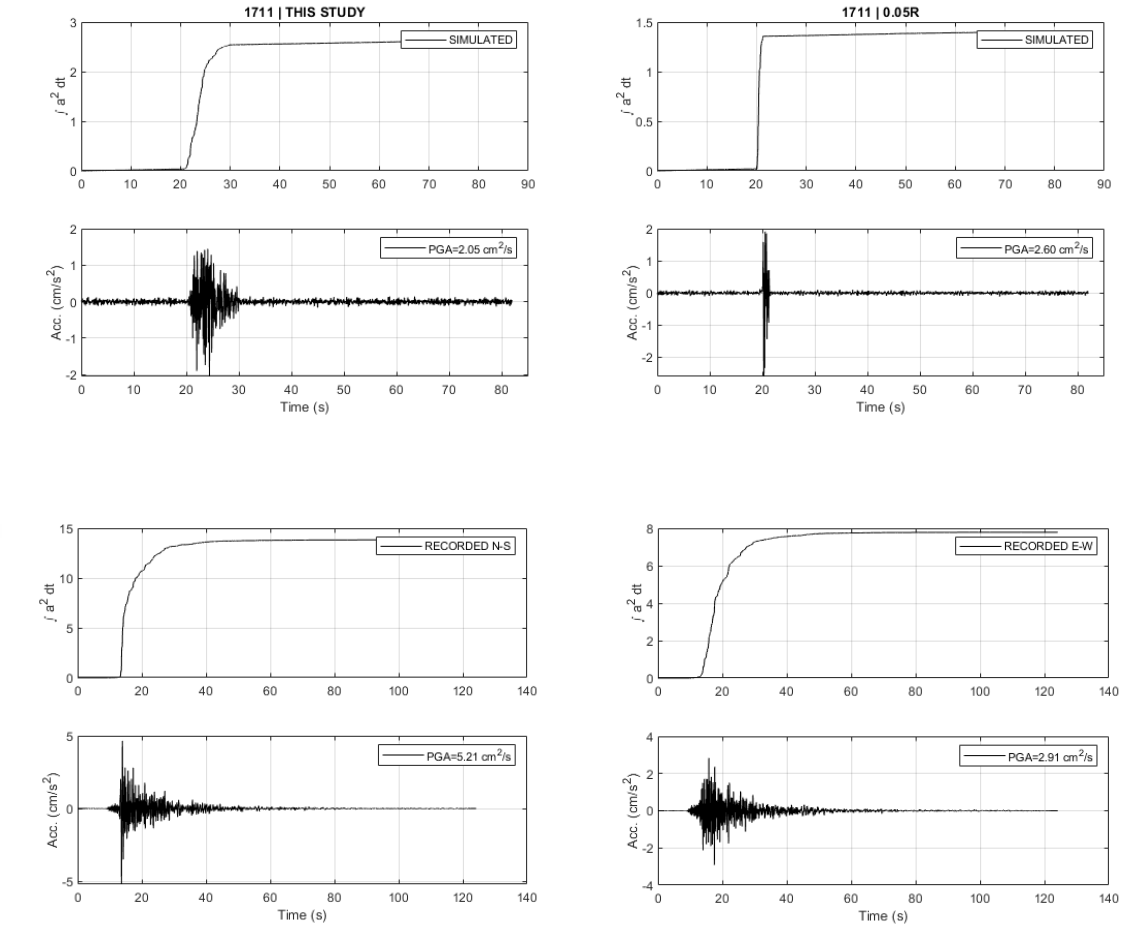

Figure 4.5. The comparison of simulated Husid plots based on the path duration models from this study (top-left) and Herrmann (1985) (top-right) as well as recorded N-S (bottom-left) and E-W (bottom-right) at station 1711, Mw 4.5.

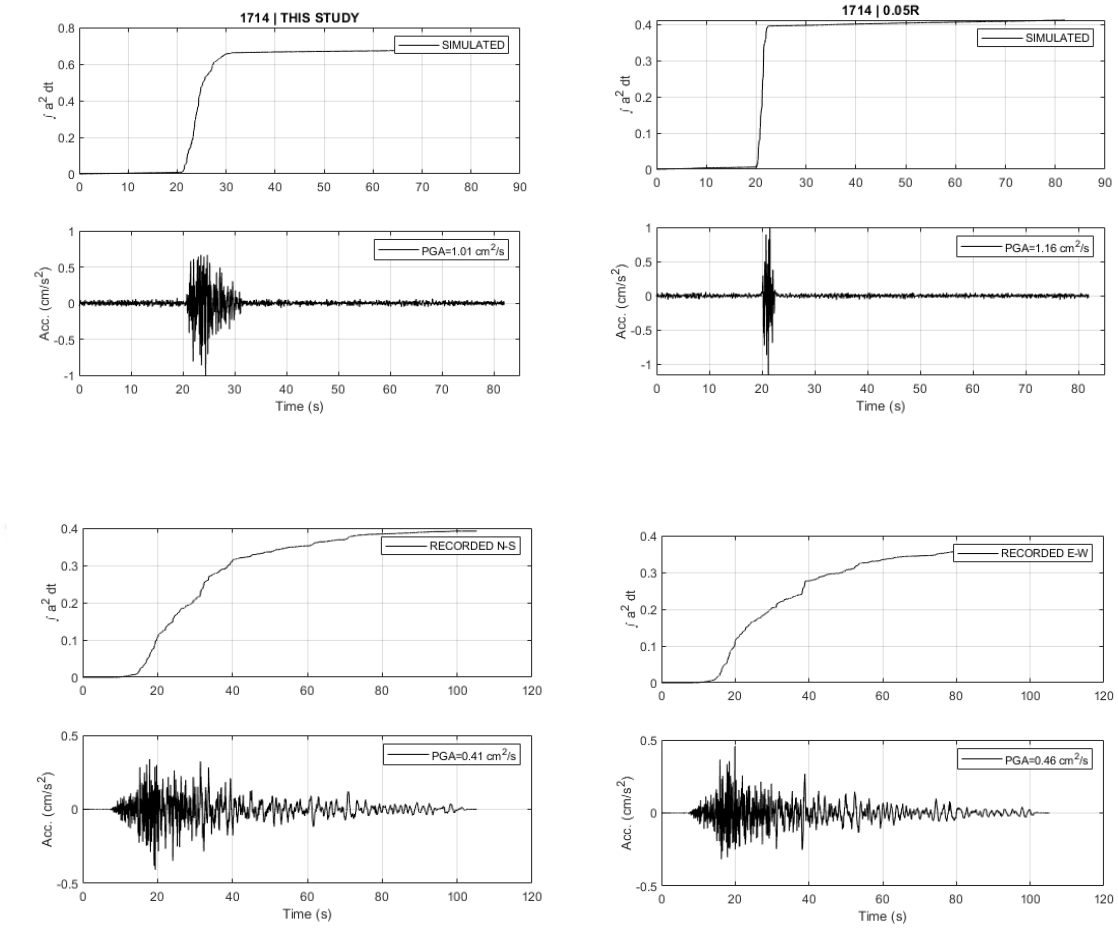

Figure 4.6. The comparison of simulated Husid plots based on the path duration models from this study (top-left) and Herrmann (1985) (top-right) as well as recorded N-S (bottom-left) and E-W (bottom-right) at station 1714, Mw 4.5.

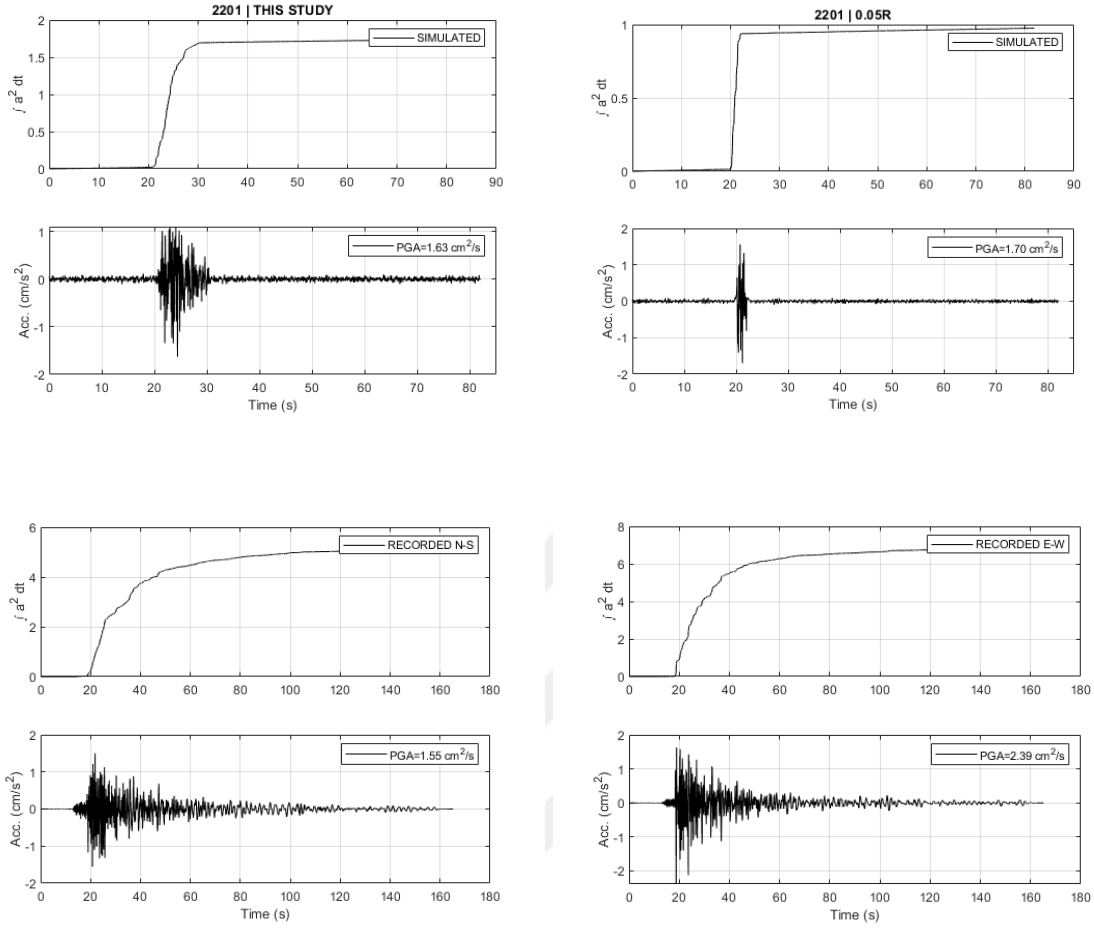

Figure 4.7. The comparison of simulated Husid plots based on the path duration models from this study (top-left) and Herrmann (1985) (top-right) as well as recorded N-S (bottom-left) and E-W (bottom-right) at station 2201, Mw 4.5.

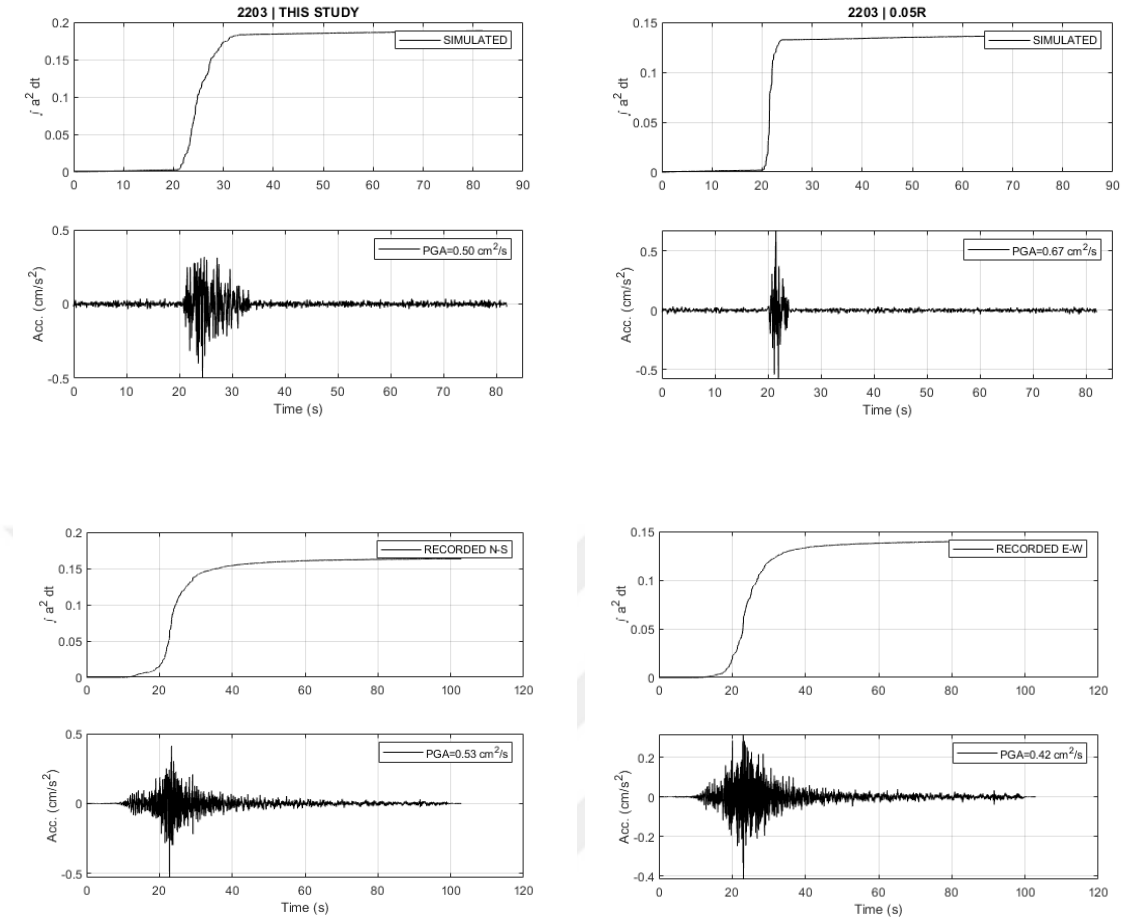

Figure 4.8. The comparison of simulated Husid plots based on the path duration models from this study (top-left) and Herrmann (1985) (top-right) as well as recorded N-S (bottom-left) and E-W (bottom-right) at station 2203, Mw 4.5.

Table 4.3. Comparison between simulated effective significant duration (D'_{95}) values for each station, Mw 4.5.

Station ID	Simulated D'_{95} (sec.) [Our study]	Simulated D'_{95} (sec.) [Herrmann, 1985]
1701	7.50	2.06
1710	8.54	1.92
1711	6.22	0.98
1714	7.80	1.56
2201	6.80	2.08
2203	8.42	1.76

4.5. Simulation of the 2014 (Mw6.9) Gökçeada Earthquake

A Mw 6.9 magnitude earthquake rattled portions of Northern Aegean, and Marmara on May 24, 2014. The quake struck at 12:25 p.m. (UTC+3) and was centered some 30 km northwest of the Island of Gökçeada. It was felt widely in cities adjacent to Çanakkale including Istanbul located approximately 300 km away from the Island. The focal depth of the earthquake has been reported as 23 km, and 25 km by RETMC-KOERI, and AFAD, respectively. This shallow earthquake damaged around 300 structures which are located mostly in the Island of Gökçeada. The largest portion of the energy released to NE-SW direction this is why the quake was felt intensely in Çanakkale and Istanbul alike. The region of the epicenter is situated western end of the North Anatolian Fault Zone (NAFZ), and the fault in question is right-lateral strike strike-slip one. The epicentral intensity (I_o) of seismic event has been reported as VII whereas this value has been specified as V at Çanakkale. Please note that the moment magnitude of Gökçeada Earthquake is considered as 6.9 in simulation.

This section actually attempts to use the regional path duration model, which is obtained in the previous section, by drawing a comparison with the former studies carried out for the 2014 Mw 6.9 Gökçeada Earthquake. In other words, our major objective here is to simulate the 2014 earthquake at strong motion stations of AFAD-TADAS to validate the propagation path characteristics including quality factor, path duration, geometrical spreading.

4.5.1. Data Set

Our goal is to carry out the closest simulation compared to the results that belong to the acceleration recordings of the stations, which are already present, located in Çanakkale. Please refer to “[13]” for R_{RUP} and R_{epi} values used in Table 4.4 below.

Table 4.4. The relevant parameters of strong ground motion stations.

Station ID	Station Coordinates	Repi (km)	R_{RUP} (km)	PGA N-S (gal)	PGA (E-W) (gal)	Vs30 (m/s)	Soil Types (NEHRP)
1701	40.14145N 26.39948E	86	48	141.04	121.26	192	Stiff Soil (D)
1710	40.42334N 26.66715E	109	59	123.15	94.40	286	Stiff Soil (D)
1711	40.19082N 25.90783E	45	24	171.44	176.60	403	Soft Rock (C)
1713	40.16216N 26.41166E	87	47.3	94.39	97.47	483	Soft Rock (C)
1714	40.11291N 26.42205E	89	51.5	45.32	51.12	429	Soft Rock (C)

4.5.2. Source Parameters

In this study, the slip distribution data that shall be used in the source model of M6.9 Gökçeada Earthquake of May 24, 2014 is in accordance with Konca et al. (2018), "[8]". All details which are intrinsic to the study of Konca et al. (2018) are elaborated in the following paragraphs.

Slip values on the fault plane are arranged in a rectangle shape, i.e., matrices. Distribution of slip values is presented in Figure 4.9. The exact corner positions of the boundary of fault segment and epicenter coordinates as well as the depth of each position are given in Table 4.5.

Table 4.5. Boundary of Fault Segment (before trimming).

Points	Longitude	Latitude	Depth (km)
A	24.58080	40.12400	1.47700
B	26.31710	40.47900	1.47700
C	26.33680	40.42270	25.62520
D	24.60060	40.06780	25.62520
E	25.30730	40.21080	

*E: Epicenter.

In the modelling, the big rectangular finite fault plane is laid out in a grid system which is made from horizontal and vertical lines crossing each other. The said segment is divided into 51 and 17 grids horizontally and vertically, respectively where the dimensions of each grid are 1.5 km wide by 3 km long.

As it can be seen, the sub-faults given above start from -1.47 km and go down to -25.63 km. The latitudes and longitudes measured from the center of the grids that represent the coordinates of each slip value has different depth at each layer. More precisely, a total of 17 different depth rows consists of 51 different columns at each layer.

As a first step, the above-mentioned map having 17 rows and 51 columns shall be strived to narrow and not to be used as it has very small displacement values around in the 0.2-1.0 cm range. That is, 153 km-width on the horizontal, and 51.5 km-length on the vertical axis shall not be used after eliminating the small displacement values. The contour map of slip distribution presented in Figure 4.9 shows the high and low displacement values located in the center of cells. Where the slip values included in per fault element along strike are presented on the x-axis – slip values included in per fault element along down dip, on the other hand, are plotted on the y-axis.

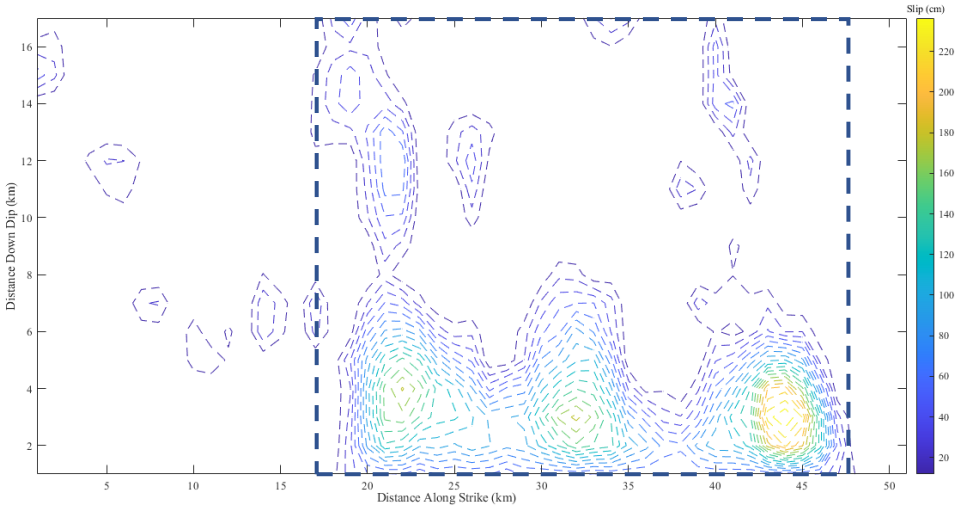

Figure 4.9. The contour map of slip distribution (Konca et al, 2018), the region shown with dashed line is the slip area considered in the simulation.

Please note that each unit of the displacements plotted in Figure 4.9 above is 3 km long on the horizontal and 1.5 km wide on the vertical axis.

According to the map, there is almost no slip value (white areas) at about the first 16 units (=48 km), and the last 4 units (=12km) situated on the horizontal axis. On the other hand, the higher slip values, approximately 0.5 to 2.5 meters, are situated in the shallow elevation of the fault segment as it can be observed on the contour map. As a matter of fact, these preliminary outcomes shed light on which values to use for data input into the EXSIM.

As for the trimming of the edges of the slip model, the criterion used here is based on Somerville et al. (1999). According to the criterion, the first 16 and last 4 edge columns included in the slip model have been removed since the slip values per fault element in these columns are less than 30 percent of the average slip of the entire fault so that the area having the high slip values can be extracted from the model.

These twenty columns including 16x17 sub-faults in the west and 4x17 sub-faults in the east have been removed from the map. Therefore, lat. and long. of upper edge of the fault as well as the location of hypocenter in along fault and down dip distance from the fault shall be updated after the elimination. In other words, the points of A and D have moved to eastwards for about 48 km.

- Latitude: 1° = 110.574 km / Longitude: 1° = 111.320 x cos(latitude) km.
- 48/111.320 x cos (0) = 0.4312°.

Table 4.6. Boundary of Fault Segment (after trimming).

Points	Longitude	Latitude	Depth (km)
A	25.01200	40.12400	1.47700
B	26.31710	40.47900	1.47700
C	26.33680	40.42270	25.62520
D	25.03180	40.06780	25.62520
E	25.30730	40.21080	

*E: Epicenter.

- The Closest Horizontal Distance: 25.30730-25.01200=0.2953°=32.8km
- The Closest Vertical Distance: 40.21080-40.12400=0.0868°=9.6km

The closest horizontal distance from hypocenter to the upper edge of the fault is found as 32.8 km while the closest vertical distance from hypocenter to the upper edge of the fault comes out 9.6 km. The slip distribution after trimming the edges of the slip model presented in Figure 4.9 (the area in dashed zone). Where the slip values included in per fault element along strike are presented on the x-axis – slip values included in per fault element along down dip, on the other hand, are plotted on the y-axis.

After trimming, the number of sub-faults has decreased by 40% as it can be seen on figure above.

Table 4.7. Input parameters of the finite fault simulation.

Parameters	Values	References
Anelastic attenuation	$Q(f)=180\ (f/1.0)^{0.45}$	Akıncı et al. (2006)
Distance dependent duration	See Table 3.7	This study
Kappa (s)	0.045	Aşkan et al. (2014)
Crustal shear wave velocity (m/s)	3500	-
Crustal density (kg/m^3)	2850	-
Geometrical spreading	See Table 4.2	Akıncı et al. (2006)
Stress drop (MPa)	Variable: 1.2-8.0	-
Pulsing area percentage (%)	Variable: 20-60	-
Slip distribution	See Figure 4.9	This study
Fault plane orientation	Strike:75° Dip:75°	Konca et al. (2018)
Depth to top of fault plane (m)	1477	Konca et al. (2018)
Source duration (s)	-	0.5/*fc* (inversely proportional to corner frequency)
Site amplification	-	Boore & Joyner (1997), Karagöz et al. (2018)

4.6. Simulation

4.6.1. Basis of Comparisons for Results

What we try to do is to observe if we achieve the close results when the outcome of simulation is compared to the real one in regard to spectral accelerations and the ground motion intensities. At the end of the simulation, PSA values and acceleration time histories

as well as ground motion parameters such as significant duration, arias intensity shall be obtained as output parameters so that the final graphs can be easily plotted, so the final waveforms obtained by the simulation shall be able to be compared with the recorded results.

Acceleration time histories and spectral acceleration graphs plotted according to the observed and simulated results of M6.9 Gökçeada Earthquake for each station are presented between Figure 4.10 and Figure 4.16 in Section 4.7 below. The relevant figures obtained at the end of the simulation shall enable us to make a comparison.

4.6.2. Number of Trials

This section shall be addressed just as it is described in Section 4.1.1 of this document.

4.6.3. Model Validation

As it can be observed in Figure 4.10 through Figure 4.14 showing the simulated and recorded results, the comparison made between these two is based on pseudo spectral accelerations. In addition to this, it can be seen how these two waveforms are close to each other in the said figures. It can be concluded from the lower graph that the modelling is done satisfactorily in case it follows zero closely.

Residuals are calculated at 22 discrete periods (from 0.02 to 2.0 sec.) as per the following equation which is applied for all stations so as to find the smallest residual value. Please refer to Eq. 4.3 for the formula utilized in model validation.

4.7. Analysis

In the calculation of stiff soil and rock site conditions, frequency dependent generic amplification factors of Karagöz et al. (2018) (hereafter K18), and Boore and Joyner (1997) (hereafter BJ97) are adopted for both sets of simulations, respectively. Each simulation has been carried out 1.2 MPa through 8 MPa range for stress drop where the

stress drop is increased by 2 bars. Moreover, the pulsing percentage values are applied between 20 and 60 by increasing 10 percent in an attempt to find the most suitable source parameters. In the first simulation which is carried out according to the K18, the minimum residual is obtained by 6.4 MPa stress drop and 60% pulsing percentage whereas the said parameter is found by 3.4 MPa stress drop, 60% pulsing percentage by using the amplification factors of Boore and Joyner (1997). The stress drop, pulsing percentage, and minimum average residual value used for each simulation are presented in Table 4.8, and comparison of recorded and simulated PSA values & residuals of geometric mean of horizontal PSAs at each station are given in Figure 4.10 through Figure 4.14.

Table 4.8. Minimum average residual, stress drop, and pulsing percentage values.

References to amplification factors	Minimum average residual	Stress drop (bar)	Pulsing percentage (%)
Karagöz et al. (2018)	0.4806	64	60
Boore and Joyner (1997)	0.4246	34	60

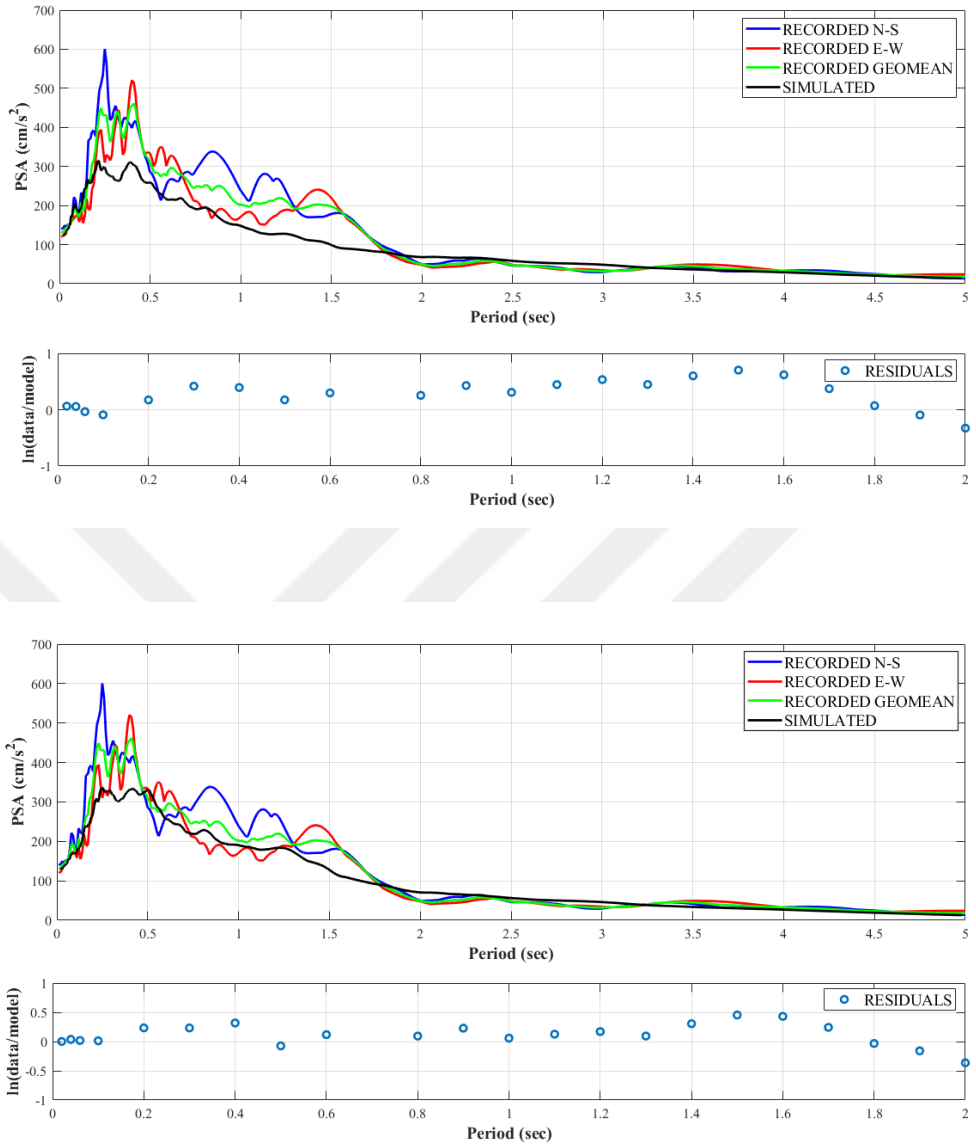

Figure 4.10. Pseudo spectral accelerations and residuals of geometric mean of horizontal PSAs at station 1701, BJ97 – top, K18 – bottom.

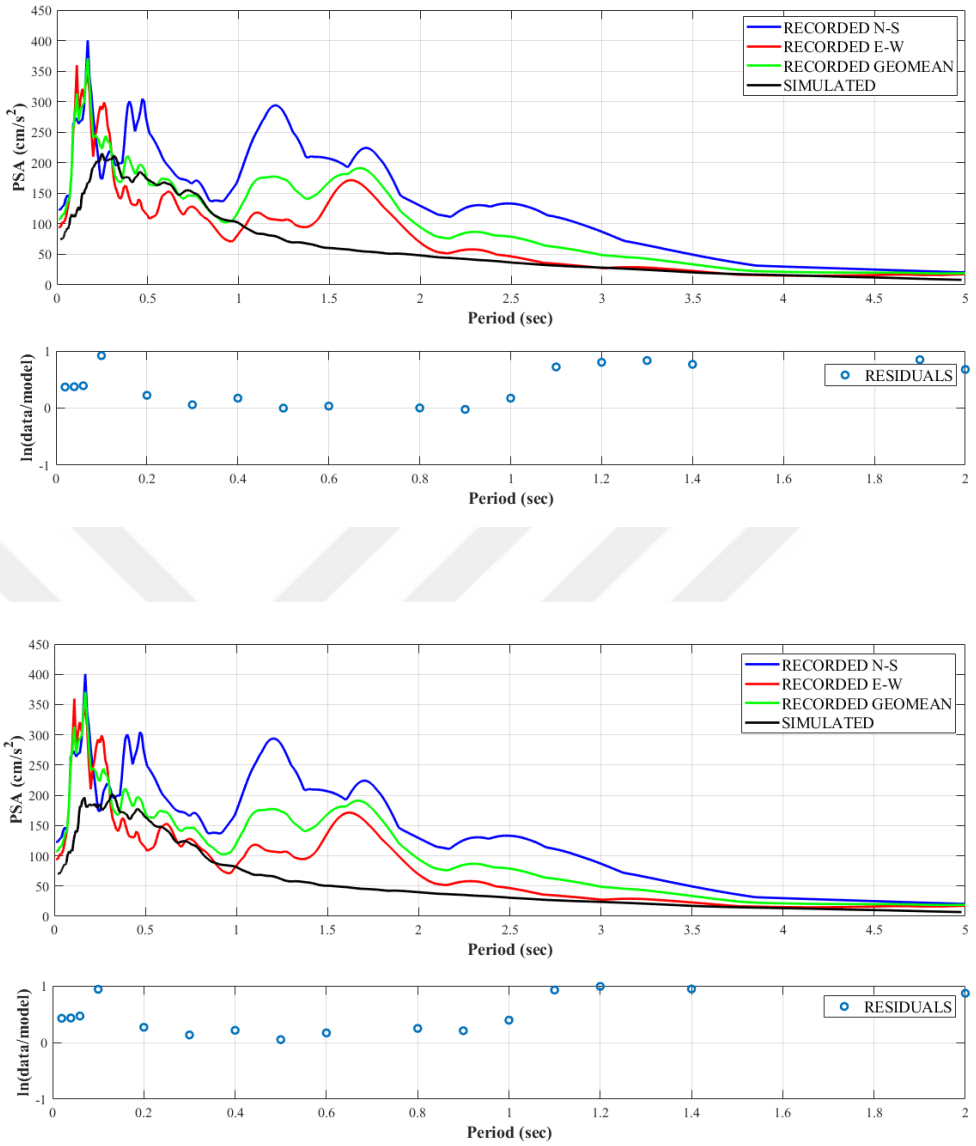

Figure 4.11. Pseudo spectral accelerations and residuals of geometric mean of horizontal PSAs at station 1710, BJ97 – top, K18 – bottom.

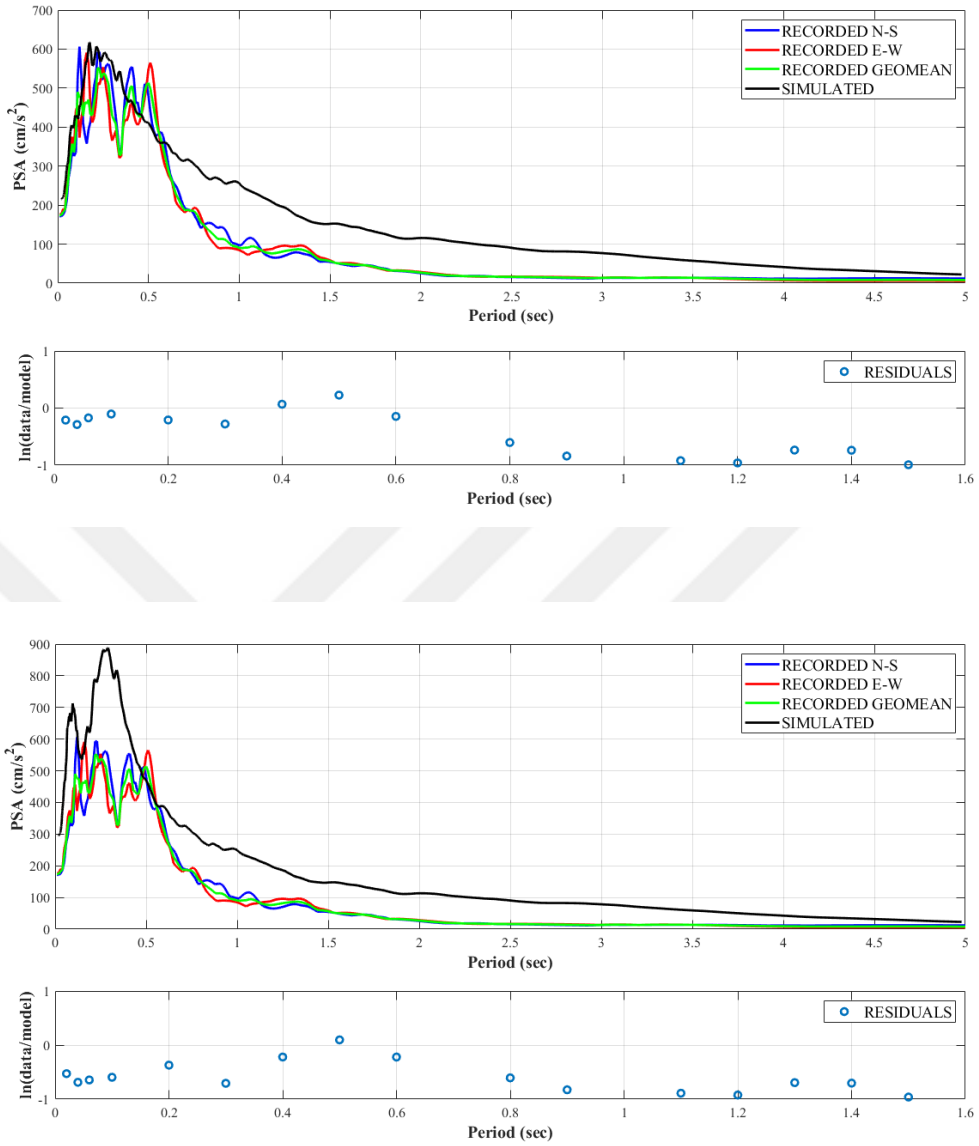

Figure 4.12. Pseudo spectral accelerations and residuals of geometric mean of horizontal PSAs at station 1711, BJ97 – top, K18 – bottom.

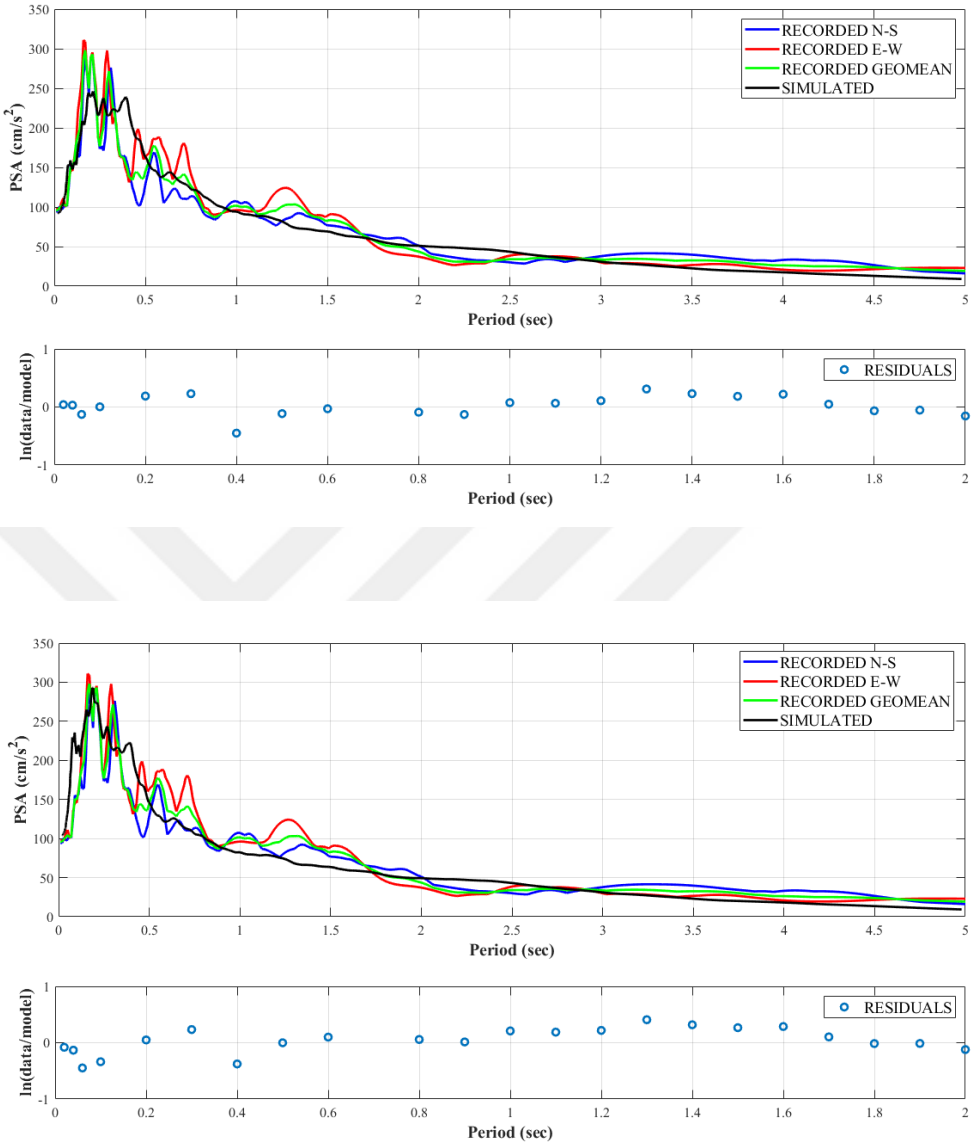

Figure 4.13. Pseudo spectral accelerations and residuals of geometric mean of horizontal PSAs at station 1713, BJ97 – top, K18 – bottom.

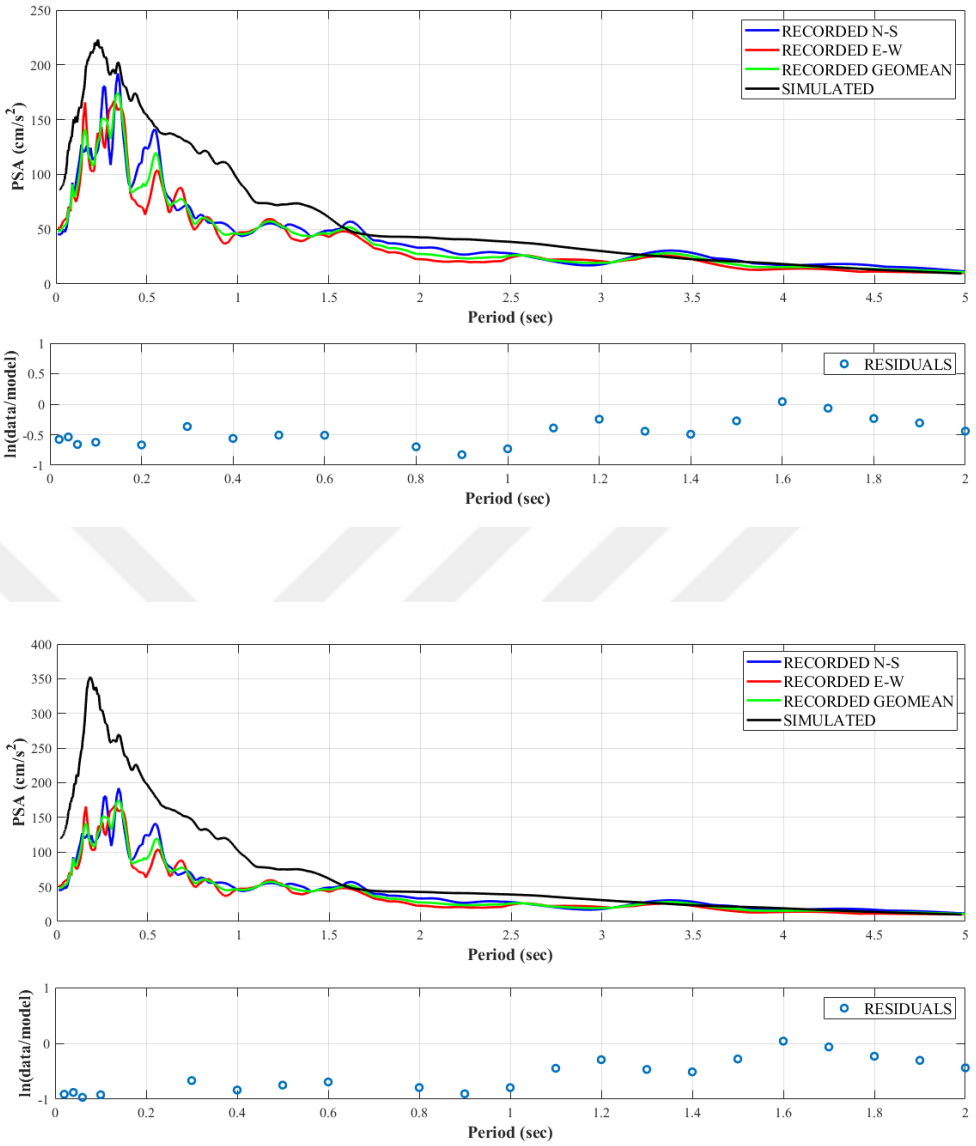

Figure 4.14. Pseudo spectral accelerations and residuals of geometric mean of horizontal PSAs at station 1714, BJ97 – top, K18 – bottom.

Acceleration time histories and velocity time histories as well are plotted according to the observed and simulated results of M6.9 Gökçeada Earthquake for each station, and they are presented between the Figure 4.15 and Figure 4.18 below. Moreover, the comparison between recorded and simulated peak ground acceleration values as well as velocities are tabulated in Table 4.9 and Table 4.10 for each station.

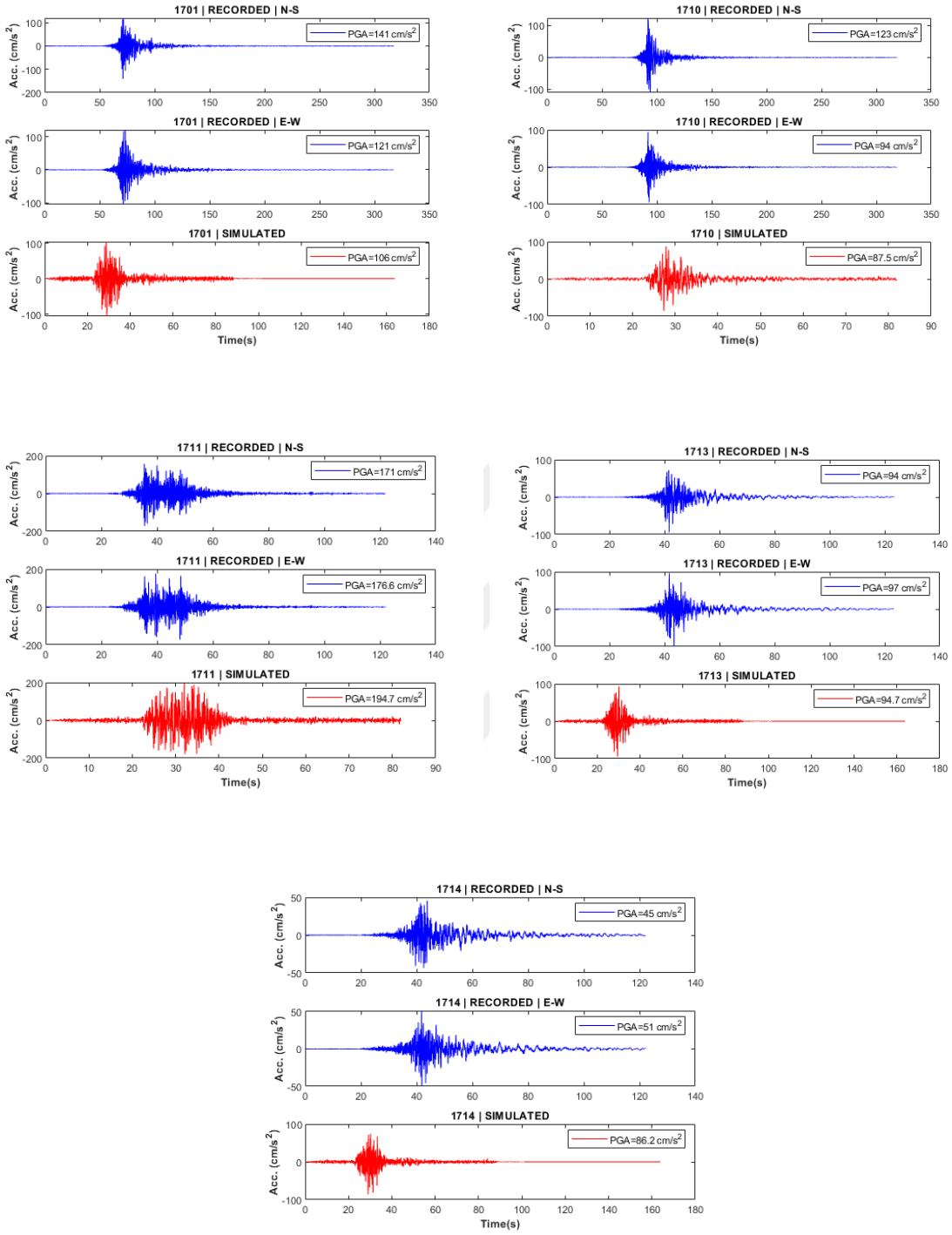

Figure 4.15. Recorded and simulated acceleration time histories at stations 1701, 1710, 1711, 1713, and 1714 – based on BJ97.

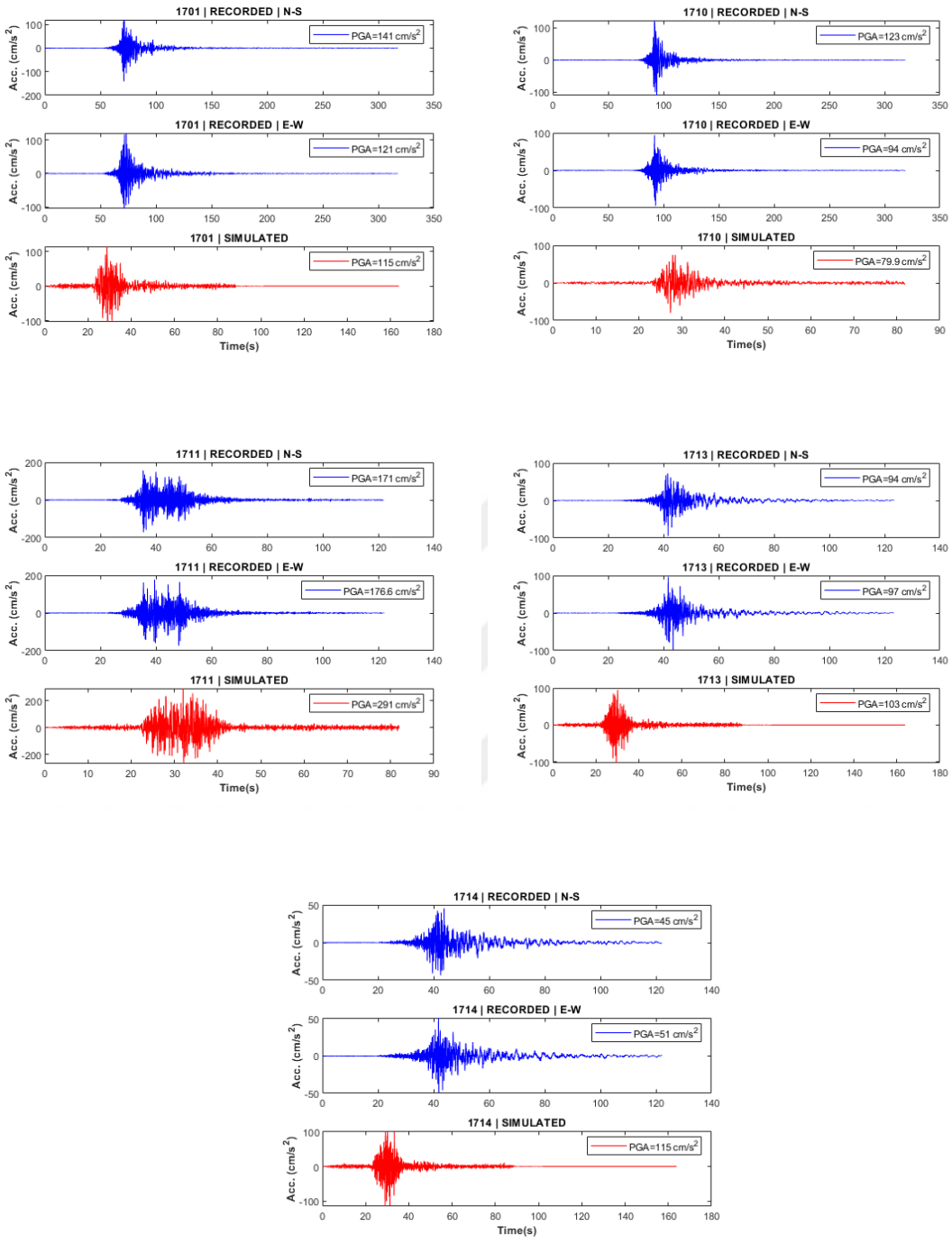

Figure 4.16. Recorded and simulated acceleration time histories at stations 1701, 1710, 1711, 1713, and 1714 – based on K18.

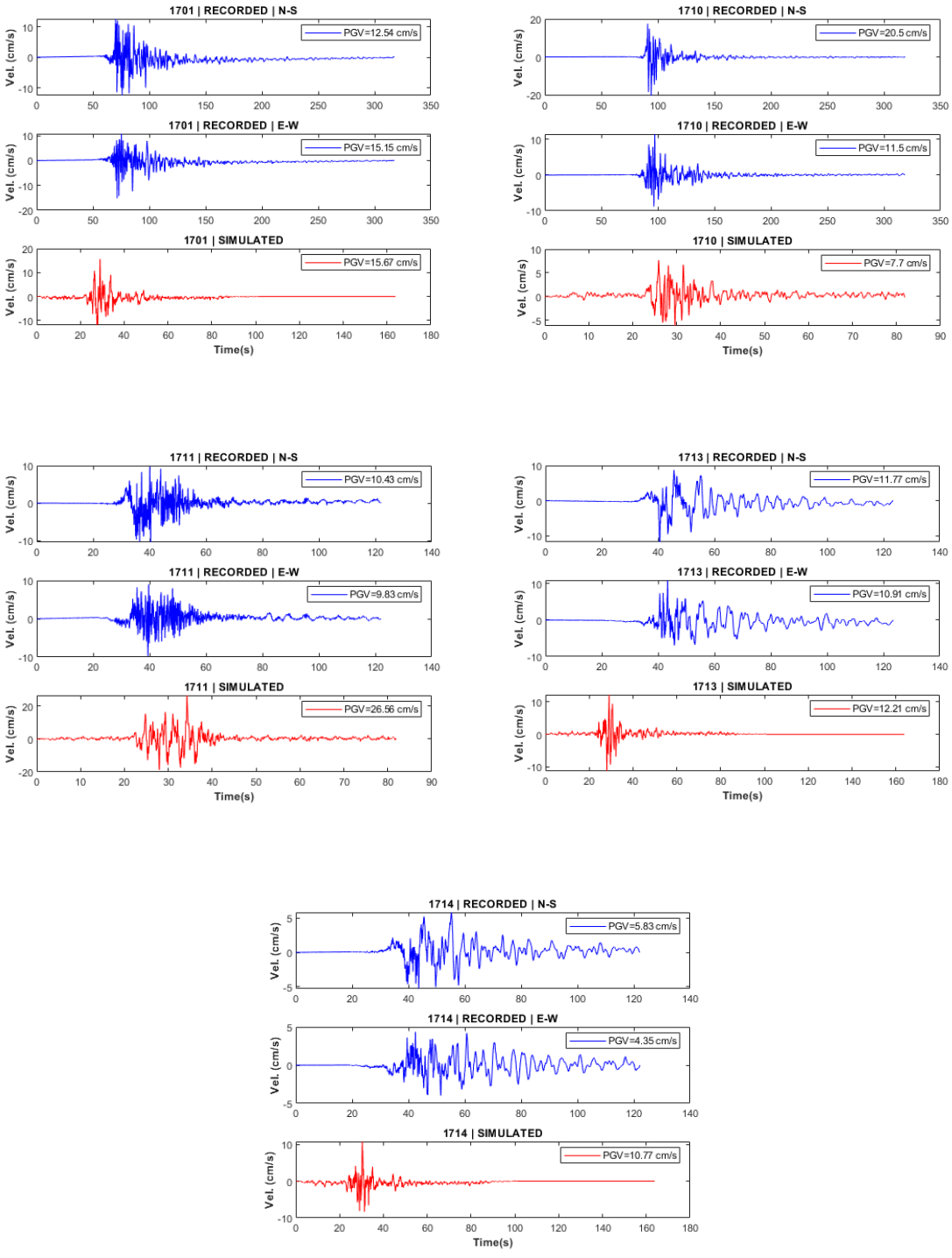

Figure 4.17. Recorded and simulated velocity time histories at stations 1701, 1710, 1711, 1713, and 1714 – based on BJ97.

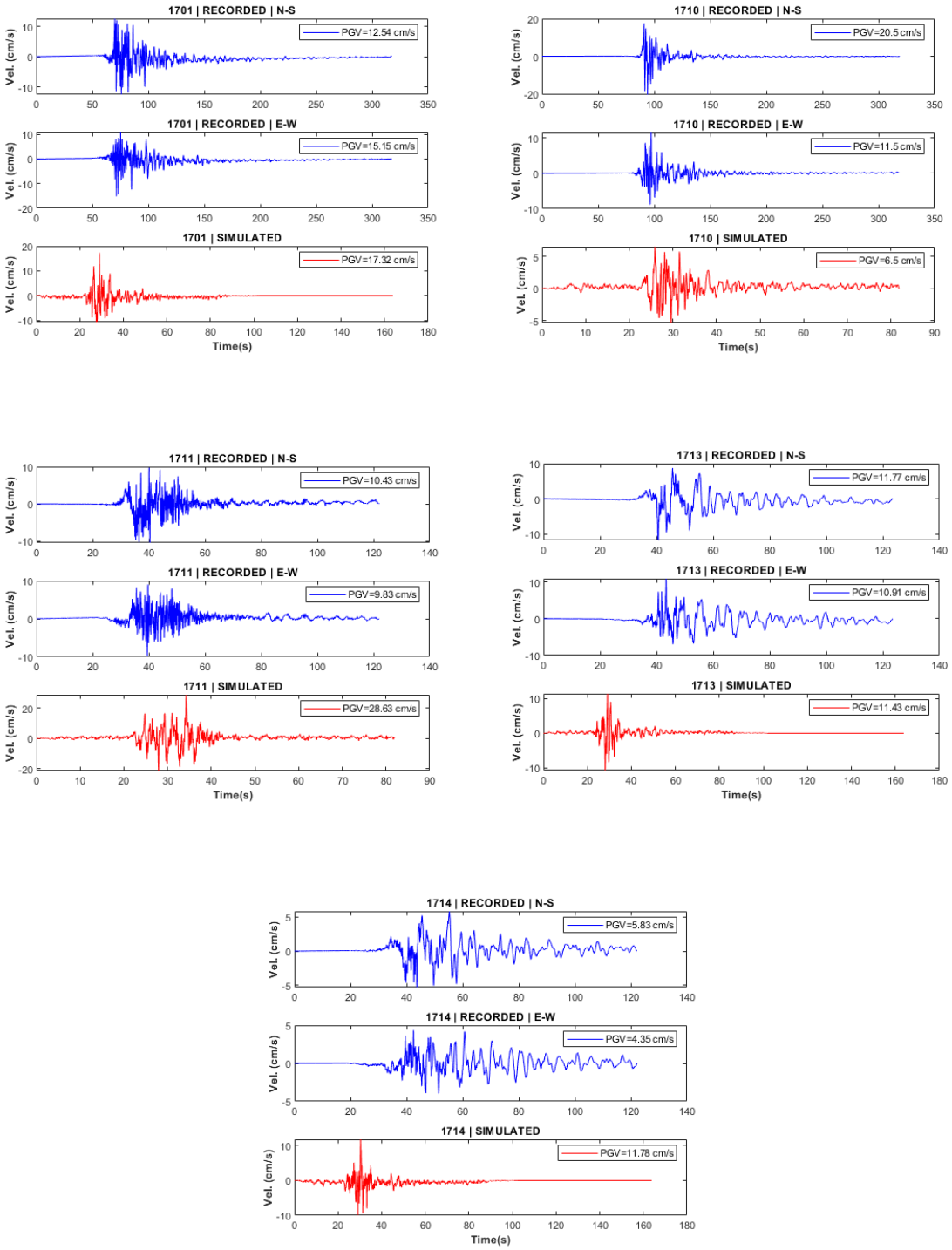

Figure 4.18. Recorded and simulated velocity time histories at stations 1701, 1710, 1711, 1713, and 1714 – based on K18.

Please note that K18 and BJ97 in Table 4.9 and 4.10 below refer to Karagöz et al. (2018), and Boore and Joyner (1997), respectively.

Table 4.9. Comparison between recorded and simulated peak ground acceleration values for each station.

Station ID	Soil types	R_{RUP} (km)	Recorded PGA (cm/s^2)		Simulated PGA (cm/s^2) BJ97	Simulated PGA (cm/s) K18
			N-S	E-W		
1701	D	48	141	121	106	115
1710	D	59	123	94	87.5	79.9
1711	C	24	171	176.6	194.7	291
1713	C	47.3	94	97	94.7	103
1714	C	51.5	45	51	86.2	115

*Please note that soil types are defined as per NEHRP where **D** represents stiff soil whereas **C** represents soft rock.

Table 4.10. Comparison between recorded and simulated peak ground velocity values for each station.

Station ID	Soil types	R_{RUP} (km)	Recorded PGV (cm/s)		Simulated PGV (cm/s) BJ97	Simulated PGV (cm/s) K18
			N-S	E-W		
1701	D	48	12.54	15.15	15.67	17.32
1710	D	59	20.5	11.5	7.7	6.5
1711	C	24	10.43	9.83	26.56	28.63
1713	C	47.3	11.77	10.91	12.21	11.43
1714	C	51.5	5.83	4.35	10.77	11.78

*Please note that soil types are defined as per NEHRP where **D** represents stiff soil whereas **C** represents soft rock.

4.8. Results and Discussions

As for the analysis results, pseudo spectral accelerations and residuals of geometric mean of horizontal PSAs are presented in Figure 4.10 through Figure 4.14 as a result of stochastic simulation based on amplification factors of BJ97, and K18, respectively. In each figure, the top graphs represent the results obtained in accordance with amplification factors intrinsic to BJ97 whereas the bottom ones show the plots derived from the factors belong to K18. This subsection of the study attempts to address the differences between

these two results presented in each figure for all stations. The overall criterion is to consider the simulation as acceptable if the residuals, which are presented right below each PSA graphs, are within ± 0.5.

At first, even though both graphics, in Figure 4.10, obtained based on either of amplification factors in station 1701 show the same results, K18 got slightly better result in the 0.8-1.0 sec. band. Considering the overall criterion, these simulations are acceptable to both assumptions of amplification factors.

Unfortunately, the simulation cannot be carried out in the 1.0-1.2, and 1.5-2.0 sec. band having hump-shaped characters at station 1710. In other words, the amplification factors that we use cannot represent for above-mentioned time range. However, it should be kept in mind that we focus on high frequencies. This being the case, it is acceptable within the 0.5 sec. range, especially considering the overall criterion.

Even though the simulation based on the amplification factor of BJ97 is successful throughout the 0.0-0.6 sec. band at station 1711, K18 is overly amplified especially at periods of 0.3 sec. On the other hand, the rate of success decreases around 1 sec. and above for both simulations. However, BJ97 is acceptable for us as we focus on high frequency levels, and it meets the criterion that we consider throughout the 0.0-0.6 sec. band.

As for the station 1713, the simulations of ground motions for both amplification factors are highly successful from spectral and residual points of view.

Finally, the spectral values are much higher than what is expected at station 1714. Even though the results with K18 is not successful, the simulation based on amplification factors of BJ97 is reasonable as the residuals are generally around ±0.5. range.

5. SYNTHESIS OF STRONG GROUND MOTION AT THE 1915 ÇANAKKALE BRIDGE

The cable supported bridges are classified and recognized by their capability to overcome spans. The 1915 Çanakkale Bridge with a 2023-meter main span becomes the longest bridge span in the world when it opens to traffic. A 2023 meter-main span flanked by two side spans of 770 m.. The 1915 Çanakkale Bridge across the Çanakkale Strait in Turkey stretches from Gelibolu province in Europe to Lapseki province in Asia. The construction of the 1915 Çanakkale Bridge located at the Northeastern end of the strait started on March 18, 2017 and shall be completed on March 18, 2022. The bridge is included in Malkara-Çanakkale Section, and it is originally a part of the Kınalı- Tekirdağ-Çanakkale-Savaştepe Motorway Project.

Main components of the bridge and their essential characteristics are as follows.

- The suspended deck - Twin stiffened steel box girder with a total height of 3.5 meters and a width of 45 meters.
- The cable - Two main cables erected by using the Pre-fabricated Parallel Wire Strand (PPWS) method. Each PWS consists of 127 nos with 5.75mm diameter wires, on the order of 4386m long in the reference state, stretching from the European side anchorage to the Asian side anchorage.
- The towers - Two identical steel towers, which are of the portal type, stretch from an elevation of +9.9m (top of the concrete foundations) to +334.0 m (including tower top enclosure).
- The anchor blocks - Gravity based including additional barrettes.

This section attempts to perform the stochastic simulation of 2014 Mw 6.9 Gökçeada Earthquake at the side span piers of the 1915 Çanakkale Bridge by using the regional path duration model obtained in this study.

5.1. Analysis and Results

In the calculation, frequency dependent generic amplification factors, the bedrock site conditions are adopted for the simulation. By using the amplification factors as per bedrock site conditions, the source parameters of stress drop, and pulsing percentage value are chosen as 3.4 MPa and 60%, respectively. The stress drop, pulsing percentage used for the simulation are presented in Table 5.1. Simulated PSA values, simulated acceleration and velocity time histories as well at side span pier, Asia and Europe are given in Figure 5.1 through Figure 5.2.

Table 5.1. Minimum average residual, stress drop, and pulsing percentage values.

References to amplification factors	Location	Stress drop (bar)	Pulsing percentage (%)
Bedrock	SPA, SPE	34	60

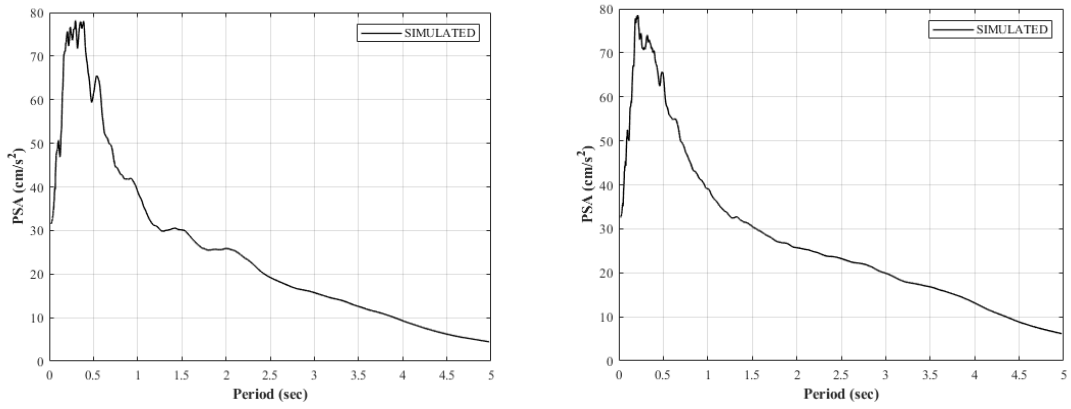

Figure 5.1. Pseudo spectral accelerations at the 1915 Çanakkale Bridge, Side Span Pier, Asia (left), and Europe (right), respectively.

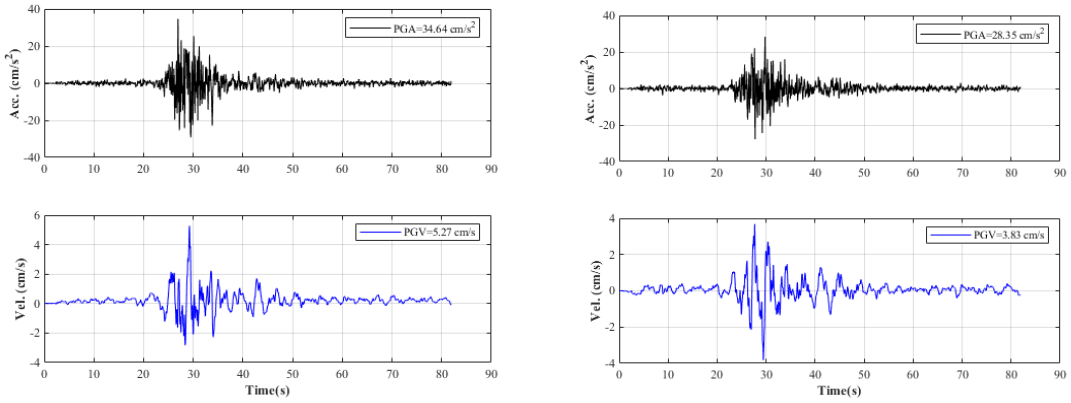

Figure 5.2. Simulated acceleration and velocity time histories at the 1915 Çanakkale Bridge, Side Span Pier, Asia (left), and Europe (right), respectively.

Table 5.2. Simulated peak ground acceleration and velocity values for side span piers.

Station ID	Soil types	Simulated PGA (cm/s^2)	Simulated PGV (cm/s)
SPA	Bedrock	34.64	5.27
SPE	Bedrock	28.35	3.83

In conclusion, pseudo spectral accelerations together with the simulated acceleration and velocity time histories are presented in Figure 5.1 and Figure 5.2 as a result of finite fault stochastic simulation. Both figures represent the results obtained by using the amplification factor in accordance with bedrock site conditions. We have performed the simulation at the side span piers simply because we have already carried out the simulation for the stations around Çanakkale region. PGA values of side span piers are pretty small as the recordings are belong to the seismic event that occurred some 90 km away from the bridge. This is why there is no drastic result.

Please note that the general information provided in this section on the 1915 Çanakkale Bridge are obtained thanks to the design department of DLSY JV.

6. CONCLUSION

It is attempted to find Turkey-specific path duration-distance function which is absent in the scientific literature so as to utilize the related data for use in EXSIM. Path duration function is one of the key parameters for use in stochastic simulation studies. The same approach outlined in Boore and Thompson (2014) has been adopted so as to make path duration calculation. In order to define the path duration which is described a simple subtraction of source duration from significant duration, an earthquake catalogue has been produced.

In the selection of ground motions, the earthquake data set comprises 477 two horizontal components recordings from 50 earthquakes having moment magnitudes of 5.5 to 7.4 is considered for the seismic events that occurred on various faults such as strike-slip, normal, and reverse and at a depth of 0.0 to 46.6 km. The final earthquake catalogue comprising 50 seismic events that occurred in Turkey starts from Jul. 1983 and goes up to Jul. 2017. Seismic grOund-motion pRediction in Europe (RESORCE) by Akkar S. et al., Pacific Earthquake Engineering Research Center (PEER NGA-West2), and Turkish Accelerometric Database and Analysis System (AFAD-TADAS) are utilized as reference databases in this study.

Corner frequencies of earthquakes are estimated following the calculation of D'_{95} of recordings adopting the method of Boore and Thompson (2014) in an attempt to obtain path duration function. Subsequent to these analyses, a trilinear regional function of path duration which is intrinsic to Turkey has been presented concluding that global and regional functions have trilinear characteristic and there is a piece of negative slope in transition in many cases even though it is not documented for the sake of simplification. It should be noted that this is also verified through personal communication with Gail M. Atkinson.

Stochastic simulations are performed at five stations for the two different seismic events that occurred at Gökçeada in the North Aegean Region. One of the aftershocks of May 24, 2014 Mw6.9 Gökçeada Earthquake is Mw4.5 dated May 24, 2014 14:49:15 is

used as the first seismic event to be dealt with. The logic behind the simulation of small event simulation is to visualize the effect of path duration on simulated time series when using conventional (0.05R) and region-dependent (this study) path duration function as source duration dominates the total duration of ground excitation and consequently path duration effect shall not be seen adequately for large magnitude events.

As for the calculation of soil conditions at each station, frequency dependent generic amplification factors of K18, and BJ97 are adopted for both sets of simulations, and acceleration time histories, pseudo spectral accelerations and residuals of geometric mean of horizontal PSAs alike are presented as per the observed and simulated results of M6.9 Gökçeada Earthquake for each station following the analysis. Residuals of spectral accelerations are calculated at 22 discrete periods (from 0.02 to 2.0 sec.) in order to find the smallest residual value where the overall criterion is to consider the simulation as acceptable if the residuals are within ± 0.5 focusing on high frequencies.

The assessments of the results are extensively carried out at each station considering the selection criteria, and it is mostly observed that simulations based on BJ97 are performed successfully. Finally, the stochastic simulation of 2014 Mw 6.9 Gökçeada Earthquake at the side span piers of the 1915 Çanakkale Bridge has been performed by using the regional path duration model obtained in this study and the results have been documented and discussed.

REFERENCES

1. Boore, D. M. and Thompson, E. M. (2014), "Path Durations for Use in the Stochastic-Method Simulation of Ground Motions", *Bulletin of the Seismological Society of America,* Vol. 104, No. 5, pp. 2541–2552, doi: 10.1785/0120140058, October 2014.

2. Andrews DJ., "Objective determination of source parameters and similarity of earthquakes of different size", *Das S, Boatwright J, Scholz SH, Editors. Earthquake source mechanics.* Washington DC: Maurice Ewing Series 6, AGU: 259-267, 1986.

3. Tanırcan, G., Hiroe, M., Yamanaka, H., Özel, A. O., "Large Stress Release During Normal Faulting Earthquakes in Western Turkey Supported by Broadband Ground Motion Simulations", *Pure and Applied Geophysics,* ©2019 Springer Nature Switzerland AG, https://doi.org/10.1007/s00024-019-02357-3, November 2019.

4. Kaklamanos, J., EERI, S.M., Baise, L.G., and Boore, D.M., "Estimating Unknown Input Parameters when Implementing the NGA Ground-Motion Prediction Equations in Engineering Practice", *Earthquake Spectra*, Volume 27, No. 4, pages 1219–1235; ©2011, Earthquake Engineering Research Institute, November 2011.

5. Sandıkkaya, M.A., Akkar, S., "Cumulative absolute velocity, Arias intensity and significant duration predictive models from a pan-European strong-motion dataset", *Bulletin of Earthquake Engineering*, doi:10.1007/s10518-016-0066-6, 2017.

6. Kalafat, D., Kekovalı, K., Pınar, A., "Source Characteristics of The January 8, 2013 (Mw=5.7) and May 24, 2014 (Mw=6.8) North Aegean Earthquakes and Their Aftershocks", *Istanbul Earth Sciences Review,* C.27, S.2, SS. 59-76, Y. 2014.

7. Durukal, E., Çatalyürekli, Y., "Spectral Analysis of Source Parameters of the 1999 Kocaeli and Düzce Earthquake Aftershock Sequences", *13th World Conference on Earthquake Engineering,* Vancouver, B.C., Canada, Paper No. 421, August 1-6,

2004.

8. Konca, A.O., Cetin, S., Karabulut, H., Reilinger, R., Dogan, U., Ergintav, S., Cakir, Z., and Tari, E., "The 2014, MW6.9 North Aegean Earthquake: Seismic and Geodetic Evidence for Coseismic Slip on Persistent Asperities", *Geophys. J. Int.*, 213, 1113–1120 doi: 10.1093/gji/ggy049 Advance Access publication 2018 February 5 GJI Seismology, 2018.

9. Özcan, Z., Özocak, A., Mert, N., Utkucu, M., and Doğan, E., "Observed Earthquake-Induced Failures from March 2, 2017 Samsat-Adıyaman Earthquake", *4th International Conference on Earthquake Engineering and Seismology*, Eskişehir–Anadolu University, October 11-13, 2017.

10. Atkinson, G.M., and Boore, D.M., "Ground-Motion Relations for Eastern North America", *Bulletin of the Seismological Society of America,* Vol. 85, No. 1, pp. 17-30, February 1995.

11. Somerville, P.G., and Smith, N.F., "Source, Path and Site Effects on Loma Prieta Strong Motions", *Second International Conference on Recent Advances in Geotechnical Earthquake Engineering and Soil Dynamics,* St. Louis, Missouri, Paper No. LP30, March 11-15, 1991.

12. Güney, A.B., and Horasan, G., "Enhanced Ground Motions Due to Large-Amplitude Critical Moho Reflections (Sms) in the Sea of Marmara, Turkey", *Geophysical Research Letters,* Vol. 29, No. 2, 1022, 10.1029/2001gl013505, 2002.

13. Karagöz, Ö., Chimoto, K., Yamanaka, H., Özel, O., and Çıtak, S., "Broadband Ground-Motion Simulation of the 24 May 2014 Gökçeada (North Aegean Sea) Earthquake (Mw 6.9) in NW Turkey Considering Local Soil Effects", *Bulletin of Earthquake Engineering,* doi:10.1007/s10518-017-0207-6, 2018.

14. Atkinson, G.M., and Asatourians, K., "Implementation and Validation of EXSIM (A Stochastic Finite-Fault Ground-Motion Simulation Algorithm) on the SCEC Broadband Platform", *Seismological Research Letters,* 86(1):48-60 doi:

10.1785/0220140097, January 2014.

15. Atkinson, G.M., D. M. Boore, K. Assatourians, K. Campbell, and D. Motazedian., "A Guide to Differences between Stochastic Point-Source and Stochastic Finite-Fault Simulations", *Bull. Seismol. Soc. Am.,* 99, 3192–3201, 2009.

16. Herrmann, R. B., "An Extension of Random Vibration Theory Estimates of Strong Ground Motion to Large Distances", *Bull. Seismol. Soc. Am.,* Vol. 75, No. 5, pp. 1447-1453, October 1985.

17. Boore, D. M., "Simulation of Ground Motion Using the Stochastic Method", *Pure appl. geophys.,* 160, 635–676 0033 – 4553/03/040635 – 42, 2003.

18. Hanks, T. C., Kanamori, H. "A Moment Magnitude Scale", *Journal of Geophysical Research,* Vol. 84, No. B5, May 10, 1979.

19. Akinci, A., Malagnini, L., Herrmann, R. B., Gok, R., and Sørensen, M. B., "Ground motion scaling in the Marmara region, Turkey", *Geophys. J. Int.,* 166, 635–651, doi: 10.1111/j.1365-246X.2006.02971, July 04, 2006.

20. Boore, D. M., and Joyner, W.B., "Site Amplifications for Generic Rock Sites", *Bulletin of the Seismological Society of America,* Vol. 87, No. 2, pp. 327-341, April 1997.

21. Boore, D. M., "Stochastic Simulation of High-Frequency Ground Motions Based on Seismological Models of the Radiated Spectra", *Bulletin of the Seismological Society of America,* Vol. 73, No. 6, pp. 1865-1894, December 1983.

22. Motazedian, D., "Stochastic Finite-Fault Modeling Based on a Dynamic Corner Frequency", *Bulletin of the Seismological Society of America,* Vol. 95, No. 3, pp. 995–1010, June 2005.

23. KOERI-RETMC: Boğaziçi University Kandilli Observatory and Earthquake Research Institute, Regional Earthquake and Tsunami Monitoring Center

http://www.koeri.boun.edu.tr/sismo/2/earthquake-catalog/. Accessed Feb. 17, 2020.

24. Akkar S., Sandıkkaya M.A., Şenyurt M., Azari Sisi A., Ay B.Ö., Traversa P., Douglas J., Cotton F., Luzi L., Hernandez B., Godey S. (2013), *Seismic grOund-motion pRediction in Europe (RESORCE).* https://www.resorce-portal.eu/edition2018/. Accessed Dec. 17, 2019.

25. *AFAD-TADAS: Turkish Accelerometric Database and Analysis System.* https://tadas.afad.gov.tr/list-event. Accessed Feb. 12, 2020.

26. *PEER NGA-West2: Pacific Earthquake Engineering Research Center.* https://ngawest2.berkeley.edu/ .Accessed Jul. 4, 2020.

27. Askan A., Sisman F.N., Pekcan O., "A Regional Near-Surface High Frequency Spectral Attenuation (kappa) Model for Northwestern Turkey", *Soil Dynamics and Earthquake Engineering*, (65), 113–125, 2014.

28. Wells D. L., and Coppersmith K. J., "New Empirical Relationships among Magnitude, Rupture Length, Rupture Width, Rupture Area, and Surface Displacement", *Bulletin of the Seismological Society of America*, Vol. 84, No. 4, pp. 974-1002, August 1994.

APPENDIX A: THE CHARACTERSITICS OF RECORDINGS

Table A.1. Selected recordings, and their key characteristics.

Earthquake	Sta.	fc_{mean}	D'_{95}	D_P	Faulting	V_{s30} (m/s)	R_{RUP}	Mw	Source
1983-07-05	2607	0.50	5.99	4.99	STRIKE SLIP	397.238	35	6.1	RESORCE
1983-07-05	2625	0.50	6.99	5.99	STRIKE SLIP	520.075	44	6.1	RESORCE
1983-07-05	0147	0.50	19.89	18.89	STRIKE SLIP	408.663	72	6.1	RESORCE
1983-10-30	0042	0.36	18.88	17.49	STRIKE SLIP	316.42	21	6.6	RESORCE
1983-10-30	2591	0.36	6.62	5.23	STRIKE SLIP	374.87	999	6.6	RESORCE
1992-03-13	0063	0.30	4.78	3.11	STRIKE SLIP	421	1	6.7	RESORCE
1992-03-13	0065	0.30	6.25	4.58	STRIKE SLIP		999	6.7	RESORCE
1992-03-13	0064	0.30	20.02	18.35	STRIKE SLIP	319.56	999	6.7	RESORCE
1992-03-15	0063	0.50	16.14	15.14	STRIKE SLIP	421	41	5.9	RESORCE
1992-03-15	0066	0.50	4.16	3.16	STRIKE SLIP	999	27	5.9	RESORCE
1992-11-06	0114	0.38	9.75	8.43	STRIKE SLIP	369.273	33	6	RESORCE
1992-11-06	3062	0.38	21.02	19.70	STRIKE SLIP	999	67	6	RESORCE
1995-10-01	0105	0.44	55.32	54.18	NORMAL	355.922	83	6.5	RESORCE
1995-10-01	0106	0.44	21.32	20.18	NORMAL	334.59	999	6.5	RESORCE
1995-10-01	0107	0.44	15.49	14.35	NORMAL	395.095	999	6.5	RESORCE
1995-10-01	0108	0.44	21.58	20.44	NORMAL	198.124	999	6.5	RESORCE
1995-10-01	3603	0.44	15.75	14.61	NORMAL	659.6	250	6.5	RESORCE
1995-12-05	0231	0.66	18.04	17.28	STRIKE SLIP	407.299	111	5.8	RESORCE
1995-12-05	0232	0.66	18.48	17.72	STRIKE SLIP	314.247	53	5.8	RESORCE
1996-08-14	2619	1.21	14.61	14.20	STRIKE SLIP	999	120	5.7	RESORCE
1996-08-14	2661	1.21	5.60	5.19	STRIKE SLIP	443.258	52	5.7	RESORCE
1996-08-14	2619	1.01	10.34	9.85	STRIKE SLIP	999	123	5.6	RESORCE
1996-08-14	2661	1.01	4.81	4.32	STRIKE SLIP	443.258	54	5.6	RESORCE
1996-08-14	3918	1.01	9.80	9.31	STRIKE SLIP	368.398	29	5.6	RESORCE
1997-01-22	2221	0.70	11.45	10.73	NORMAL	469.525	24	5.7	RESORCE
1997-01-22	2399	0.70	24.59	23.87	NORMAL	466.185	173	5.7	RESORCE
1997-11-14	0147	0.59	14.43	13.58	STRIKE SLIP	408.663	273	5.9	RESORCE
1997-11-14	0153	0.59	22.04	21.19	STRIKE SLIP	191.835	147	5.9	RESORCE
1998-06-27	2221	0.58	14.25	13.38	STRIKE SLIP	469.525	115	6.3	RESORCE
1998-06-27	2274	0.58	6.26	5.39	STRIKE SLIP	366.433	54	6.3	RESORCE
1998-06-27	2317	0.58	8.62	7.75	STRIKE SLIP	263.81	45	6.3	RESORCE
1998-06-27	2399	0.58	51.95	51.08	STRIKE SLIP	466.185	156	6.3	RESORCE
1999-08-17	1146	0.07	48.98	41.84	STRIKE SLIP	225.60	207.8	7.4	PEER
1999-08-17	1147	0.07	23.70	16.56	STRIKE SLIP	175.00	69.62	7.4	PEER
1999-08-17	1148	0.07	7.59	0.45	STRIKE SLIP	523.00	13.49	7.4	PEER

Earthquake	Sta.	fc_{mean}	D'_{95}	D_P	Faulting	V_{s30} (m/s)	R_{RUP}	Mw	Source
1999-08-17	1149	0.07	21.75	14.60	STRIKE SLIP	310.01	58.28	7.4	PEER
1999-08-17	1150	0.07	98.56	91.41	STRIKE SLIP	310.90	349.6	7.4	PEER
1999-08-17	1151	0.07	29.96	22.81	STRIKE SLIP	468.44	180.2	7.4	PEER
1999-08-17	1152	0.07	49.71	42.56	STRIKE SLIP	306.37	315.9	7.4	PEER
1999-08-17	1153	0.07	13.07	5.93	STRIKE SLIP	341.56	127.1	7.4	PEER
1999-08-17	1154	0.07	48.54	41.40	STRIKE SLIP	612.78	65.53	7.4	PEER
1999-08-17	1155	0.07	50.59	43.45	STRIKE SLIP	289.69	60.43	7.4	PEER
1999-08-17	1156	0.07	55.49	48.35	STRIKE SLIP	289.69	266.2	7.4	PEER
1999-08-17	1157	0.07	24.44	17.30	STRIKE SLIP	346.00	66.69	7.4	PEER
1999-08-17	1158	0.07	6.32	-0.83	STRIKE SLIP	281.86	15.37	7.4	PEER
1999-08-17	1159	0.07	12.19	5.04	STRIKE SLIP	585.09	142.3	7.4	PEER
1999-08-17	1160	0.07	40.69	33.55	STRIKE SLIP	386.75	55.48	7.4	PEER
1999-08-17	1161	0.07	8.27	1.12	STRIKE SLIP	792.00	10.92	7.4	PEER
1999-08-17	1162	0.07	9.64	2.50	STRIKE SLIP	347.62	31.74	7.4	PEER
1999-08-17	1163	0.07	18.45	11.31	STRIKE SLIP	354.37	60.05	7.4	PEER
1999-08-17	1164	0.07	35.07	27.92	STRIKE SLIP	595.20	51.95	7.4	PEER
1999-08-17	1165	0.07	14.46	7.32	STRIKE SLIP	811.00	7.21	7.4	PEER
1999-08-17	1166	0.07	18.30	11.16	STRIKE SLIP	476.62	30.73	7.4	PEER
1999-08-17	1167	0.07	49.09	41.94	STRIKE SLIP	399.61	145.1	7.4	PEER
1999-08-17	1168	0.07	56.33	49.19	STRIKE SLIP	612.78	293.4	7.4	PEER
1999-08-17	1169	0.07	28.46	21.32	STRIKE SLIP	445.66	55.3	7.4	PEER
1999-08-17	1170	0.07	12.07	4.93	STRIKE SLIP	384.86	53.43	7.4	PEER
1999-08-17	1172	0.07	8.40	1.26	STRIKE SLIP	521.76	165	7.4	PEER
1999-08-17	1173	0.07	56.38	49.23	STRIKE SLIP	323.80	472.6	7.4	PEER
1999-08-17	1174	0.07	50.81	43.66	STRIKE SLIP	361.80	256.9	7.4	PEER
1999-08-17	1175	0.07	39.52	32.37	STRIKE SLIP	356.39	226.7	7.4	PEER
1999-08-17	1176	0.07	12.07	4.93	STRIKE SLIP	297.00	4.83	7.4	PEER
1999-08-17	1177	0.07	42.17	35.03	STRIKE SLIP	341.56	53.88	7.4	PEER
1999-09-13	0136	0.46	24.74	23.64	STRIKE SLIP	285.50	236	5.8	RESORCE
1999-09-13	0138	0.46	27.88	26.78	STRIKE SLIP	242.50	148	5.8	RESORCE
1999-09-13	0139	0.46	15.82	14.72	STRIKE SLIP	661.99	219	5.8	RESORCE
1999-09-13	0140	0.46	8.93	7.83	STRIKE SLIP	456.59	97	5.8	RESORCE
1999-09-13	0143	0.46	7.12	6.02	STRIKE SLIP	196.66	42	5.8	RESORCE
1999-09-13	0145	0.46	1.76	0.66	STRIKE SLIP	826.11	14	5.8	RESORCE
1999-09-13	0147	0.46	17.69	16.59	STRIKE SLIP	408.66	210	5.8	RESORCE
1999-09-13	0149	0.46	9.86	8.76	STRIKE SLIP	595.17	90	5.8	RESORCE
1999-09-13	0155	0.46	6.00	4.90	STRIKE SLIP	412.04	26	5.8	RESORCE
1999-09-13	0182	0.46	11.98	10.88	STRIKE SLIP	448.22	65	5.8	RESORCE
1999-09-13	0183	0.46	11.04	9.94	STRIKE SLIP	455.68	59	5.8	RESORCE
1999-09-13	0187	0.46	9.97	8.87	STRIKE SLIP	481.27	66	5.8	RESORCE
1999-09-13	0189	0.46	12.67	11.57	STRIKE SLIP	719.29	78	5.8	RESORCE

Earthquake	Sta.	fc_{mean}	D'_{95}	D_P	Faulting	V_{s30} (m/s)	R_{RUP}	Mw	Source
1999-09-13	0190	0.46	9.04	7.94	STRIKE SLIP	616.38	45	5.8	RESORCE
1999-09-13	0146	0.46	4.01	2.91	STRIKE SLIP	281.98	89	5.8	RESORCE
1999-09-13	0144	0.46	9.80	8.70	STRIKE SLIP	701.08	47	5.8	RESORCE
1999-09-13	3251	0.46	28.22	27.12	STRIKE SLIP	999.00	35	5.8	RESORCE
1999-09-13	3260	0.46	6.95	5.85	STRIKE SLIP	999.00	14	5.8	RESORCE
1999-09-13	3261	0.46	6.55	5.45	STRIKE SLIP	999.00	50	5.8	RESORCE
1999-09-13	3257	0.46	72.67	71.57	STRIKE SLIP	999.00	77	5.8	RESORCE
1999-09-13	3263	0.46	4.44	3.34	STRIKE SLIP	999.00	12	5.8	RESORCE
1999-09-13	3264	0.46	11.74	10.64	STRIKE SLIP	999.00	23	5.8	RESORCE
1999-09-13	3274	0.46	28.96	27.86	STRIKE SLIP	276.00	90	5.8	RESORCE
1999-09-13	3288	0.46	8.63	7.53	STRIKE SLIP	999.00	42	5.8	RESORCE
1999-09-13	3289	0.46	9.73	8.63	STRIKE SLIP	999.00	21	5.8	RESORCE
1999-09-13	3295	0.46	7.66	6.56	STRIKE SLIP	999.00	21	5.8	RESORCE
1999-09-13	3296	0.46	15.71	14.61	STRIKE SLIP	999.00	44	5.8	RESORCE
1999-09-13	3292	0.46	8.76	7.66	STRIKE SLIP	999.00	21	5.8	RESORCE
1999-09-13	3293	0.46	14.62	13.52	STRIKE SLIP	999.00	27	5.8	RESORCE
1999-09-13	3297	0.46	5.91	4.81	STRIKE SLIP	999.00	26	5.8	RESORCE
1999-09-13	3294	0.46	21.66	20.56	STRIKE SLIP	999.00	27	5.8	RESORCE
1999-09-13	0164	0.46	11.42	10.32	STRIKE SLIP	659.60	91	5.8	RESORCE
1999-09-13	0159	0.46	21.11	20.01	STRIKE SLIP	230.00	96	5.8	RESORCE
1999-09-13	0177	0.46	5.66	4.56	STRIKE SLIP	999.00	24	5.8	RESORCE
1999-09-13	0173	0.46	24.02	22.92	STRIKE SLIP	999.00	28	5.8	RESORCE
1999-09-13	0179	0.46	35.27	34.17	STRIKE SLIP	170.00	27	5.8	RESORCE
1999-09-13	3323	0.46	63.37	62.27	STRIKE SLIP	999.00	50	5.8	RESORCE
1999-09-13	0175	0.46	27.12	26.02	STRIKE SLIP	999.00	38	5.8	RESORCE
1999-09-13	3600	0.46	5.88	4.78	STRIKE SLIP	999.00	26	5.8	RESORCE
1999-09-13	0178	0.46	33.36	32.26	STRIKE SLIP	175.00	28	5.8	RESORCE
1999-09-13	0157	0.46	6.09	4.99	STRIKE SLIP	523.11	55	5.8	RESORCE
1999-09-13	0161	0.46	34.04	32.94	STRIKE SLIP	173.42	113	5.8	RESORCE
1999-09-13	0152	0.46	17.25	16.15	STRIKE SLIP	274.50	172	5.8	RESORCE
1999-09-13	0154	0.46	20.25	19.15	STRIKE SLIP	274.50	95	5.8	RESORCE
1999-09-13	0148	0.46	19.43	18.33	STRIKE SLIP	283.30	109	5.8	RESORCE
1999-09-13	0192	0.46	9.83	8.73	STRIKE SLIP	274.50	54	5.8	RESORCE
1999-09-13	0158	0.46	24.18	23.08	STRIKE SLIP	424.80	103	5.8	RESORCE
1999-09-13	0162	0.46	7.33	6.23	STRIKE SLIP	338.60	93	5.8	RESORCE
1999-09-13	0202	0.46	13.09	11.99	STRIKE SLIP	999.00	90	5.8	RESORCE
1999-09-13	3324	0.46	22.92	21.82	STRIKE SLIP	999.00	27	5.8	RESORCE
1999-09-13	0169	0.46	15.01	13.91	STRIKE SLIP	338.60	94	5.8	RESORCE
1999-09-13	3325	0.46	14.22	13.12	STRIKE SLIP	999.00	26	5.8	RESORCE
1999-09-13	0170	0.46	10.47	9.37	STRIKE SLIP	999.00	91	5.8	RESORCE
1999-09-13	0156	0.46	10.11	9.01	STRIKE SLIP	297.47	23	5.8	RESORCE

Earthquake	Sta.	fc_{mean}	D'_{95}	D_P	Faulting	V_{s30} (m/s)	R_{RUP}	Mw	Source
1999-09-13	3598	0.46	12.02	10.92	STRIKE SLIP	999.00	65	5.8	RESORCE
1999-11-11	0138	0.51	20.55	19.57	STRIKE SLIP	242.50	151	5.6	RESORCE
1999-11-11	0139	0.51	29.94	28.96	STRIKE SLIP	661.99	235	5.6	RESORCE
1999-11-11	0140	0.51	19.17	18.19	STRIKE SLIP	456.59	112	5.6	RESORCE
1999-11-11	0147	0.51	19.97	18.99	STRIKE SLIP	408.66	228	5.6	RESORCE
1999-11-11	0149	0.51	17.69	16.71	STRIKE SLIP	595.17	106	5.6	RESORCE
1999-11-11	0155	0.51	1.30	0.32	STRIKE SLIP	412.04	18	5.6	RESORCE
1999-11-11	0181	0.51	10.01	9.03	STRIKE SLIP	454.78	41	5.6	RESORCE
1999-11-11	0182	0.51	5.15	4.17	STRIKE SLIP	448.22	54	5.6	RESORCE
1999-11-11	0183	0.51	5.95	4.97	STRIKE SLIP	455.68	49	5.6	RESORCE
1999-11-11	0184	0.51	8.62	7.64	STRIKE SLIP	315.98	51	5.6	RESORCE
1999-11-11	0187	0.51	5.94	4.96	STRIKE SLIP	481.27	55	5.6	RESORCE
1999-11-11	0189	0.51	9.15	8.17	STRIKE SLIP	719.29	66	5.6	RESORCE
1999-11-11	0190	0.51	5.87	4.89	STRIKE SLIP	616.38	33	5.6	RESORCE
1999-11-11	0194	0.51	6.35	5.37	STRIKE SLIP	440.00	55	5.6	RESORCE
1999-11-11	0185	0.51	17.52	16.54	STRIKE SLIP	300.00	35	5.6	RESORCE
1999-11-11	0159	0.51	29.87	28.89	STRIKE SLIP	230.00	112	5.6	RESORCE
1999-11-11	0157	0.51	12.67	11.69	STRIKE SLIP	523.11	72	5.6	RESORCE
1999-11-11	0161	0.51	42.24	41.26	STRIKE SLIP	173.42	130	5.6	RESORCE
1999-11-11	0197	0.51	17.48	16.50	STRIKE SLIP	999.00	80	5.6	RESORCE
1999-11-11	0152	0.51	28.87	27.89	STRIKE SLIP	274.50	189	5.6	RESORCE
1999-11-11	0154	0.51	43.75	42.77	STRIKE SLIP	274.50	112	5.6	RESORCE
1999-11-11	0148	0.51	28.47	27.49	STRIKE SLIP	283.30	126	5.6	RESORCE
1999-11-11	0192	0.51	10.56	9.58	STRIKE SLIP	274.50	72	5.6	RESORCE
1999-11-11	0158	0.51	33.11	32.13	STRIKE SLIP	424.80	120	5.6	RESORCE
1999-11-11	0162	0.51	30.06	29.08	STRIKE SLIP	338.60	110	5.6	RESORCE
1999-11-11	0202	0.51	33.37	32.39	STRIKE SLIP	999.00	107	5.6	RESORCE
1999-11-11	0169	0.51	24.88	23.90	STRIKE SLIP	338.60	111	5.6	RESORCE
1999-11-11	0170	0.51	22.54	21.56	STRIKE SLIP	999.00	107	5.6	RESORCE
1999-11-11	0156	0.51	17.60	16.62	STRIKE SLIP	297.47	39	5.6	RESORCE
1999-11-12	0136	0.31	49.64	48.04	STRIKE SLIP	285.50	260	7.1	RESORCE
1999-11-12	0137	0.31	43.54	41.94	STRIKE SLIP	225.61	220	7.1	RESORCE
1999-11-12	0138	0.31	42.24	40.64	STRIKE SLIP	242.50	163	7.1	RESORCE
1999-11-12	0139	0.31	75.08	73.48	STRIKE SLIP	661.99	280	7.1	RESORCE
1999-11-12	0140	0.31	26.84	25.24	STRIKE SLIP	456.59	156	7.1	RESORCE
1999-11-12	0146	0.31	14.00	12.40	STRIKE SLIP	281.98	8	7.1	RESORCE
1999-11-12	0147	0.31	19.86	18.26	STRIKE SLIP	408.66	278	7.1	RESORCE
1999-11-12	0148	0.31	23.80	22.20	STRIKE SLIP	283.30	175	7.1	RESORCE
1999-11-12	0149	0.31	21.23	19.63	STRIKE SLIP	595.17	155	7.1	RESORCE
1999-11-12	0150	0.31	39.85	38.25	STRIKE SLIP	361.82	207	7.1	RESORCE
1999-11-12	0154	0.31	38.55	36.95	STRIKE SLIP	274.50	158	7.1	RESORCE

Earthquake	Sta.	fc_{mean}	D'_{95}	D_P	Faulting	V_{s30} (m/s)	R_{RUP}	Mw	Source
1999-11-12	0155	0.31	23.09	21.49	STRIKE SLIP	412.04	37	7.1	RESORCE
1999-11-12	0156	0.31	38.92	37.32	STRIKE SLIP	297.47	89	7.1	RESORCE
1999-11-12	0157	0.31	21.89	20.29	STRIKE SLIP	523.11	123	7.1	RESORCE
1999-11-12	0158	0.31	20.71	19.11	STRIKE SLIP	424.80	169	7.1	RESORCE
1999-11-12	0159	0.31	27.81	26.21	STRIKE SLIP	230.00	162	7.1	RESORCE
1999-11-12	0160	0.31	25.34	23.74	STRIKE SLIP	274.50	167	7.1	RESORCE
1999-11-12	0161	0.31	32.47	30.87	STRIKE SLIP	173.42	180	7.1	RESORCE
1999-11-12	0162	0.31	22.51	20.91	STRIKE SLIP	338.60	159	7.1	RESORCE
1999-11-12	0169	0.31	31.61	30.01	STRIKE SLIP	338.60	161	7.1	RESORCE
1999-11-12	0181	0.31	19.64	18.04	STRIKE SLIP	454.78	15	7.1	RESORCE
1999-11-12	0182	0.31	19.33	17.73	STRIKE SLIP	448.22	4	7.1	RESORCE
1999-11-12	0183	0.31	17.62	16.02	STRIKE SLIP	455.68	3	7.1	RESORCE
1999-11-12	0184	0.31	18.34	16.74	STRIKE SLIP	315.98	2	7.1	RESORCE
1999-11-12	0185	0.31	34.10	32.50	STRIKE SLIP	300.00	85	7.1	RESORCE
1999-11-12	0187	0.31	19.26	17.66	STRIKE SLIP	481.27	0	7.1	RESORCE
1999-11-12	0188	0.31	3.74	2.14	STRIKE SLIP	293.58	6	7.1	RESORCE
1999-11-12	0189	0.31	11.00	9.40	STRIKE SLIP	719.29	0	7.1	RESORCE
1999-11-12	0190	0.31	19.69	18.09	STRIKE SLIP	616.38	18	7.1	RESORCE
1999-11-12	0192	0.31	43.47	41.87	STRIKE SLIP	274.50	122	7.1	RESORCE
1999-11-12	0193	0.31	16.56	14.96	STRIKE SLIP	355.38	33	7.1	RESORCE
1999-11-12	0194	0.31	17.97	16.37	STRIKE SLIP	441.00	0	7.1	RESORCE
1999-11-12	0195	0.31	28.74	27.14	STRIKE SLIP	146.78	132	7.1	RESORCE
1999-11-12	0196	0.31	33.36	31.76	STRIKE SLIP	999.00	131	7.1	RESORCE
1999-11-12	0197	0.31	28.93	27.33	STRIKE SLIP	999.00	130	7.1	RESORCE
1999-11-12	0198	0.31	29.35	27.75	STRIKE SLIP	250.50	132	7.1	RESORCE
1999-11-12	0199	0.31	27.71	26.11	STRIKE SLIP	999.00	131	7.1	RESORCE
1999-11-12	0200	0.31	38.43	36.83	STRIKE SLIP	999.00	129	7.1	RESORCE
1999-11-12	0201	0.31	33.83	32.23	STRIKE SLIP	999.00	133	7.1	RESORCE
1999-11-12	0202	0.31	50.73	49.13	STRIKE SLIP	999.00	156	7.1	RESORCE
1999-11-12	0105	0.31	46.06	44.46	STRIKE SLIP	355.92	357	7.1	RESORCE
1999-11-12	0142	0.31	21.71	20.11	STRIKE SLIP	347.69	38	7.1	RESORCE
1999-11-12	0152	0.31	55.35	53.75	STRIKE SLIP	274.50	239	7.1	RESORCE
1999-11-12	3252	0.31	51.68	50.08	STRIKE SLIP	999.00	0	7.1	RESORCE
1999-11-12	3253	0.31	45.33	43.73	STRIKE SLIP	999.00	0	7.1	RESORCE
1999-11-12	3254	0.31	45.23	43.63	STRIKE SLIP	999.00	0	7.1	RESORCE
1999-11-12	3322	0.31	68.72	67.12	STRIKE SLIP	999.00	129	7.1	RESORCE
2000-06-06	0138	0.32	45.37	43.80	NORMAL	242.50	282	6	RESORCE
2000-06-06	0150	0.32	19.03	17.46	NORMAL	361.82	96	6	RESORCE
2000-06-06	0228	0.32	20.43	18.86	NORMAL	702.62	51	6	RESORCE
2000-06-06	2665	0.32	26.37	24.80	NORMAL	347.90	8	6	RESORCE
2000-08-23	0138	0.81	25.94	25.32	STRIKE SLIP	242.50	150	5.5	RESORCE

Earthquake	Sta.	fc_{mean}	D'_{95}	D_P	Faulting	V_{s30} (m/s)	R_{RUP}	Mw	Source
2000-08-23	0140	0.81	16.64	16.02	STRIKE SLIP	456.59	143	5.5	RESORCE
2000-08-23	0143	0.81	12.76	12.14	STRIKE SLIP	196.66	86	5.5	RESORCE
2000-08-23	0146	0.81	12.67	12.05	STRIKE SLIP	281.98	40	5.5	RESORCE
2000-08-23	0148	0.81	12.71	12.09	STRIKE SLIP	283.30	167	5.5	RESORCE
2000-08-23	0149	0.81	8.61	7.99	STRIKE SLIP	595.17	147	5.5	RESORCE
2000-08-23	0155	0.81	5.55	4.93	STRIKE SLIP	412.04	30	5.5	RESORCE
2000-08-23	0157	0.81	6.17	5.55	STRIKE SLIP	523.11	113	5.5	RESORCE
2000-08-23	0161	0.81	19.27	18.65	STRIKE SLIP	173.42	171	5.5	RESORCE
2000-08-23	0162	0.81	8.61	7.99	STRIKE SLIP	338.60	151	5.5	RESORCE
2000-08-23	0169	0.81	11.38	10.76	STRIKE SLIP	338.60	152	5.5	RESORCE
2000-08-23	0170	0.81	7.18	6.56	STRIKE SLIP	999.00	148	5.5	RESORCE
2000-08-23	0188	0.81	20.98	20.36	STRIKE SLIP	293.58	73	5.5	RESORCE
2000-08-23	0226	0.81	15.57	14.95	STRIKE SLIP	321.00	231	5.5	RESORCE
2000-08-23	0227	0.81	6.03	5.41	STRIKE SLIP	271.61	14	5.5	RESORCE
2000-08-23	0228	0.81	18.64	18.02	STRIKE SLIP	702.62	167	5.5	RESORCE
2000-08-23	0158	0.81	31.34	30.72	STRIKE SLIP	424.80	161	5.5	RESORCE
2001-07-26	0133	0.27	45.53	43.66	REVERSE	310.87	334	6.4	RESORCE
2001-07-26	0134	0.27	46.38	44.51	REVERSE	269.99	258	6.4	RESORCE
2002-02-03	0136	0.26	17.74	15.80	NORMAL	285.50	140	6.5	RESORCE
2002-02-03	0137	0.26	14.69	12.75	NORMAL	225.61	47	6.5	RESORCE
2002-02-03	0138	0.26	21.52	19.58	NORMAL	242.50	126	6.5	RESORCE
2002-02-03	0155	0.26	36.36	34.42	NORMAL	412.04	242	6.5	RESORCE
2002-02-03	0226	0.26	34.81	32.87	NORMAL	321.00	322	6.5	RESORCE
2002-02-03	2430	0.26	27.26	25.32	NORMAL	294.11	116	6.5	RESORCE
2002-02-03	0139	0.26	59.81	57.87	NORMAL	661.99	296	6.5	RESORCE
2002-02-03	0136	0.50	26.51	25.52	NORMAL	285.50	125	5.8	RESORCE
2002-02-03	0137	0.50	19.15	18.16	NORMAL	225.61	32	5.8	RESORCE
2002-02-03	0138	0.50	27.51	26.52	NORMAL	242.50	111	5.8	RESORCE
2002-02-03	0155	0.50	15.72	14.73	NORMAL	412.04	233	5.8	RESORCE
2002-02-03	2430	0.50	21.40	20.41	NORMAL	294.11	113	5.8	RESORCE
2003-01-27	0064	0.71	25.02	24.31	STRIKE SLIP	319.56	62	6	RESORCE
2003-01-27	0229	0.71	16.27	15.56	STRIKE SLIP	528.66	89	6	RESORCE
2003-01-27	0231	0.71	25.20	24.49	STRIKE SLIP	407.30	94	6	RESORCE
2003-04-10	0134	0.62	8.74	7.94	STRIKE SLIP	269.99	38	5.7	RESORCE
2003-04-10	0139	0.62	17.69	16.89	STRIKE SLIP	661.99	178	5.7	RESORCE
2003-04-10	2322	0.62	12.25	11.45	STRIKE SLIP	746.91	139	5.7	RESORCE
2003-04-10	2459	0.62	25.01	24.21	STRIKE SLIP	366.89	105	5.7	RESORCE
2003-04-10	2462	0.62	26.50	25.70	STRIKE SLIP	354.77	112	5.7	RESORCE
2003-04-10	2465	0.62	28.14	27.34	STRIKE SLIP	267.39	127	5.7	RESORCE
2003-04-10	2466	0.62	48.62	47.82	STRIKE SLIP	232.92	176	5.7	RESORCE
2003-04-10	2624	0.62	27.63	26.83	STRIKE SLIP	416.73	251	5.7	RESORCE

Earthquake	Sta.	fc_{mean}	D'_{95}	D_P	Faulting	V_{s30} (m/s)	R_{RUP}	Mw	Source
2003-04-10	0226	0.62	27.75	26.95	STRIKE SLIP	321.00	252	5.7	RESORCE
2003-05-01	0229	0.46	5.22	4.14	STRIKE SLIP	528.66	13	6.3	RESORCE
2003-05-01	0231	0.46	28.86	27.78	STRIKE SLIP	407.30	106	6.3	RESORCE
2003-05-01	0232	0.46	42.77	41.69	STRIKE SLIP	314.25	107	6.3	RESORCE
2003-05-01	0233	0.46	17.51	16.43	STRIKE SLIP	416.68	85	6.3	RESORCE
2003-07-06	0139	0.62	13.02	12.21	STRIKE SLIP	661.99	168	5.7	RESORCE
2003-07-06	0147	0.62	10.83	10.02	STRIKE SLIP	408.66	130	5.7	RESORCE
2003-07-06	0153	0.62	31.06	30.25	STRIKE SLIP	191.84	38	5.7	RESORCE
2003-07-06	2611	0.62	42.24	41.43	STRIKE SLIP	249.07	247	5.7	RESORCE
2003-07-06	2627	0.62	19.07	18.26	STRIKE SLIP	301.25	250	5.7	RESORCE
2003-07-06	2629	0.62	42.36	41.55	STRIKE SLIP	176.30	248	5.7	RESORCE
2003-07-13	0231	0.50	16.86	15.85	STRIKE SLIP	407.30	47	5.5	RESORCE
2003-07-13	2503	0.50	10.02	9.01	STRIKE SLIP	480.78	56	5.5	RESORCE
2003-07-13	2519	0.50	32.37	31.36	STRIKE SLIP	999.00	154	5.5	RESORCE
2004-08-04	2322	0.41	4.65	3.44	NORMAL	746.91	35	5.5	RESORCE
2004-08-04	2459	0.41	30.48	29.27	NORMAL	366.89	114	5.5	RESORCE
2004-08-04	2462	0.41	33.63	32.42	NORMAL	354.77	119	5.5	RESORCE
2004-08-04	2465	0.41	32.63	31.42	NORMAL	267.39	127	5.5	RESORCE
2004-08-04	2466	0.41	49.79	48.58	NORMAL	232.92	156	5.5	RESORCE
2004-08-11	0231	0.45	11.75	10.64	NORMAL	407.30	30	5.6	RESORCE
2004-08-11	2503	0.45	15.06	13.95	NORMAL	480.78	76	5.6	RESORCE
2005-01-23	2240	0.56	13.61	12.72	STRIKE SLIP	299.38	62	5.8	RESORCE
2005-01-23	2466	0.56	74.12	73.23	STRIKE SLIP	232.92	237	5.8	RESORCE
2005-03-14	0233	0.31	29.90	28.31	STRIKE SLIP	416.68	60	5.8	RESORCE
2005-03-14	2591	0.31	19.02	17.43	STRIKE SLIP	374.87	71	5.8	RESORCE
2005-03-23	0233	0.39	31.04	29.76	STRIKE SLIP	416.68	54	5.6	RESORCE
2005-03-23	2591	0.39	12.90	11.62	STRIKE SLIP	374.87	69	5.6	RESORCE
2005-06-06	0229	0.36	8.56	7.17	STRIKE SLIP	528.66	64	5.7	RESORCE
2005-06-06	2526	0.36	8.18	6.79	STRIKE SLIP	484.75	42	5.7	RESORCE
2005-06-06	2591	0.36	8.43	7.04	STRIKE SLIP	374.87	67	5.7	RESORCE
2005-10-17	0134	0.74	12.61	11.93	STRIKE SLIP	269.99	56	5.5	RESORCE
2005-10-17	0135	0.74	8.40	7.72	STRIKE SLIP	340.32	76	5.5	RESORCE
2005-10-17	0139	0.74	19.57	18.89	STRIKE SLIP	661.99	190	5.5	RESORCE
2005-10-17	2459	0.74	30.30	29.62	STRIKE SLIP	366.89	124	5.5	RESORCE
2005-10-17	0134	0.43	12.18	11.02	STRIKE SLIP	269.99	53	5.8	RESORCE
2005-10-17	0135	0.43	11.74	10.58	STRIKE SLIP	340.32	74	5.8	RESORCE
2005-10-17	0139	0.43	14.72	13.56	STRIKE SLIP	661.99	188	5.8	RESORCE
2005-10-17	2322	0.43	14.09	12.93	STRIKE SLIP	746.91	145	5.8	RESORCE
2005-10-17	2459	0.43	33.69	32.53	STRIKE SLIP	366.89	125	5.8	RESORCE
2005-10-17	2465	0.43	36.59	35.43	STRIKE SLIP	267.39	148	5.8	RESORCE
2005-10-17	2466	0.43	58.72	57.56	STRIKE SLIP	232.92	197	5.8	RESORCE

Earthquake	Sta.	fc_{mean}	D'_{95}	D_P	Faulting	V_{s30} (m/s)	R_{RUP}	Mw	Source
2005-10-20	0134	0.49	14.29	13.26	STRIKE SLIP	269.99	48	5.8	RESORCE
2005-10-20	0135	0.49	8.16	7.13	STRIKE SLIP	340.32	69	5.8	RESORCE
2005-10-20	0139	0.49	13.75	12.72	STRIKE SLIP	661.99	186	5.8	RESORCE
2005-10-20	2459	0.49	41.76	40.73	STRIKE SLIP	366.89	115	5.8	RESORCE
2005-10-20	2465	0.49	50.27	49.24	STRIKE SLIP	267.39	138	5.8	RESORCE
2005-10-20	2466	0.49	56.87	55.84	STRIKE SLIP	232.92	187	5.8	RESORCE
2007-02-09	0229	0.65	35.43	34.66	STRIKE SLIP	528.66	132	5.5	RESORCE
2007-02-09	0231	0.65	7.92	7.15	STRIKE SLIP	407.30	34	5.5	RESORCE
2007-02-09	2503	0.65	15.78	15.01	STRIKE SLIP	480.78	64	5.5	RESORCE
2007-02-21	0229	0.38	27.40	26.08	NORMAL	528.66	116	5.7	RESORCE
2007-02-21	0231	0.38	12.75	11.43	NORMAL	407.30	33	5.7	RESORCE
2007-02-21	2381	0.38	23.40	22.08	NORMAL	671.11	197	5.7	RESORCE
2007-02-21	2503	0.38	11.58	10.26	NORMAL	480.78	79	5.7	RESORCE
2007-12-20	0137	0.57	46.73	45.85	STRIKE SLIP	225.61	232	5.7	RESORCE
2007-12-20	2509	0.57	41.33	40.45	STRIKE SLIP	388.24	188	5.7	RESORCE
2007-12-20	2568	0.57	45.77	44.89	STRIKE SLIP	480.87	164	5.7	RESORCE
2007-12-20	2586	0.57	83.00	82.12	STRIKE SLIP	237.09	224	5.7	RESORCE
2007-12-20	2588	0.57	53.52	52.64	STRIKE SLIP	279.60	256	5.7	RESORCE
2007-12-26	0137	0.37	45.57	44.23	STRIKE SLIP	225.61	233	5.6	RESORCE
2007-12-26	2509	0.37	29.72	28.38	STRIKE SLIP	388.24	190	5.6	RESORCE
2007-12-26	2568	0.37	30.64	29.30	STRIKE SLIP	480.87	164	5.6	RESORCE
2007-12-26	2586	0.37	60.42	59.08	STRIKE SLIP	237.09	223	5.6	RESORCE
2010-03-08	2436	0.31	52.14	50.53	STRIKE SLIP	390.54	194	6.1	RESORCE
2010-03-08	0229	0.31	8.84	7.23	STRIKE SLIP	528.66	30	6.1	RESORCE
2010-03-08	2540	0.31	20.69	19.08	STRIKE SLIP	356.01	89	6.1	RESORCE
2010-03-08	3921	0.31	39.66	38.05	STRIKE SLIP	519.00	95	6.1	RESORCE
2010-03-08	0231	0.31	41.91	40.30	STRIKE SLIP	407.30	77	6.1	RESORCE
2010-03-08	3922	0.31	9.65	8.04	STRIKE SLIP	329.00	16	6.1	RESORCE
2010-03-08	3923	0.31	21.03	19.42	STRIKE SLIP	709.00	171	6.1	RESORCE
2010-03-08	0229	0.43	11.98	10.82	STRIKE SLIP	528.66	46	5.6	RESORCE
2010-03-08	2540	0.43	30.57	29.41	STRIKE SLIP	356.01	102	5.6	RESORCE
2010-03-08	0231	0.43	45.92	44.76	STRIKE SLIP	407.30	66	5.6	RESORCE
2011-05-19	0108	0.40	35.01	33.78	NORMAL	198.12	147	5.9	RESORCE
2011-05-19	0114	0.40	26.04	24.81	NORMAL	369.27	208	5.9	RESORCE
2011-05-19	3924	0.40	38.08	36.85	NORMAL	271.00	179	5.9	RESORCE
2011-05-19	0226	0.40	13.70	12.47	NORMAL	321.00	156	5.9	RESORCE
2011-05-19	2575	0.40	15.19	13.96	NORMAL	560.74	57	5.9	RESORCE
2011-05-19	2607	0.40	23.77	22.54	NORMAL	397.24	158	5.9	RESORCE
2011-05-19	2592	0.40	9.71	8.48	NORMAL	401.79	115	5.9	RESORCE
2011-05-19	2611	0.40	26.56	25.33	NORMAL	249.07	117	5.9	RESORCE
2011-05-19	2629	0.40	21.87	20.64	NORMAL	176.30	136	5.9	RESORCE

Earthquake	Sta.	fc_{mean}	D'_{95}	D_P	Faulting	V_{s30} (m/s)	R_{RUP}	Mw	Source
2011-05-19	2632	0.40	11.64	10.41	NORMAL	366.16	138	5.9	RESORCE
2011-05-19	2635	0.40	23.79	22.56	NORMAL	228.73	139	5.9	RESORCE
2011-05-19	2594	0.40	14.80	13.57	NORMAL	412.39	84	5.9	RESORCE
2011-05-19	2603	0.40	7.20	5.97	NORMAL	264.93	110	5.9	RESORCE
2011-05-19	2633	0.40	18.85	17.62	NORMAL	348.69	140	5.9	RESORCE
2011-05-19	2638	0.40	12.68	11.45	NORMAL	571.79	143	5.9	RESORCE
2011-05-19	3925	0.40	13.28	12.05	NORMAL	1597.73	148	5.9	RESORCE
2011-05-19	3926	0.40	7.06	5.83	NORMAL	999.00	131	5.9	RESORCE
2011-05-19	3927	0.40	46.72	45.49	NORMAL	999.00	146	5.9	RESORCE
2011-05-19	3928	0.40	47.05	45.82	NORMAL	999.00	133	5.9	RESORCE
2011-05-19	3929	0.40	38.35	37.12	NORMAL	356.00	152	5.9	RESORCE
2011-05-19	2586	0.40	18.20	16.97	NORMAL	237.09	140	5.9	RESORCE
2011-05-19	2585	0.40	28.20	26.97	NORMAL	328.37	136	5.9	RESORCE
2011-05-19	2589	0.40	9.20	7.97	NORMAL	630.99	139	5.9	RESORCE
2011-05-19	2584	0.40	11.36	10.13	NORMAL	248.29	136	5.9	RESORCE
2011-05-19	2583	0.40	9.29	8.06	NORMAL	999.00	135	5.9	RESORCE
2011-05-19	2588	0.40	29.26	28.03	NORMAL	279.60	114	5.9	RESORCE
2011-05-19	2568	0.40	29.63	28.40	NORMAL	480.87	180	5.9	RESORCE
2011-05-19	3930	0.40	20.26	19.03	NORMAL	999.00	133	5.9	RESORCE
2011-05-19	3931	0.40	25.54	24.31	NORMAL	999.00	132	5.9	RESORCE
2011-05-19	3932	0.40	19.15	17.92	NORMAL	999.00	140	5.9	RESORCE
2011-05-19	3933	0.40	11.84	10.61	NORMAL	999.00	139	5.9	RESORCE
2011-05-19	3934	0.40	21.84	20.61	NORMAL	999.00	145	5.9	RESORCE
2011-05-19	3935	0.40	17.28	16.05	NORMAL	999.00	141	5.9	RESORCE
2011-05-19	3936	0.40	17.17	15.94	NORMAL	999.00	193	5.9	RESORCE
2011-05-19	3937	0.40	18.08	16.85	NORMAL	999.00	205	5.9	RESORCE
2011-05-19	3938	0.40	18.19	16.96	NORMAL	283.00	207	5.9	RESORCE
2011-05-19	3939	0.40	21.91	20.68	NORMAL	999.00	227	5.9	RESORCE
2011-05-19	2532	0.40	39.33	38.10	NORMAL	193.19	184	5.9	RESORCE
2011-05-19	0015	0.40	10.17	8.94	NORMAL	770.69	187	5.9	RESORCE
2011-05-19	3940	0.40	16.26	15.03	NORMAL	999.00	189	5.9	RESORCE
2011-05-19	3941	0.40	13.67	12.44	NORMAL	270.00	172	5.9	RESORCE
2011-05-19	3942	0.40	17.96	16.73	NORMAL	999.00	181	5.9	RESORCE
2011-05-19	3943	0.40	14.25	13.02	NORMAL	999.00	177	5.9	RESORCE
2011-05-19	3944	0.40	17.02	15.79	NORMAL	999.00	183	5.9	RESORCE
2011-05-19	3945	0.40	25.21	23.98	NORMAL	999.00	179	5.9	RESORCE
2011-05-19	3946	0.40	18.81	17.58	NORMAL	999.00	180	5.9	RESORCE
2011-05-19	3947	0.40	34.17	32.94	NORMAL	999.00	182	5.9	RESORCE
2011-05-19	3948	0.40	17.84	16.61	NORMAL	999.00	173	5.9	RESORCE
2011-05-19	3949	0.40	29.12	27.89	NORMAL	999.00	184	5.9	RESORCE
2011-05-19	3950	0.40	25.15	23.92	NORMAL	999.00	176	5.9	RESORCE

Earthquake	Sta.	fc_{mean}	D'_{95}	D_P	Faulting	V_{s30} (m/s)	R_{RUP}	Mw	Source
2011-05-19	3951	0.40	16.05	14.82	NORMAL	999.00	180	5.9	RESORCE
2011-05-19	3952	0.40	15.08	13.85	NORMAL	999.00	186	5.9	RESORCE
2011-05-19	3953	0.40	15.32	14.09	NORMAL	999.00	173	5.9	RESORCE
2011-05-19	3954	0.40	27.16	25.93	NORMAL	999.95	197	5.9	RESORCE
2011-05-19	3955	0.40	16.45	15.22	NORMAL	769.76	185	5.9	RESORCE
2011-05-19	3956	0.40	17.62	16.39	NORMAL	276.85	184	5.9	RESORCE
2011-05-19	0144	0.40	19.70	18.47	NORMAL	701.08	182	5.9	RESORCE
2011-05-19	3999	0.40	36.07	34.84	NORMAL	305.00	192	5.9	RESORCE
2011-05-19	3957	0.40	44.23	43.00	NORMAL	999.00	189	5.9	RESORCE
2011-05-19	3958	0.40	47.14	45.91	NORMAL	380.00	231	5.9	RESORCE
2011-05-19	3959	0.40	14.14	12.91	NORMAL	300.00	174	5.9	RESORCE
2011-05-19	3960	0.40	27.76	26.53	NORMAL	300.00	188	5.9	RESORCE
2011-05-19	3961	0.40	38.77	37.54	NORMAL	999.00	185	5.9	RESORCE
2011-05-19	3962	0.40	38.96	37.73	NORMAL	999.00	186	5.9	RESORCE
2011-05-19	2553	0.40	15.66	14.43	NORMAL	266.60	80	5.9	RESORCE
2011-05-19	2529	0.40	9.60	8.37	NORMAL	343.32	29	5.9	RESORCE
2011-05-19	3963	0.40	9.17	7.94	NORMAL	304.00	25	5.9	RESORCE
2011-05-19	0135	0.40	31.45	30.22	NORMAL	340.32	153	5.9	RESORCE
2011-05-19	2522	0.40	24.52	23.29	NORMAL	291.71	107	5.9	RESORCE
2011-05-19	2530	0.40	4.85	3.62	NORMAL	335.81	36	5.9	RESORCE
2011-05-19	2507	0.40	38.65	37.42	NORMAL	272.93	107	5.9	RESORCE
2011-05-19	3964	0.40	16.91	15.68	NORMAL	999.00	237	5.9	RESORCE
2011-05-19	0136	0.40	7.92	6.69	NORMAL	285.50	55	5.9	RESORCE
2011-05-19	2647	0.40	10.62	9.39	NORMAL	388.43	156	5.9	RESORCE
2011-05-19	2653	0.40	6.63	5.40	NORMAL	357.77	158	5.9	RESORCE
2011-05-19	3965	0.40	43.90	42.67	NORMAL	999.00	258	5.9	RESORCE
2011-05-19	3966	0.40	68.68	67.45	NORMAL	999.00	258	5.9	RESORCE
2011-05-19	3967	0.40	54.96	53.73	NORMAL	999.00	260	5.9	RESORCE
2011-05-19	3968	0.40	76.56	75.33	NORMAL	999.00	252	5.9	RESORCE
2011-05-19	3969	0.40	40.07	38.84	NORMAL	999.00	261	5.9	RESORCE
2011-05-19	3970	0.40	17.96	16.73	NORMAL	999.00	214	5.9	RESORCE
2011-10-23	2581	0.18	77.51	74.72	REVERSE	294.79	105	7.1	RESORCE
2011-10-23	3971	0.18	6.70	3.91	REVERSE	999.00	84	7.1	RESORCE
2011-10-23	3972	0.18	26.94	24.15	REVERSE	311.00	74	7.1	RESORCE
2011-10-23	2912	0.18	20.40	17.61	REVERSE	292.63	20	7.1	RESORCE
2011-10-23	3973	0.18	31.92	29.13	REVERSE	999.00	123	7.1	RESORCE
2011-10-23	3974	0.18	35.69	32.90	REVERSE	450.00	188	7.1	RESORCE
2011-10-23	2514	0.18	39.50	36.71	REVERSE	314.55	135	7.1	RESORCE
2011-10-23	3975	0.18	80.85	78.06	REVERSE	463.00	175	7.1	RESORCE
2011-10-23	2540	0.18	53.80	51.01	REVERSE	356.01	188	7.1	RESORCE
2011-10-23	3976	0.18	79.03	76.24	REVERSE	320.00	257	7.1	RESORCE

Earthquake	Sta.	fc_{mean}	D'_{95}	D_P	Faulting	V_{s30} (m/s)	R_{RUP}	Mw	Source
2011-10-23	3923	0.18	73.79	71.00	REVERSE	709.00	249	7.1	RESORCE
2011-10-23	3977	0.18	78.81	76.02	REVERSE	999.00	252	7.1	RESORCE
2011-10-23	3978	0.18	101.40	98.61	REVERSE	329.00	269	7.1	RESORCE
2011-10-23	3979	0.18	91.50	88.71	REVERSE	999.00	275	7.1	RESORCE
2011-10-23	3980	0.18	54.96	52.17	REVERSE	999.00	297	7.1	RESORCE
2011-10-23	0232	0.18	93.80	91.01	REVERSE	314.25	324	7.1	RESORCE
2011-10-23	3981	0.18	43.04	40.25	REVERSE	999.00	340	7.1	RESORCE
2011-10-23	3982	0.18	56.92	54.13	REVERSE	999.00	346	7.1	RESORCE
2011-10-23	3984	0.18	99.88	97.09	REVERSE	999.00	366	7.1	RESORCE
2011-10-23	3987	0.18	24.10	21.31	REVERSE	999.00	58	7.1	RESORCE
2011-10-23	2541	0.18	20.89	18.10	REVERSE	652.00	77	7.1	RESORCE
2011-10-23	3988	0.18	35.90	33.11	REVERSE	999.00	95	7.1	RESORCE
2011-10-23	3989	0.18	26.84	24.05	REVERSE	999.00	51	7.1	RESORCE
2011-10-23	3990	0.18	26.61	23.82	REVERSE	999.00	96	7.1	RESORCE
2011-10-23	3991	0.18	35.54	32.75	REVERSE	999.00	105	7.1	RESORCE
2011-10-23	3992	0.18	36.45	33.66	REVERSE	999.00	91	7.1	RESORCE
2011-10-23	3993	0.18	28.10	25.31	REVERSE	999.00	55	7.1	RESORCE
2011-10-23	3994	0.18	27.05	24.26	REVERSE	999.00	117	7.1	RESORCE
2011-10-23	3995	0.18	40.18	37.39	REVERSE	999.00	152	7.1	RESORCE
2011-10-23	3996	0.18	26.07	23.28	REVERSE	999.00	68	7.1	RESORCE
2011-11-09	3971	0.32	21.18	19.61	STRIKE SLIP	999.00	93	5.6	RESORCE
2011-11-09	2508	0.32	5.61	4.04	STRIKE SLIP	363.13	16	5.6	RESORCE
2011-11-09	3997	0.32	24.06	22.49	STRIKE SLIP	293.00	75	5.6	RESORCE
2011-11-09	3998	0.32	14.90	13.33	STRIKE SLIP	999.00	6	5.6	RESORCE
20120610124415	0705	0.26	10.13	8.21	STRIKE SLIP	1113.00	70.11	6.1	AFAD
20120610124415	0910	0.26	34.03	32.11	STRIKE SLIP	271.00	179.2	6.1	AFAD
20120610124415	3511	0.26	41.58	39.66	STRIKE SLIP	827.00	258.9	6.1	AFAD
20120610124415	4801	0.26	11.25	9.32	STRIKE SLIP	466.00	93.89	6.1	AFAD
20120610124415	4803	0.26	9.09	7.17	STRIKE SLIP	248.00	19.7	6.1	AFAD
20120610124415	4809	0.26	11.53	9.61	STRIKE SLIP	747.00	145.6	6.1	AFAD
20120610124415	4810	0.26	17.45	15.53	STRIKE SLIP	393.00	72.35	6.1	AFAD
20120610124415	4811	0.26	14.46	12.54	STRIKE SLIP	372.00	56.22	6.1	AFAD
20130108141604	1005	0.17	9.45	6.51	STRIKE SLIP	387.00	96.59	5.8	AFAD
20130108141604	1701	0.17	29.09	26.15	STRIKE SLIP	192.00	85.38	5.8	AFAD
20130108141604	1710	0.17	18.66	15.72	STRIKE SLIP	286.00	123	5.8	AFAD
20140524092500	1701	0.08	20.57	14.32	STRIKE SLIP	192.00	57.95	6.5	AFAD
20140524092500	1704	0.08	22.76	16.51	STRIKE SLIP	403.00	79.92	6.5	AFAD
20140524092500	1707	0.08	15.69	9.44	STRIKE SLIP	324.00	173	6.5	AFAD
20140524092500	1710	0.08	14.29	8.04	STRIKE SLIP	286.00	75.84	6.5	AFAD
20140524092500	1712	0.08	12.32	6.07	STRIKE SLIP	683.00	128.3	6.5	AFAD
20140524092500	3415	0.08	21.52	15.27	STRIKE SLIP	283.00	261	6.5	AFAD

Earthquake	Sta.	fc_{mean}	D'_{95}	D_P	Faulting	V_{s30} (m/s)	R_{RUP}	Mw	Source
20140524092500	5904	0.08	22.04	15.79	STRIKE SLIP	225.00	117	6.5	AFAD
20170302110725	0201	0.44	9.62	8.48	STRIKE SLIP	391.00	34.6	5.5	AFAD
20170302110725	0208	0.44	17.62	16.48	STRIKE SLIP	469.00	78.87	5.5	AFAD
20170302110725	2703	0.44	19.69	18.56	STRIKE SLIP	758.00	110.8	5.5	AFAD
20170302110725	4401	0.44	24.80	23.66	STRIKE SLIP	481.00	94.62	5.5	AFAD
20170302110725	4404	0.44	15.85	14.72	STRIKE SLIP	1380.00	83.96	5.5	AFAD
20170302110725	4614	0.44	13.92	12.78	STRIKE SLIP	671.00	104.4	5.5	AFAD
20170302110725	4616	0.44	14.25	13.12	STRIKE SLIP	390.00	144.8	5.5	AFAD
20170302110725	6301	0.44	13.86	12.73	STRIKE SLIP	652.00	41.57	5.5	AFAD
20170612122837	1005	0.25	15.10	13.10	NORMAL	387.00	58.11	6.2	AFAD
20170612122837	1704	0.25	13.41	11.41	NORMAL	403.00	96.65	6.2	AFAD
20170612122837	3503	0.25	16.69	14.69	NORMAL	193.00	49.54	6.2	AFAD
20170612122837	3508	0.25	9.97	7.97	NORMAL	558.00	87.43	6.2	AFAD
20170612122837	3510	0.25	12.41	10.41	NORMAL	313.00	72.53	6.2	AFAD
20170612122837	3511	0.25	16.59	14.59	NORMAL	827.00	86.34	6.2	AFAD
20170612122837	3512	0.25	16.12	14.12	NORMAL	468.00	80.3	6.2	AFAD
20170612122837	3514	0.25	16.04	14.04	NORMAL	836.00	75.99	6.2	AFAD
20170612122837	3515	0.25	14.55	12.55	NORMAL	171.00	72.12	6.2	AFAD
20170612122837	3516	0.25	15.57	13.57	NORMAL	460.00	66.09	6.2	AFAD
20170612122837	3520	0.25	18.48	16.48	NORMAL	875.00	79.76	6.2	AFAD
20170612122837	3523	0.25	12.90	10.90	NORMAL	414.00	63.34	6.2	AFAD
20170612122837	3524	0.25	11.20	9.20	NORMAL	459.00	71.09	6.2	AFAD
20170612122837	3525	0.25	13.84	11.84	NORMAL	745.00	79.4	6.2	AFAD
20170612122837	3527	0.25	13.64	11.64	NORMAL	207.00	26.17	6.2	AFAD
20170612122837	3528	0.25	13.47	11.47	NORMAL	532.00	56.21	6.2	AFAD
20170612122837	3534	0.25	17.07	15.07	NORMAL	328.00	36.79	6.2	AFAD
20170720223110	0916	0.36	46.43	45.04	NORMAL	371.00	107.2	6.6	AFAD
20170720223110	3528	0.36	43.04	41.65	NORMAL	532.00	162.8	6.6	AFAD
20170720223110	4806	0.36	11.39	10.00	NORMAL	323.00	44.97	6.6	AFAD
20170720223110	4807	0.36	9.02	7.63	NORMAL	696.00	66.95	6.6	AFAD
20170720223110	4809	0.36	5.93	4.54	NORMAL	747.00	19.47	6.6	AFAD
20170720223110	4810	0.36	10.88	9.49	NORMAL	393.00	63.57	6.6	AFAD